FELIPE RODRIGUES

Core-top calibration of paleotemperature geochemical proxies: A case study in the Southeast Brazilian continental margin

A thesis submitted to the Oceanographic Institute of the University of São Paulo in partial fulfillment of the requirements for the degree of Master of Science, in the Oceanography Program, with a concentration in Geological Oceanography.

Supervisor: Prof. Dr. Michel Michaelovitch de Mahiques

Co-advisor: Dr. Renata Hanae Nagai

São Paulo
2019

University of São Paulo
Oceanographic Institute

Core-top calibration of paleotemperature geochemical proxies: A case study in the Southeast Brazilian continental margin

FELIPE RODRIGUES

A thesis submitted to the Oceanographic Institute of the University of São Paulo in partial fulfillment of the requirements for the degree of Master of Science, in the Oceanography Program, with a concentration in Geological Oceanography.

Revised Version

Judged on May 27th 2019, by:

Prof. Dr. Michel Michaelovitch de Mahiques (IOUSP)	Grade
Prof. Dr. Cesar de Castro Martins (CEM/UFPR)	Grade
Prof. Dr. María Alejandra Gómez Pivel (UFRGS)	Grade

São Paulo
2019

University of São Paulo
Oceanographic Institute

Core-top calibration of paleotemperature geochemical proxies:
a case study in the Southeast Brazilian continental margin

FELIPE RODRIGUES

A thesis submitted to the Oceanographic Institute of the University of São Paulo in partial fulfillment of the requirements for the degree of Master of Science, in the Oceanography Program, with a concentration in Geological Oceanography.

Judged on 27 / 05 / 2019 by:

Prof. Dr. Michel M. Mahiques	Aprovado Grade
Prof. Dr. César de Castro Martins	APROVADO Grade
Prof. Dr. Maria Alejandra Gomez Pivel	Aprovado Grade

São Paulo
2019

Acknowledgments

First of all, my research would have been impossible without the financial aid and support provided by the São Paulo Research Foundation (FAPESP), under grant number 2017/14205-4, and to the Research Internship Abroad (BEPE), under grant number 2018/04518-8. Also, this study was financed in part by the Coordenação de Aperfeiçoamento de Pessoal de Nível Superior – Brasil (CAPES) – Finance Code 001.

I would like to express my sincere gratitude to my advisor Dr. Michel Michaelovitch de Mahiques and to my co-advisor Dr. Renata Hanae Nagai, for the continuous support to the construction of this study. Thank you for your patience, motivation, enthusiasm, and immense knowledge. Thank you for accepting me as your student!

I wish to thanks Dr. Silvia Melo, for allowing me to use your lab facilities (aka microscopes and coffee maker) for months! Our conversations were always extraordinary.

I am profoundly grateful to Dr. Julie Richey for accepting as a summer intern at the USGS in St. Pete. You have been giving me invaluable help with the elemental data, literature, and writing. I am very thankful for all your assistance!

I thank my fellow labmates from LAMA. Thank you, Jorge, for the QGIS tips; Ligia for the chats; and Pits for the coffee and support. I also would like to thanks my second labhouse, the LABQOM, especially Naty, Felipe, Dani, Dóris and Aline. You are an amazing team.

I am so thankful for all the emotional and personal assistance that Amanda gave me during this journey. Thank you for being such a great person, for the charanaga's parties, the candies and sugar specialties, and so on. You can count on me whenever you need!

Thank you, my family, for supporting me.

Last but not least, I would like to thank my fiancé Tom. When your happiness is someone else's happiness, that is love.

Thank you all!

Abstract

Reconstructing past sea surface temperature conditions is valuable to observe and evaluate the climate of the past. In the SW Atlantic, so far, few studies have exanimated the applicability of paleotemperature equations, which may reflect in fewer reliable SST estimates. This study aimed to evaluate two marine proxies for SST reconstructions: the alkenones unsaturation index ($U^{K'}_{37}$) and the ratio Mg/Ca in different planktonic foraminifera species and size fractions (*G. ruber* pink; *G. ruber* white *senso stricto* and *senso lato;* between 250 - 300 µm and 300 - 355 µm; *G. truncatulinoides* (d) crusted and non-crusted forms, between 380 – 620 µm; and *G. inflata* 300 – 425 µm). The samples were collected in the shelf break of South Brazilian Bight (SBB, 22 °S to 27 °S). The proxies were converted into SSTs and then compared to modern SSTs from the World Ocean Atlas and satellite images. The first chapter describes the $U^{K'}_{37}$ signals and the applicability of three different paleotemperature equations, and the second chapter describes the Mg/Ca a proxy for past SSTs and water mass conditions after applying the most used paleotemperature equations for the ratio Mg/Ca. The $U^{K'}_{37}$ seems to record mostly autumn conditions at 0m, and the most recent Bayspline equation results into more similar temperature averages when compared to modern annual SSTs (*p*-value of 0.81, n = 47, Δ_{SST} of -0.03°C ± 0.27), while the most used linear equations result into SSTs similar to autumn conditions. In subtropical regions with low-temperature variations (~4°C), the function $U^{K'}_{37}$ versus SSTs works in an exponential relation, and they are related to seasonal temperatures. For the Mg/Ca in planktonic foraminifera species, the Mg/Ca-inferred temperatures agree well with modern ocean temperatures. Our data suggest that in different size fractions the tested species respond differently to the most used species-specific and general species paleotemperature equations. All the upper water column species agree well with temperatures at 0-meter depth. The *G. ruber* (p) responds well to the SS equation, where the smallest and the largest size results into annual and autumn estimates, respectively (*p*-value of 0.81 and 0.71, n = 23); the smallest size of *G. ruber* (w) *s.s.* provides summer estimates applying the GE equation (*p*-value of 0.21, n = 7), while the largest size provides annual estimates (*p*-value of 0.86, n = 13). The *G. ruber* (w) *s.l.* has significant averages when compared the largest size with autumn and summer conditions (*p*-value of 0.21 for both, n = 16); the deep-dwelling species *G. inflata* and the *G. truncatulinoides* (d) crusted form reflect the uplift of the SACW, calcifying at 10 and 20 m depth (*p*-value of 0.89, n = 10 and *p*-value of 0.06, n = 14, respectively), while the *G. truncatulinoides* (d) non-crusted form records annual temperature in deep water layers conditions (*p*-value of 0.06, n = 16). This is the first study to report Mg/Ca ratios in surface-dwelling and deep-dwelling planktonic foraminifera tests obtained in core-top samples at the SBB. This validation will inform the reconstruction of past environmental conditions of SW Atlantic, especially in the SBB.

Keywords: Marine geochemistry, paleotemperature, foraminifera, alkenones unsaturation index, Mg/Ca-based, paleoceanography, water masses, paleotemperature equations, marine proxies.

Resumo

As reconstruções das condições da temperatura superficial do mar são importantes para avaliar o clima do passado da Terra. No Atlântico SE, no entanto, poucos estudos avaliaram a aplicabilidade das equações de conversão dos indicadores geoquímicos para temperatura, o que pode resultar em estimativas de paleotemperatura de menor acurácia. Este estudo avaliou dois indicadores marinhos de paleotemperatura: o índice de insaturação de alquenonas ($U^{K'}_{37}$), e a razão Mg/Ca em testas de foraminíferos planctônicos de diferentes espécies e frações de tamanho (*G. ruber* pink; *G. ruber* white *senso stricto* e *senso lato;* entre 250 - 300 µm e 300 - 355 µm; *G. truncatulinoides* (d) encrustadas e não-encrustadas, entre 380 – 620 µm; e *G. inflata* 300 – 425 µm). As amostras são provenientes da plataforma externa e quebra da plataforma do Embaiamento de São Paulo (22°S a 27°S). Os indicadores foram transformados em TSM e então comparados com as temperaturas obtidas por meio do World Ocean Atlas e de imagens de satélite. O primeiro capítulo apresenta os dados de $U^{K'}_{37}$ e a aplicabilidade de três equações de paleotemperatura. O segundo capítulo apresenta dados da razão Mg/Ca como indicador de TSM e condições de massa d'água após a aplicação das equações de conversão. O $U^{K'}_{37}$ apresenta influência do outono em 0 m de profundidade em seus registros, e a mais recente equação *Bayspline* resulta em médias de TSM mais similares com as condições atuais, principalmente quando comparado com a média anual de TSM (*p*-valor de 0.81, n = 47, Δ_{SST} de -0.03°C ± 0.27), já as equações lineares mais conhecidas resultam em TSM mais parecidas com condições de outono. No geral, em regiões com pouca variação de TSM (~1.5 °C), o $U^{K'}_{37}$ responde em uma relação exponencial com a temperatura. A razão Mg/Ca em testas de foraminíferos planctônicos, quando convertidas em TSM, resultam em médias similares com as condições atuais de temperatura. Os nossos dados sugerem que as equações específicas para cada espécie (SS) e as equações gerais (GE) resultam em diferentes médias de TSM para cada espécie/fração de tamanho. Todas as espécies de superfície respondem bem com as temperaturas em 0 metros de profundidade. A *G. ruber* (p) responde bem à equação SS, onde a menor e a maior fração de tamanho resulta em médias similares às TSM anuais e de outono, respectivamente (p-valor de 0.81 e 0.71, n = 23); a menor fração de tamanho da espécie *G. ruber* (w) *s.s.* resulta em médias similares às TSM de verão com a equação GE (*p*-valor de 0.21, n = 7), enquanto a maior fração de tamanho resulta em TSM anual (*p*-valor de 0.86, n = 13). A maior fração de tamanho da espécie *G. ruber* (w) *s.l.* resulta em médias significativas quando comparadas com TSM de outono e de verão (*p*-valor de 0.21 para ambas, n = 16). Os registros geoquímicos das espécies de subsuperfície, como a *G. inflata* e a *G. truncatulinoides* (d) encrustada registram a subida da ACAS para a superfície na área de estudo, calcificando em 10 e 20 metros de profundidade, respectivamente (*p*-valor de 0.89, n = 10 e de 0.06, n = 14, respectivamente), enquanto a *G. truncatulinoides* (d) não-encrustada aparenta registrar as condições anuais de temperatura em profundidades mais próximas da ACAS, com médias um pouco mais elevadas que as duas espécies de subsuperfície (*p*-valor de 0.06, n = 16). Este é o primeiro estudo que relata as razões Mg/Ca em diferentes espécies de foraminíferos planctônicos no SBB. Esta validação auxiliará a aprimorar futuras estimações de TSM com este indicador.

Palavras-chave: Geoquímica marinha, paleotemperatura, índice de insaturação de alquenonas, razão Mg/Ca, paleoceanografia, massas d'água, foraminíferos, calcificação, equações de paleotemperatura, indicadores marinhos.

Table Index

Figure Index

Table of Contents

General Introduction

The reconstruction of past Sea Surface Temperature (SST) conditions is a powerful tool to evaluate past climatic variations (ELDERFIELD AND GANSONS, 2000; ROSENTHAL AND LOHMANN, 2002; EVANS et al., 2016). SST can be reconstructed using physico-chemical composition of marine sediments (WEFER et al., 1999; KUCERA, 2007), and these records can be observed through the geochemical proxies, such as the alkenones unsaturation index ($U^{K'}_{37}$) (e.g. PRAHL AND WAKEHAM, 1987; MUELLER et al., 1998; Conte et al., 2006; amongst others), and with the major elements presented in foraminifera tests (e.g. ratio Mg/Ca; NÜRNBGERG et al., 1996; ANAND et al., 2003; amongst others). Each of these proxies varies as the sea temperature changes and, after the sediment deposition, they are usually found well preserved within the sediment fractions.

To convert the geochemical proxy data to quantitative temperature estimative, both for foraminifera tests and $U^{K'}_{37}$, a conversion equation is applied. These equations have different coefficients, which may change according to different locations (PRAHL et al., 1988; MUELLER et al., 1998; CONTE et al., 2006; TIERNEY AND TINGLEY, 2018), species and/or size fractions (ANAND et al., 2003; CONTE et al*.,* 2006; RICHEY et al., 2012; RIVEIROS et al*.,* 2016; THIRUMALAI et al., 2016).

Within the paleotemperature context, the number of paleoceanographic studies in the SW Atlantic has increased during the past decades (e.g. LEDUC et al., 2010; PIVEL et al., 2013; CHIESSI et al., 2014; SANTOS et al., 2014; CORDEIRO et al., 2014; LESSA et al., 2016; SANTOS et al., 2017; LOURENÇO et al., 2017; DAUNER et al., 2019), and, so far, one study has tested the applicability of $U^{K'}_{37}$-based paleotemperature equations (COCCEPIORI et al., 2018). Despite the growth in interest of paleotemperature in the region, the SW Atlantic still lacks validation studies for the SST proxies that are commonly used for this purpose.

The aim of this thesis was to validate the different paleotemperature calibrations for these proxies in the SW Atlantic Ocean. This is enable more SST accurate estimates and, consequently, more robust paleoceanographic reconstructions. To do so, this master's thesis was divided into two chapters to assess two different marine paleotemperature proxies. In the first chapter the alkenones unsaturation index proxy is presented and discussed, and in the second chapter, the Mg/Ca ratio of different species of planktonic foraminifera tests was analyzed.

CHAPTER 1

Testing global calibrations for reconstruction of sea surface temperatures using $U^{K'}_{37}$ as a proxy: Which is the best model for the SW Atlantic Ocean?

1.1. Introduction

The alkenones are a group of long chain (C_{37}-C_{39}) di-, tri- and tetra-unsaturated methyl and ethyl ketones. They are synthesized by coccolithophores of the class *Prymnesiophyceae*, mainly the Haptophyte algae *Emiliania huxleyi* and *Gephyrocapsa oceanica* (VOLKMAN et al., 1980; DE LEEUW et al., 1980). These species inhabit the upper mixed layer in open waters (about 20 – 30-meter depth; WINTER et al., 1994), and in the South Atlantic, they are associated to waters with a high content of nutrients and low temperatures (BOECKEL et al., 2006).

The unsaturation level of the alkenones ($U^{K'}_{37}$) shows a temperature response, such that the lower the sea water temperature, the higher the unsaturation level of this index (BRASSELL et al., 1986a; PRAHL AND WAKEHAM, 1987; PRAHL et al., 1988; SIKES et al., 1997). The index itself was first calculated after Brassell et al. (1986b) and readjusted by Prahl and Wakeham (1987) (Equation 1), where:

$$U^{K'}_{37} = \frac{[C37{:}2]}{[C37{:}2+C37{:}3]} \qquad \text{(Equation 1)}$$

Prahl and Wakeham (1987) observed the linear correlation between $U^{K'}_{37}$ and temperature in laboratory culture using the *E. huxleyi*. From there, Prahl et al. (1988) used samples from sediment traps collected along the Pacific Ocean and developed the most widely used global calibration of $U^{K'}_{37}$ as a paleotemperature proxy, which is defined as $U^{K'}_{37} = 0.034T + 0.043$ (Equation 1). This equation has been globally applied for palaeoceanographic studies regarding reconstruction of SST based on $U^{K'}_{37}$ (SIKES et al., 1991; ROSELL-MELÉ et al., 1995; MUELLER et al., 1998; amongst others).

Conte et al. (2006) gathered core-top samples throughout different ocean basins, as well as previous published $U^{K'}_{37}$ data around the globe, to develop a global alkenones equation. In contrast to the linear relationship of Prahl et al. (1988), they found that on a global scale, the $U^{K'}_{37}$ shows a polynomial correlation with the SST ($T = -0.957 + 54.293(U^{K'}_{37}) - 52.894(U^{K'}_{37})^2 + 28.231(U^{K'}_{37})^3$ – Equation 2). Then, they proposed a third level polynomial equation to reconstruct past SST.

Other equations for the $U^{K'}_{37}$ have also been performed in different regions/basins to observed possible variations among them (e.g., SIKES et al., 1991; ROSELL-MELÉ et al., 1995; PELEJERO AND CALVO, 2003; MULLER et al., 1998). These authors found, mostly, a linear correlation between their $U^{K'}_{37}$ values and the SST.

For the South Atlantic Ocean, Muller et al. (1998) developed an equation for the SE portion of this basin using core-top samples. These authors found a similar linear equation to the Prahl et al. (1988) equation ($U^{K'}_{37} = 0.033T + 0.069$ – Equation 3), suggesting that both equations can be properly applied in their study basins, as well as in other regions.

Ceccopieri et al. (2018) were the first authors to test different alkenone equations (i.e., PRAHL et al., 1988; MULLER et al. 1998 and TIERNEY AND TINGLEY, 2018) in the SW Atlantic aiming to observe which calibration results in most reliable SSTs reconstructions for the region. They found that in the Campos Basin (20.5 °S to 24 °S), the $U^{K'}_{37}$ correlates best to modern mean annual SSTs when the Mueller et al. (1998) equation is applied. They also observed a strong correlation of $U^{K'}_{37}$ SST estimates with winter SSTs which, according to these authors, might be a consequence of the upwelling of the South Atlantic Central Water (SAWC), which carries cold water and high nutrients content to the surface. This phenome is very significant and frequent in the area, especially in the Cabo Frio (22 °S) region.

The South Brazilian Bight (SBB - 23°S - 28°S), is a region that lacks paleotemperature studies even though it plays an important role in the global ocean circulation system (PETERSON AND STRAMMA, 1991), transporting salty and warm waters southwards. Yet, in the SBB, the $U^{K'}_{37}$-SST reconstructions have assumed that Prahl et al. (1988) is the one that provides most reliable estimates (i.e. BENTHIEN AND MÜLLER, 2000; LOURENÇO et al., 2018). The reliability of the inferred results from this equation, however, has not been tested so far.

As previously mentioned, in the SW Atlantic, there is only one study regarding the applicability of the equations for SST reconstructions based on $U^{K'}_{37}$ (i.e. CECCOPIERI et al., 2018), and it covers an area north of the SBB, which shows different oceanographic conditions. Considering that the SW Atlantic has not been much explored in the paleoceanographic field, analyzing what is the influence of the temperature on the marine sediments of this basins improve the understanding of past ocean conditions in the area.

Therefore, this study tested the applicability of four SST-$U^{K'}_{37}$ based equations in the SBB in order to identify which one provides SSTs that are more similar to observed SSTs. In this first chapter, the main goal will be to perform a regional calibration of the $U^{K'}_{37}$ index to compare with previously published calibrations. This validation is important to the understanding paleotemperature estimates in the SW Atlantic in the context of data gathered from other regions.

1.2. Objectives

The main goal of this chapter was to validate what SST-$U^{K'}_{37}$ based calibrations are more suitable for the SBB. The validation will help to improve future paleotemperature data that will be analyzed in the study area and, therefore, to understand the palaeoceanographic and paleoclimate evolution of the SW Atlantic.

To reach the main goal of this chapter the following targets were established:

i. Generate data from the geochemical proxies in marine sediments ($U^{K'}_{37}$), from samples collected along the South Brazilian Bight;
ii. Compare the $U^{K'}_{37}$ data to observed modern SST and verify what is or is there is a correlation between them;
iii. Compare the SST generated by the $U^{K'}_{37}$ in this study to previously published data from the literature;
iv. Verify/Validate if the available paleotemperature coefficients are adequate for the study area.

1.3. Study Area

The SBB is located on the SE Atlantic Ocean, extending from Cabo Frio to Cabo de Santa Marta (23°S - 28°S, Figure 1). The area presents an arc-shape orientation, and its continental shelf is very wide, ranging from 71 to 231 km wide (ZEMBRUSKI, 1979). The SBB does not receive large a fluvial discharge due to the uplift of the Serra do Mar mountain formation, that deviates the largest rivers towards the continent, (MAHIQUES et al., 2002; 2004). Therefore, the sedimentary processes in the area are dominated by the local ocean circulation (MAHIQUES et al., 2004).

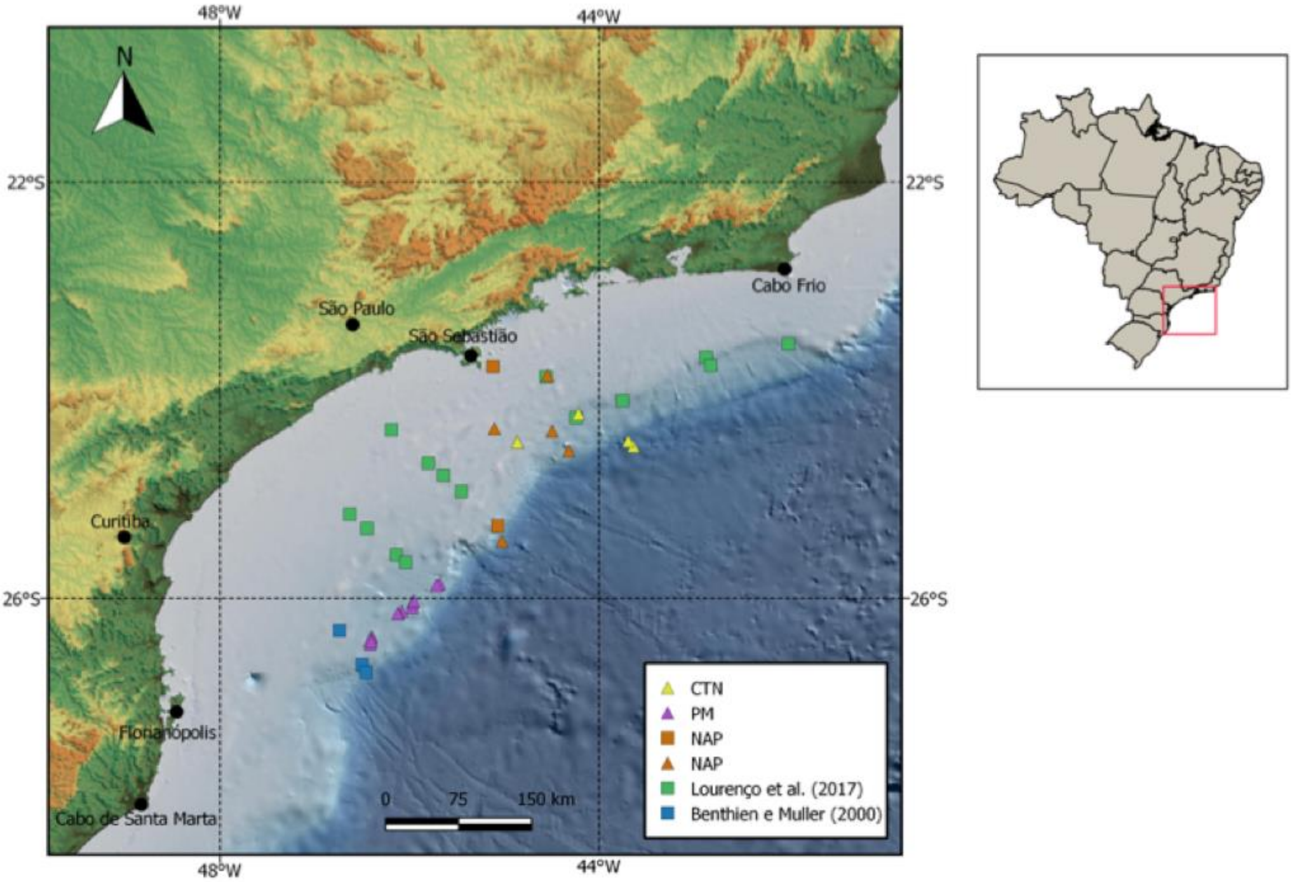

Figure 1 - Map of the study area and sample locations, as the triangles represent the locations where the samples were retrieved. The yellow, green and the orange triangles represent the Contornitos (CTN - FAPESP n° 2016/03381-3), Pockmarks (PM - FAPESP n° 2016/22194-0), and GEOSEDEx (GEO) projects respectively. The squares represent the data that were available on the literature and were used in this study.

The Sao Sebastião Island is marked as a division point of the sea floor composition, where southwards of the island, the sea floor is composed of mud, and northwards, calcium carbonate (MAHIQUES et al., 2004). In the outer continental shelf, the presence of coarse sediments is higher, and their presence is related to the sediment depositions during the events of regression of the sea level (MAHIQUES et al., 2011).

The SBB is dominated by the Brazil Current (BC), which flows southwards over the shelf break and continental slope (CAMPOS et al., 1995; 2000; STRAMMA AND ENGLAND, 1999, Figure 2). The BC transports two water masses: the Tropical Water (TW; Temperature > 20°C; Salinity > 36), which is a superficial water mass and it is known for presenting warm, salty and oligotrophic waters; and the SACW (Temperature > 6°C < 20°C, Salinity > 34.6 and < 36), with colder, less saline and nutrient-enriched waters, which flows at the pycnocline levels (MIRANDA, 1985; SILVEIRA et al., 2000).

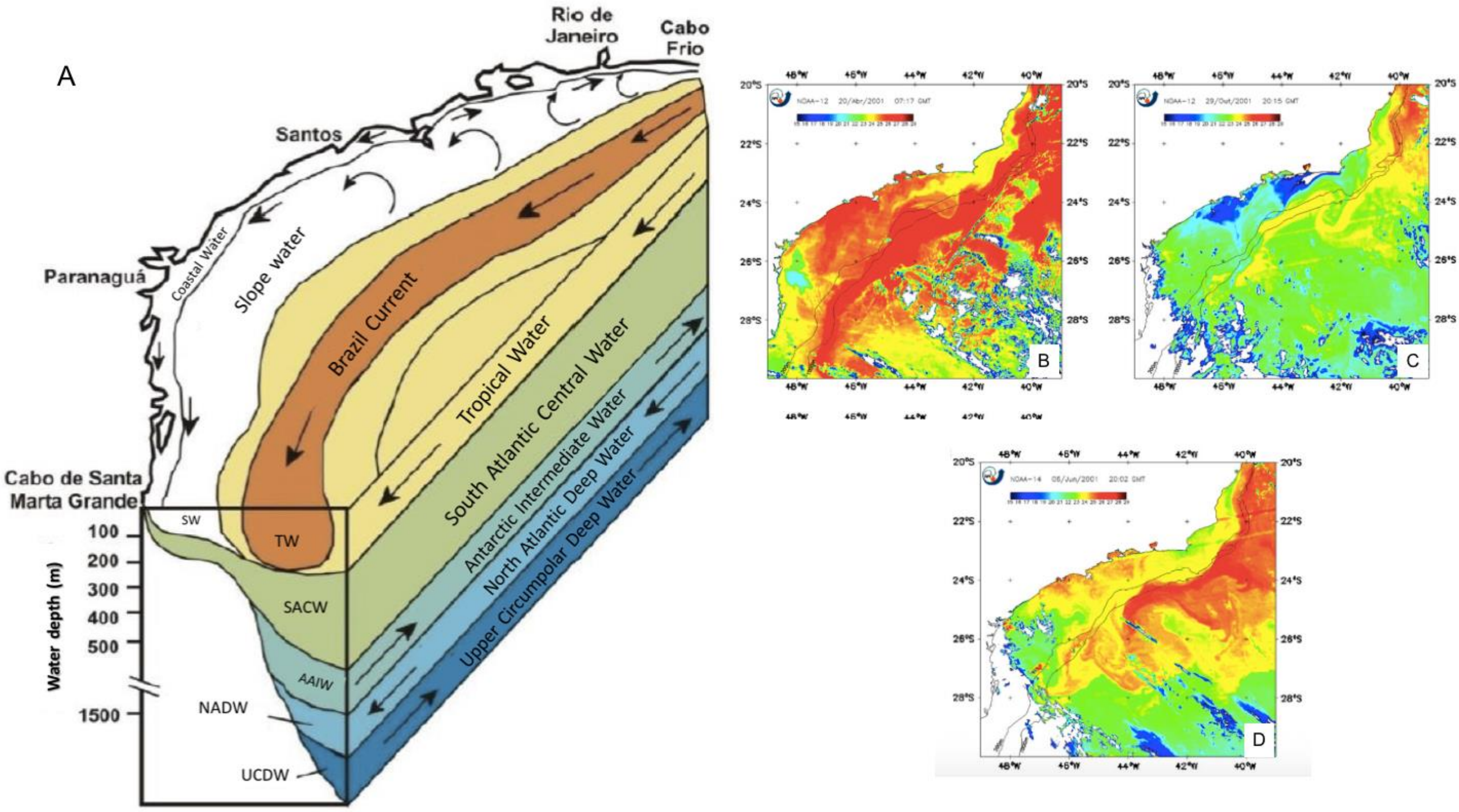

Figure 2 – On Figure 2A represents the vertical structure of the BC over the SBB (Adapted from Maatsura, 1986). The meanders caused by the BC can be observed through satellite images on Figures 2B, 2C and 2D (Adapted from Calado et al., 2008).

The BC forms meanders and eddies on, especially north of the SBB, due to the abrupt changes in the coastline orientation (CAMPOS et al., 2000, Figure 2). The presence of the clockwise meanders leads to the rise of cold waters (e.g., SACW) into the upper water column, generating an upwelling structure (CAMPOS et al., 1996; 2000; LIMA, 1997; SILVEIRA et al., 2008), making the mixed layer and the nutricline shallower (JIN et al., 2016; MCGILLICUDDY, 2016). This upwelling structure can be very significant in some parts of the shelf break in the austral summer, as reported by Brandini et al. (1990), where they observed that in some parts of the shelf break the primary productivity was higher than in coastal zones. The seasonal enhanced of the upwelling is caused mainly by the increase of the strength of the northeasterly (NE) winds (MATSUURA, 1986, CASTELÃO et al., 2004), which, besides bringing the SAWC to the surface, also favors the Coastal Water (CW) to move offshore.

The uplift of cold waters changes the spatial variation of SST, salinity, nutrients and suspended material, causing changes on the light availability in the photic zones (BRANDINI et al., 1990a; BRANDINI, 2014), resulting in the variation in chlorophyll-a (chl-*a*) concentration, biomass and phytoplankton dynamics throughout the SBB (ODEBRECHT AND CASTELLO, 2001; GAETA AND BRANDINI, 2006; BRAGA et al., 2008; BRANDINI et al., 2014).

1.4. Material and Methods

1.4.1. Alkenones analyses and Nannoplankton Identification

The material analyzed in this thesis comes from 25 core-tops (5 core-tops in 0 – 0.5 cm, and 20 core-tops in 0 - 1 cm, Figure 1, Table 1, Appendix) retrieved with multiple-corers (MUC) and box-corers, from the inner and outer shelf, as well as upper slope off the SE Brazilian margin (24°S to 27°S) during three oceanographic cruises, conducted on board the R/V Alpha Crucis, from the Oceanographic Institute of the University of São Paulo, as part of three other projects.

Previously published core-top $U^{K'}_{37}$ data from the study area (BENTHIEN AND MÜLLER, 2000; LOURENÇO et al., 2017, Table 1, Appendix) were also added into the data set to improve the statistical analysis and precision of the results.

The samples were extracted and purified at the Laboratory of Marine Organic Chemistry (LABQOM) at the Oceanographic Institute of the University of São Paulo (IOUSP), as part of other researches.

The analytical procedure to alkenones determination was adapted from Lourenço (2007). About 10 g of freeze-dried sediments of each sample were used. After the samples being macerated and weighed, 80 mL of a mixture of dichloromethane (DCM) and *n*-hexane were added into the samples for them to be submitted to the Soxhlet for 8 h. In all samples, it was added 50 µL of a solution of standard 1-hexadecane and 1-eicosene (50 ng μL^{-1}) to them be used as a surrogate. At the end of the extraction process, the samples had their volume reduced (concentrated) to, approximately, 0.5 mL in a rotary evaporator in 45 °C.

The purification of the total organic extract (fraction) was performed by adsorption column, where the sample was submitted onto 1 g of alumina and 2 g of silica, both deactivated at 5% with water and extracted 5 times with *n*-hexane and sodium sulfate. The concentrated organic fraction was eluted in the column with 6 mL of *n*-hexane, as well as 10 mL of DCM/*n*-hexane. These solutions provide aliphatic hydrocarbons and alkenones. The eluate had its volume reduced to, approximately, 0.5 mL in the rotary vapor and then transferred to amber glass ampoules, where 50 µL of a solution containing 50 g μL^{-1} of the internal chromatographic standard (1-tetradecene) was added. After extraction of a batch of samples, it was performed an analytical blank (sodium sulfate).

The alkenones were identified and quantified through the injection of 1 µL of the final extraction through a gas chromatograph with automatic injector coupled to a flame ionization detector (GC-FID; Agilent GC System 6890 Series). A chromatographic column of 50 m of length x 0.32 mm of intern diameter x 0.17 µm of film thickness, where the stationary phase was composed by 5% difenil and 95% dimetilpolisioloxane. The carrier gas was H_2 (purity > 99.999%), with a constant pressure of 7.24 psi. The injector temperature was constantly maintained at 280 °C and the injections were conducted in the splitless mode, with the detector kept at 325 °C.

The quantification of the compounds was performed through the software HP Chemstation (G2070 BA). The criteria applied to accept the analytical curve of the compound was the Pearson linear correlation equal or superior to 99.5% (R^2 = 0.995). The identification was made of the ratio of mass and area of the surrogate standards with the internal chromatographic standard. For the alkenones, the $C_{37:3}$, $C_{37:2}$, $C_{38:3Et}$, $C_{38:3Me}$, $C_{38:2Et}$, $C_{38:2Me}$ compounds were identified and quantified. It was calculated the total concentration of the alkenones (i.e. $C_{37:3}$ + $C_{37:2}$), and the $U^{K'}_{37}$ were calculated after Prahl et al. (1988), as described in Equation 1. A correlation analyses was then used to verify if the total alkenones concentration responded to the chl-*a* concentrations (see the next topic).

The nannofossil identification was performed by the South Atlantic Paleoceanography Laboratory (LaPAS) team, also at IOUSP. At LaPAS, the identification and counting of the coccolithophores (i.e., *E. huxleyi* and *G. oceanica*) from the samples of this thesis was performed under a light polarizing microscope (1000 x). To do this, slides were prepared, according to the Koch and Young (2007) method. The cells were counted according to the visual sight method (QUADROS, 2007), where at least 300 specimens on each slide were counted and identified. The taxonomic classification to identify the nanoplanktonic species was performed after Young et al. (2003) and Antunes (2007), using as support material the Nannotax3 website (YOUNG et al., 2014).

Even though all samples were retrieved above the lysocline, located at 4300 m depth in the South Atlantic (DITTERT et al., 1999), the *E. huxleyi-C.leptoporus* dissolution index, in here including the Boeckel and Baumann (2004) modification (CEX’; Equation 4), was applied to observe if the samples were submitted to high dissolution. In this study, the large *Gephyrocapsa* sp. (< 3 µm) was considered instead of *G. ericsonii,* as Saavedra-Pellitero et al. (2010) have executed.

$$\mathrm{CEX}' = \frac{E.huxleyi + Gephyrocapsa\ \mathrm{sp.}}{E.huxleyi + Gephyrocapsa\ \mathrm{sp.} + C.leptoporus} \qquad \text{(Equation 4)}$$

1.4.2. Acquisition Sea Surface Temperatures, Chlorophyll-*a,* and Statistical Analysis

The annual (SST_{AN}) and austral seasonal (summer – SST_{SU}, autumn – SST_{AU}, winter – SST_{WI}, and spring – SST_{SP}) SSTs, and the chl-*a* concentrations were obtained from the Aqua (EOS PM) satellite with the Moderate Resolution Imaging Spectroradiometer (MODIS) sensor. All the images were acquired in the NASA's website "Ocean Color" at *https://oceancolor.gsfc.nasa.gov/cgi/l3.*

For this thesis, third level daytime images were used, with a 4 km resolution. The images were treated using the SeaDAS software (version 7.5.1, available on *https://seadas.gsfc.nasa.gov/)*. It was possible to SSTs ranging from 2002 to 2017. The SSTs and chl-*a* concentrations from the satellites represent the austral seasonal and annual sea surface conditions. Data from the temperature of the water column was obtained with the World Ocean Atlas 2013 (WOA13) (LOCARNINI et al., 2013) up to 25 m, because deeper than that, the data became not available.

After obtaining the satellite and water column sea temperatures for each sample location, it was tested the normality of the data with the Shapiro-Wilk test, and it was observed if the dataset had outliers. Afterward, a correlation analysis (Pearson's correlation) was performed between the $U^{K'}_{37}$ and the sea temperature with the Past software (version 3.18), to observe the correlation between them in order to observe what season/water depth may be being recorded in the $U^{K'}_{37}$ signals.

The $U^{K'}_{37}$ signals were then converted into SST after four paleotemperature equations (PRAHL et al., 1988; MULLER et al., 1998; CONTE et al., 2006; TIERNEY AND TINGLEY, 2018). These equations were selected because: i) Prahl et al. (1988) is the widely used paleo-proxy paleotemperature equation for $U^{K'}_{37}$; ii) Muller et al. (1998) performed their analyses in the SE Atlantic Ocean; iii) Conte et al. (2006) performed a global calibration, including a few samples from SBB and; iv) Tierney and Tingley (2018) created a new global equation using Bayesian B-spline regression model (BAYSPLINE) for regions where temperatures can get above 24°C.

The ANOVA test was performed to detect what paleotemperature equations based on $U^{K'}_{37}$ show the lowest difference of averages within themselves, as well as between the satellites and the WOA13 sea temperatures (seasonal and annual sea temperatures).

A *p*-value < 0.05 (at 95% of significance) is the value where the null hypothesis (H_0) were rejected and, where, in all cases:

H_0: the averages of the calculated SSTs from the equations are equal to the obtained sea temperatures (satellites and WOA13);

H_1: the averages of the calculated SSTs from the equations are different from the obtained sea temperatures (satellites and WOA13).

Afterward, the difference between the $U^{K'}_{37}$-inferred SSTs and the satellite gathered SSTs (SST anomalies - Δ_{SST}) were estimated from the difference between the average of the $U^{K'}_{37}$ equations against the sea temperatures gathered from MODIS. The Δ_{SST} shows what equation shows lower discrepancies between the calculated SST against the satellite SST.

1.5. Results

The extracted values of the $U^{K'}_{37}$ from all samples, as well as the seasonal and annual SST gathered from the Aqua MODIS Mission, are shown in Table 2 (Appendix) and in Figure 3.

The $U^{K'}_{37}$ showed an average of 0.863 (± 0.02, N = 45), where the highest index showed the value of 0.962, and the lowest 0.804. The $U^{K'}_{37}$ data in this study do not present outliers and present normal distribution (Table 2, Appendix). The total concentration of the alkenones had values between 0.03 ng/g to 0.92 ng/g (average of 0.23 ng/g; ± 0.19, N = 42; Table 3, Appendix).

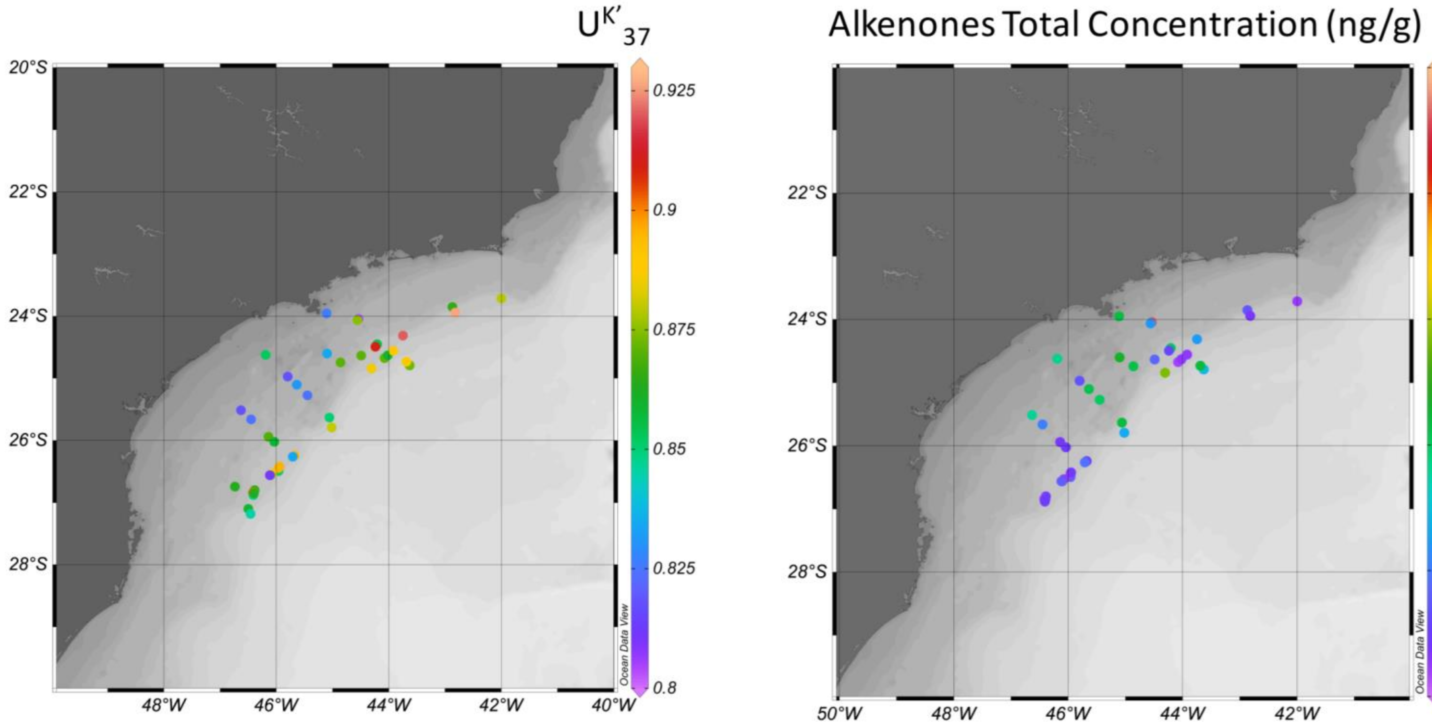

Figure 3 - Values of the $U^{K'}_{37}$ and the total concentration of the alkenones (ng/g) along the SBB.

The summary of the results from the satellite SSTs is listed in Table 4 (Appendix) and Figure 4. In general, SST_{SU} showed the warmest temperatures, and SST_{WI} showed the coolest temperatures. The SST_{AN} and SST_{AU} showed temperatures within the 24 °C, and the SST_{SP} averages in the 23 °C. The water column temperatures are listed in Table 5 (Appendix).

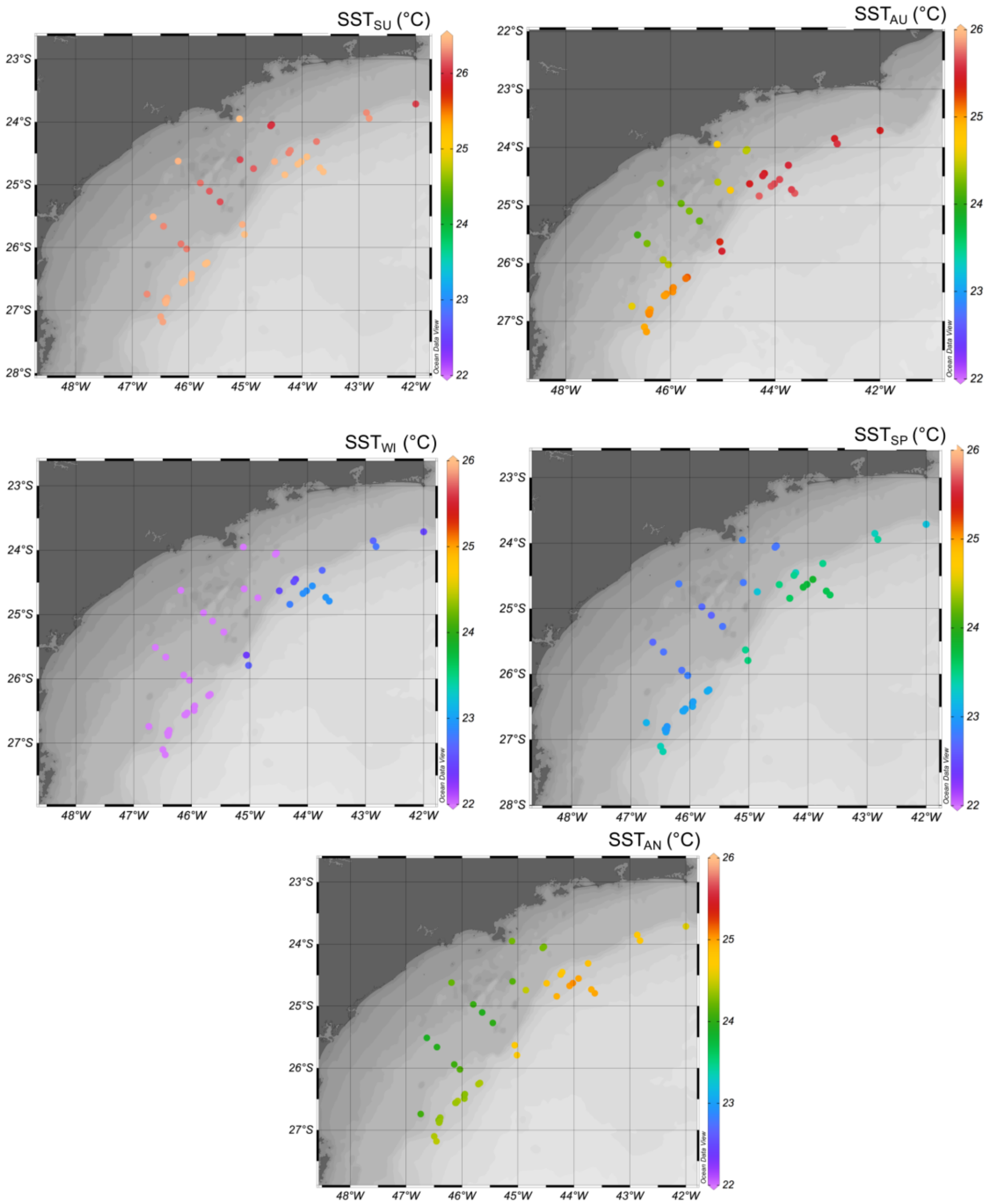

Figure 4 – Distribution of the seasonal and annual SSTs (in °C) from the samples retrieved along with the SBB.

The annual and seasonal SSTs obtained from the satellite images did not present any outliers and, except for SST$_{SU}$, the temperatures do not present a normal distribution even after transforming them into log scale. The temperatures gathered from the WOA13, on the other hand, presented outliers and did not present a normal distribution. Therefore, a non-parametric analysis of non-transformed data for the statistical analysis was performed in this study.

For the satellite image temperatures, all seasonal SSTs, except for SST_{SU}, presented a strong correlation with the $U^{K'}_{37}$ (R > 0.5, N = 45) (Table 6, Appendix). The $U^{K'}_{37}$ presented highest correlation with the SST_{AU} (R = 0.61, $p < 0.05$, N = 45). For the sea temperatures obtained with the WOA13, in general, the depth of 10 m showed the highest correlations with the $U^{K'}_{37}$, (Table 7, Appendix) where the highest was observed with the autumn temperatures at 10 m deep (R = 0.43, *p*-value < 0.05, N = 42).

The inferred SSTs-$U^{K'}_{37}$ based in published equations are listed in Table 8. Overall, all equations result in temperatures that are similar to modern SSTs. The average of Prahl et al. (1988) equation is 24.85 °C (± 0.86, N = 45). The Mueller et al. (1998) equation shows an average of 24.91 °C (± 0.94, N = 45). The polynomial equation developed by Conte et al. (2006) results in an average of 26.64 °C (± 0.74, N = 45), and the Bayesian equation created by Tierney and Tingley (2018) shows an average of 24.40 °C (± 1.08, N = 45).

The results of the Δ_{SST} calculated after the Prahl et al. (1988), Muller et al. (1998), Conte et al. (2006) and Tierney and Tingley (2018) are shown in Tables Table 9, Table 10, Table 11, Table 12, respectively (Appendix). In general, the lowest Δ_{SST} within the published equations and the satellite SSTs was between SST_{AN} and the Tierney and Tingley (2018) equation (-0.03 °C ± 0.27). In Figure 5, it is possible to observe how the data from this study (purple line) fits in a scatterplot when compared to the previously published global calibrations.

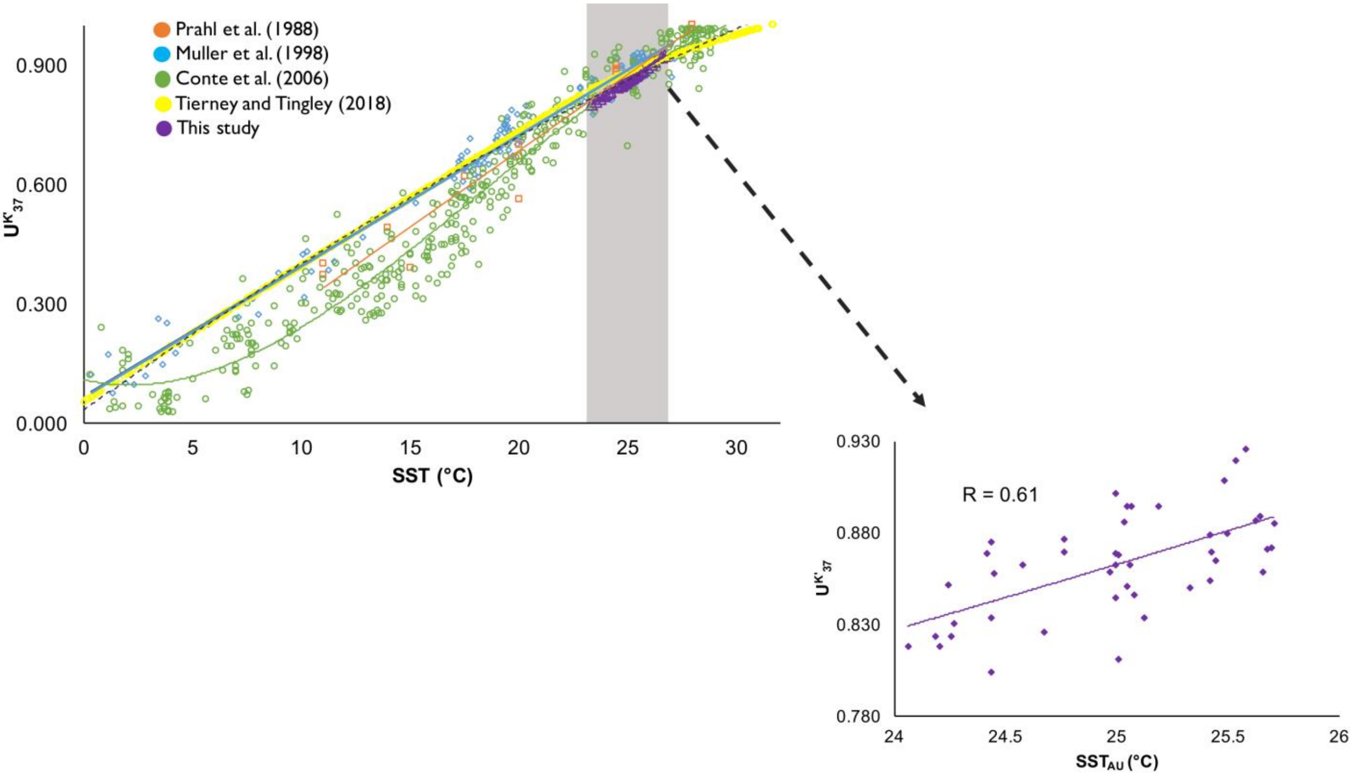

Figure 5 - Scatterplot integrating all $U^{K'}_{37}$ data from previous equations used in this study against SST_{AU}, where Prahl et al. (1988), Muller et al. (1998), Conte et al., (2006), and Tierney and Tingley (2018) are represented as orange, blue, green and yellow, respectively. The gray area highlights the range of temperature from the gathered in the samples of this study (purple line).

On Table 13 (Appendix) it is possible to observe the results of the *p*-values of the Kruskal-Wallis test, where it the averages of the $U^{K'}_{37}$-inferred SSTs obtained with the published equations are compared to the annual and seasonal SSTs gathered from the satellite images. Our data suggest that there is no significant difference between the Prahl et al. (1988) and Mueller et al. (1998) SSTs estimates with the SST_{AU} (*p*-value of 0.48 and 0.61, respectively).

The Tierney and Tingley (2018) equation presented the most similar averages with modern temperatures within all equations, with strong signifancy with the SST_{AN} (*p*-value of 0.87). On the other hand, the Conte et al. (2006) is the equation that gives less representative results, showing its highest (but low) *p*-value with SST_{SU} (*p*-value of 0.007). When compared with the water column temperatures gathered with the WOA13 (0 to 25 m), none of the equations result in significant similar averages.

The chl-*a* concentrations had the lowest values in the austral summer (0.16 mg dm^{-3} ± 0.09, N = 45), while the highest concentrations were found in the winter (0.27 mg dm^{-3} ± 0.16, N = 45, Table 14, Appendix). All chl-*a* concentrations showed significant negative correlation with the $U^{K'}_{37}$ values (R < - 0.5). The most negative correlation was observed with the winter season (R – 0.55, $p < 0.001$, N = 45) (Table 15, Appendix).

Between the two known species considered to synthesize alkenones, the coccolithophore *G. oceanica* was the most abundant species (Table 16, Appendix), composing about 19.56% of the total sample (± 5.98, N = 21), while *E. huxleyi* species correspond to approximately 17.14% of the total assemblage (± 8.66, N = 21).

The CEX' (Table 17, Appendix), showed values higher than 0.80, and an average of 0.96 ± 0.03, where the lowest index was 0.89 and highest was 1.0, suggesting that the samples have not been under dissolution processes.

1.6. Discussion

1.6.1. $U^{K'}_{37}$ records and its synthesizers in the SBB

The $U^{K'}_{37}$ signals from the samples of this study suggest that, except for the SST_{SU}, all seasons show a strong correlation with the $U^{K'}_{37}$ signals at 0 m, especially the SST_{AU}, which seems to play a major role in these records.

Previous proxy validation studies in different basins have also reported the imprint of $U^{K'}_{37}$ during autumn. For instance, Rosell-Melé et al. (1995) noted that in the Northeastern Atlantic (2°S – 75°N) the alkenones temperature signals reflect SST_{AU} rather than SST_{AN} at 0 m depth. They obtained their SST data from the WOA82, and, even though they found the highest correlation at surface, they suggested that their surface temperature should be considered not only to the 0 m depth, but to the mixed layer, since their samples come from a large latitudinal gradient.

Ternois et al. (1996) observed that the production of $U^{K'}_{37}$ in the Northwestern Mediterranean Sea takes in the upper water column during autumn from their sediment trap samples, when the production of coccolithophores is higher. They suggest that the seasonality and the depth of the alkenones production must be considered when reconstructing SSTs based on $U^{K'}_{37}$, as well as the interannual viability of the coccolithophores production. Also, Prahl et al.

(1993) reported that the $U^{K'}_{37}$ signals collected from their sediment traps in the Mediterranean Sea are cold-biased records, influenced mainly by episodic upwelling events near the coast, which induces to the high productivity of the alkenones producers.

The *G. oceanica* and the *E. huxleyi* prefer to inhabit nutrient-rich waters (BOECKEL et al., 2006), and in the study area they bloom mainly during summer (BRANDINI et al., 2004). The weakest correlation of $U^{K'}_{37}$ with SST occurs during summer, which can be a result of habitat competition within the phytoplankton community. As in the study area, during summer, blooms of diatoms and microflagellates have been previously reported (BRANDINI et al., 1989; BRANDINI, 1990; CASTRO et al., 2006, BRANDINI et al., 2014).

The data from this study suggests that the coccolithophores also bloom during summer, once the total alkenones concentration shows its highest correlation with that season. However, the total assemblage of nannoplankton from this study shows that, overall, the *E. huxleyi* and *G. oceanica* are not the most abundant species in the region, suggesting that there is a seasonal bloom variation between diatoms and coccolithophores throughout the year.

It is possible to hypothesize that the coccolithophores that synthesize the alkenones have habitat advantage during cooler seasons, as the water has lower temperatures, as well as lower nutrient content, while other nannoplankton are more abundant over them during warm seasons. The same patter has been suggested by Dauner et al. (2019). It is possible to suggest that as they dominate the environment during cooler seasons, they also record the temperature conditions of the upper water column, especially the 10 m depth.

1.6.2. Which $U^{K'}_{37}$-paleotemperature model is the most suitable for the SBB?

Most of the temperatures inferred from the $U^{K'}_{37}$ based equations applied in this study show similar results within them. In general, Mueller et al. (1998) and Prahl et al. (1988) averages are similar to each other, and they both agree well with modern SST_{AU}. Northwards from the SBB, Ceccopieri et al. (2018) used core-top samples retrieved in the Campos Basin to observe the similarities within the temperatures gathered from the WOA13 to the data from $U^{K'}_{37}$. These authors detected that the $U^{K'}_{37}$ values reflect colder temperatures, and that the Mueller et al. (1998) equation is also the most suitable for paleotemperature reconstruction in the area, reflecting SST_{AN}.

In this study, the equation that agrees the most with modern temperatures is the Bayesian equation developed by Tierney and Tingley (2018), as it provides strong similar averages when compared to SST_{AN}. Since the Bayspline equation, developed by Tierney and Tingley (2018), were proposed to decrease the effector and slope attenuation of the data. Our results show that this model is more reliable statistical paleotemperature SST-$U^{K'}_{37}$ estimates.

1.7. Final Considerations

This study suggests that the signatures of $U^{K'}_{37}$ in the SW Atlantic, especially between 22°S to 27°S, can be used as paleoceanographic proxies for reconstructing past sea temperature conditions. The $U^{K'}_{37}$ index responds more to seasonal SSTs than to annual SSTs. Apparently, in the SBB, the $U^{K'}_{37}$ records cooler temperatures, especially from the autumn season, which agrees well to surface and upper water column sea temperatures.

In the SBB, the inferred SST-$U^{K'}_{37}$ equation that results in more similar temperatures to modern SSTs is the Bayspline equation developed by Tierney and Tingley (2018), providing annual SSTs. For seasonal SSTs, especially SST_{AU} estimates, it is suggested to apply the Mueller et al. (1998) equation.

This study suggests that in regions with low-temperature ranges (~4 °C), the function $U^{K'}_{37}$ versus SSTs works in an exponential relation, and they are related to seasonal temperatures. In order to verify this hypothesis, more paleotemperature studies with the application of $U^{K'}_{37}$ in subtropical regions should be performed.

CHAPTER 2

Regional calibration of marine proxies in the SW Atlantic: A planktonic foraminifera proxy-based calibration

2.1. Introduction

The understanding of how climate has varied throughout Earth's history is a major key to evaluate and comprehend natural climate variations (WEFER et al., 1999), and to predict future environmental changes (BRADLEY, 2000). The oceans play an important role in climate due to the exchange of heat with the atmosphere (ROSENTHAL, 2007), what makes the reconstruction of past sea surface temperatures (SST) one of the main variables to observe past temperature changes.

A method that has been widely used to reconstruct past ocean hydrographic parameters is the ratio Mg/Ca in planktonic foraminifera tests (NÜRNBERG et al., 1996; LEA et al., 1999; ELDERFIELD AND GANSSEN, 2000; ANAND et al., 2003; CLÉROUX et al., 2007; amongst others). Planktonic foraminifera tests sink to the ocean floor where their tests are commonly found well-preserved within the marine sediment (KUCERA, 2007). Past ocean temperature and water column structure reconstructions commonly use individually or together surface-dwelling species (e.g., *Globigerinoides ruber*), intermediate dwellers species (e.g., *Globorotalia inflata*), and deep-dwelling species (e.g., *Globorotalia truncatulinoides*) (ELDERFIELD AND GANSSEN, 2000; WELDEAB et al., 2006; FARMER *et al.,* 2011; CHIESSI et al., 2014, REYNOLDS et al., 2018, amongst others).

The Mg/Ca ratio in planktonic foraminifera tests is one among many proxies in paleoceanographic studies for SST reconstructions. The incorporation of magnesium ions (Mg^{+2}) in the foraminifera calcite is temperature dependent where, during test calcification, as sea temperature increases, the foraminifera calcite Mg/Ca ratio increases exponentially (NÜRNBERG et al., 1996; LEA et al., 1999; ELDERFIELD AND GANSSEN, 2000; BARKER et al., 2003; DEKENS et al., 2002; ANAND et al., 2003; EGGINS et al., 2003; amongst others).

The Mg/Ca ratio obtained from analysis of the foraminifera tests can be converted into temperature using an empirical relationship between Mg/Ca and temperature (e.g., ANAND et al., 2003, GRAY et al., 2018). Other variables such as test size, vital effects, salinity, and pH may also influence foraminiferal Mg/Ca (e.g., ANAND et al., 2003; RICHEY et al., 2012; RIVEIROS et al., 2016). As a result, testing the Mg/Ca-SST calibrations in different regions and oceanographic settings is highly recommended before interpreting palaeoceanographic results (ANAND et al., 2003; RICHEY et al., 2012).

The number of paleoceanographic studies in the SW Atlantic has increased recently (e.g., LEDUC et al., 2010; PIVEL et al., 2013; CHIESSI et al., 2014; SANTOS et al., 2014; LESSA et al., 2016; SANTOS et al., 2017). Despite the increase in interest and the continuous use of Mg/Ca-based SST estimates, the SW Atlantic still lacks calibration studies for the most commonly used planktonic foraminifera species (i.e., *G. ruber, G. inflata*, and *G. truncatulinoides*).

Two previous studies performed in the SW Atlantic are related to calibration of planktonic foraminifera proxies: *G. ruber* (white) $\delta^{18}O$ calibration by Franco-Fragas et al. (2011), and the *G. inflata* SST based Mg/Ca ratio calibration by Groeneveld and Chiessi (2011). Currently, most of the SW Atlantic palaeoceanographic studies involving *G. ruber* (pink and white morphotypes) SST based Mg/Ca estimates apply the conversion equation suggested by Anand et al. (2003), which was calculated for specimens collected in the North Atlantic.

Overall, good interpretations of prior SSTs conditions rely on the validation and accuracy of the analyzing data (LEE et al., 2008), and the lack of regional inferred Mg/Ca-SST validation may reflect in less robust SST assessments. Hence, testing the paleotemperature equations is essential to improve past temperature estimates, providing more reliable results.

Against this background, this study conducted an elemental analysis in four planktonic foraminifera species retrieved from 26 core-top samples along the South Brazilian Bight (SBB – 24°S to 27°S), SW Atlantic. The ratio Mg/Ca will be used to test the most applied paleotemperature equation for Mg/Ca-SST estimates (e.g. ANAND et al., 2003). This is the first comparison based on Mg/Ca performed on various size fractions of different planktonic foraminifera species and variants (e.g. white *s.s.* and *s.l.*) in the SW Atlantic.

2.2. Objectives

The main goal of this chapter was to test the Mg/Ca-paleotemperature based equations of different planktonic foraminifera species in different size fractions from marine surface sediments retrieved from the SBB. From these analyses, this is study is aimed to:

i. Generate data from the paleotemperature proxies (e.g. Mg/Ca) in tests of four species of planktonic foraminifera, and in different size fractions, from core-top sediment samples collected along the SBB;
ii. Compare the Mg/Ca among the selected species/size fractions
iii. Transform the Mg/Ca into temperature and compare to modern SST to observe what is or is there is a correlation between them;
iv. Identify what season the sea temperature has most significant impact on the ratio Mg/Ca records in upper water planktonic foraminifera shells;
v. Compare the SST generated by the Mg/Ca in this study to previously published data from the literature;
vi. Verify/Validate if the available paleotemperature coefficients are adequate for the study area.

This validation will inform the reconstruction of past environmental conditions of SW Atlantic, especially in the Southern Brazilian margin.

2.3. Study Area

The samples from this study come from the outer shelf and shelf break of SBB, ranging the latitudes of 24°S to 28°S (Figure 6). Presenting a wide continental shelf, extending from 71 to 231 km wide, the area has an arc-shape morphology, and it does not receive significant fluvial discharge (ZEMBRUSKI 1979, MAHIQUES et al., 2004).

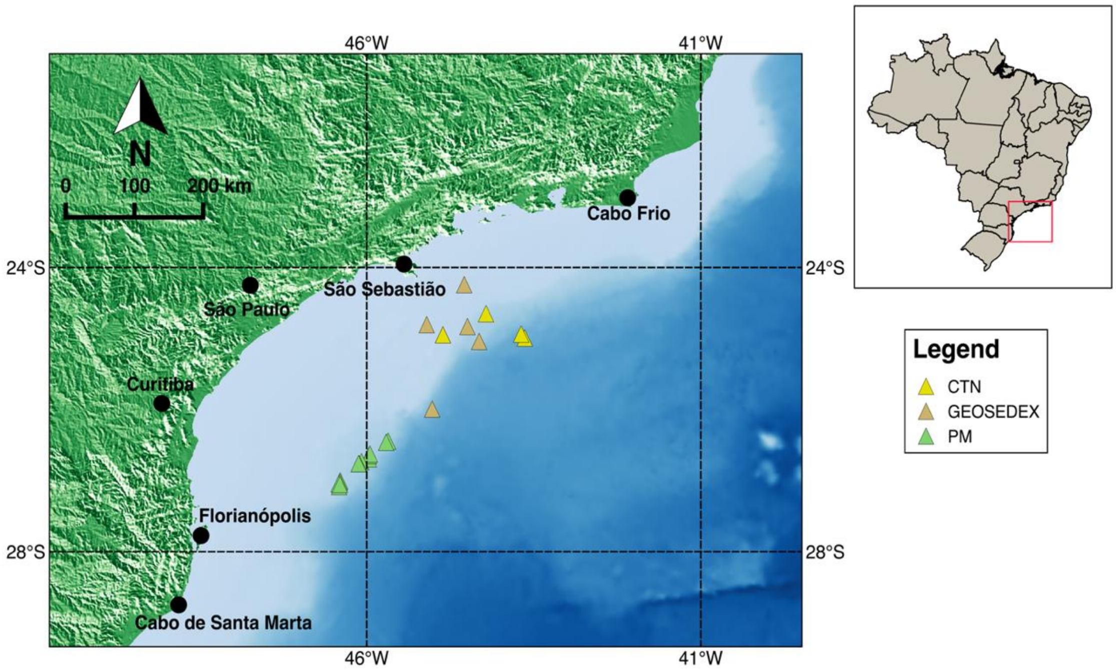

Figure 6 - Map of the study area and sample locations, as the triangles represent the locations where the samples were retrieved. The yellow, green and the orange triangles represent the Contornitos (CTN - FAPESP n° 2016/03381-3), Pockmarks (PM - FAPESP n° 2016/22194-0), and GEOSEDEx (GEO) projects respectively.

On the continental shelf, the sediment composition is composed of very fine sands (MAHIQUES et al., 2004). In offshore areas, the meanders and eddies formed by the Brazil Current (BC) play a major role in the sediment transport (SILVEIRA et al., 2000; MAHIQUES et al., 2007), and the sediments are mostly composed of clay and calcium carbonate (MAHIQUES et al., 2004), as well as coarse sediments, which are related to the sediment depositions during the events of regression of the sea level (MAHIQUES et al., 2011).

The BC is the main current systems that flows on the SBB. This current flows towards south, and its path goes over the shelf break and continental slope (CAMPOS et al., 1995; 2000; STRAMMA AND ENGLAND, 1999). The BC transports two water masses: the Tropical Water (TW; Temperature > 20°C; Salinity > 36), a superficial water mass and it can be recognize for carrying warm, salty and oligotrophic waters; and the South Atlantic Central Water (SACW, Temperature > 6°C < 20°C, Salinity > 34.6 and < 36), carrying colder, less saline and nutrient-enriched waters, flowing at the pycnocline levels (MIRANDA, 1985; SILVEIRA et al., 2000).

The meanders and eddies that the BC develops is caused because of the abrupt changes in the coastline orientation along the SBB (CAMPOS et al., 2000). These systems flow offshore and their presence lead to the rise of the SACW to the photic zone, and resulting in the fertilization of the upper water column (CAMPOS et al., 1996; 2000; LIMA, 1997; SILVEIRA et al., 2008).

The rise of the SACW changes the spatial variation of sea temperature, salinity, nutrients in the upper water column (BRANDINI et al., 1990a; BRANDINI, 2014), modifies the chlorophyll-a (chl-*a*) concentration, biomass and phytoplankton dynamics throughout the SBB (ODEBRECHT AND CASTELLO, 2001; GAETA AND BRANDINI, 2006; BRAGA et al., 2008; BRANDINI et al., 2014).

2.4. Material and Methods

2.4.1. Sample procedures

Samples from 25 core-tops (5 core-tops in 0 – 0.5 cm, and 20 core-tops in 0 – 1 cm) retrieved with multiple-corer (MUC) and box-corer, from the shelf, outer shelf and upper slope of the SE Brazilian margin (from water depths of 121 m to 1557 m; latitudes of 24°S to 27°S) during three oceanographic cruises conducted on board the R/V Alpha Crucis, from the Oceanographic Institute of the University of São Paulo (IOUSP), as described in chapter 1 (Figure 6).

The samples were washed with a 63 µm mesh and oven dried (T < 40°C). After they were dried, the samples were sieved into different size fractions in order to obtain the planktonic foraminifera tests that were selected for this study: *G. ruber* (morphotypes pink and white *s.s*. and *s.l.* in the size fractions of 250 – 300 µm and 300 – 355 µm; *G. inflata*, within the size fraction of 300 – 425 µm, and the *G. truncatulinoides* right coiling (i.e., dextral), in the size fraction of 380 – 620 µm).

The *G. ruber* white *s.s*. and *s.l*. morphotypes were visually separated under a binocular microscope according to the characteristic cited by Wang (2000) (Figure 7 and Figure 8, respectively). This separation was performed because both white morphotypes present different habitat preferences in some regions, where the *s.l.* is a cold-biased species, and shows larger depths variation, while the *s.s.* tends to inhabit the upper depths (WANG, 2000; STEINKE et al., 2005).

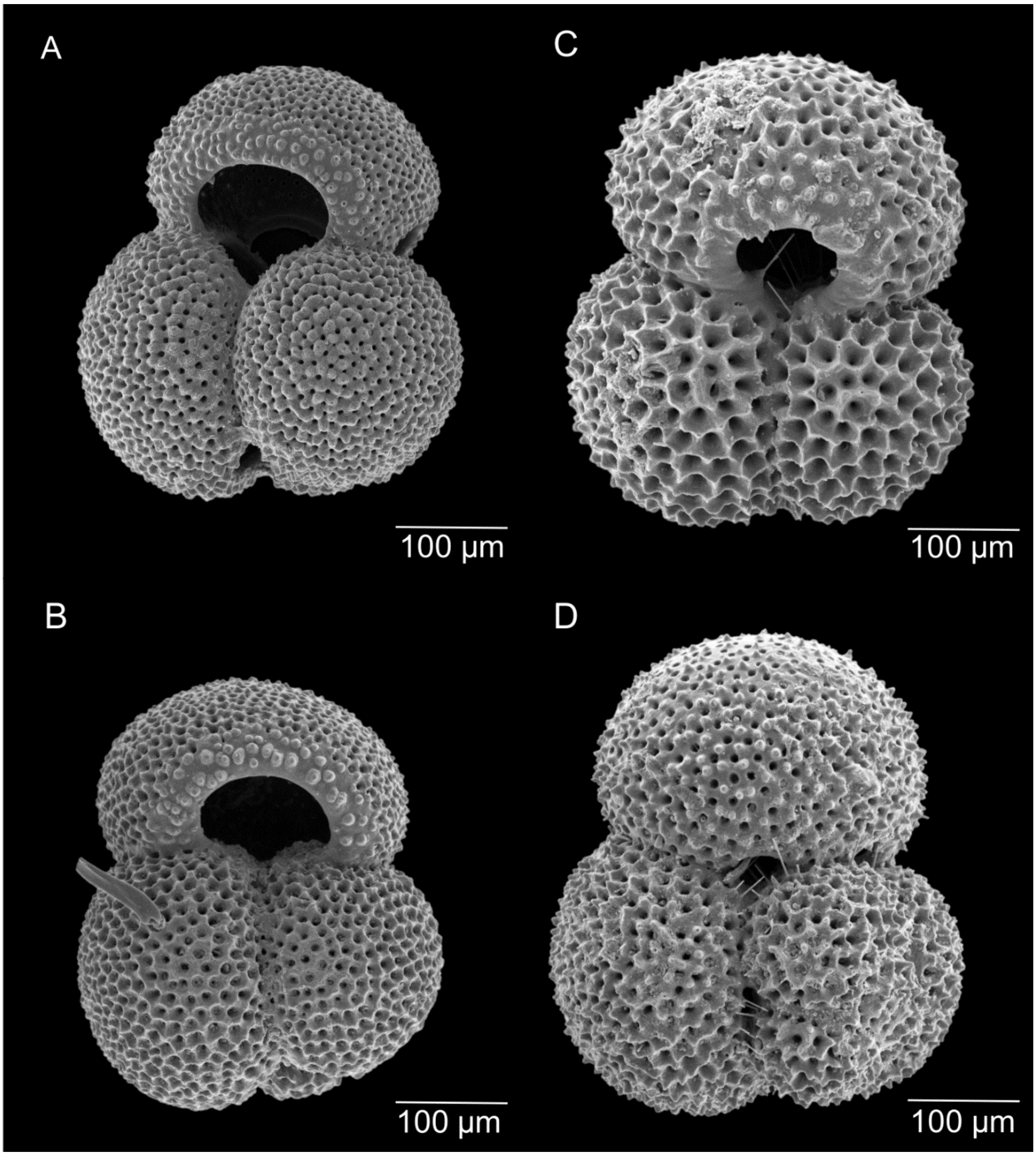

Figure 7 - Specimens of the *G. ruber* (w) *senso stricto* collected from samples of this study. The attachment on 13B is part of a bristle of the brush used to pick the tests.

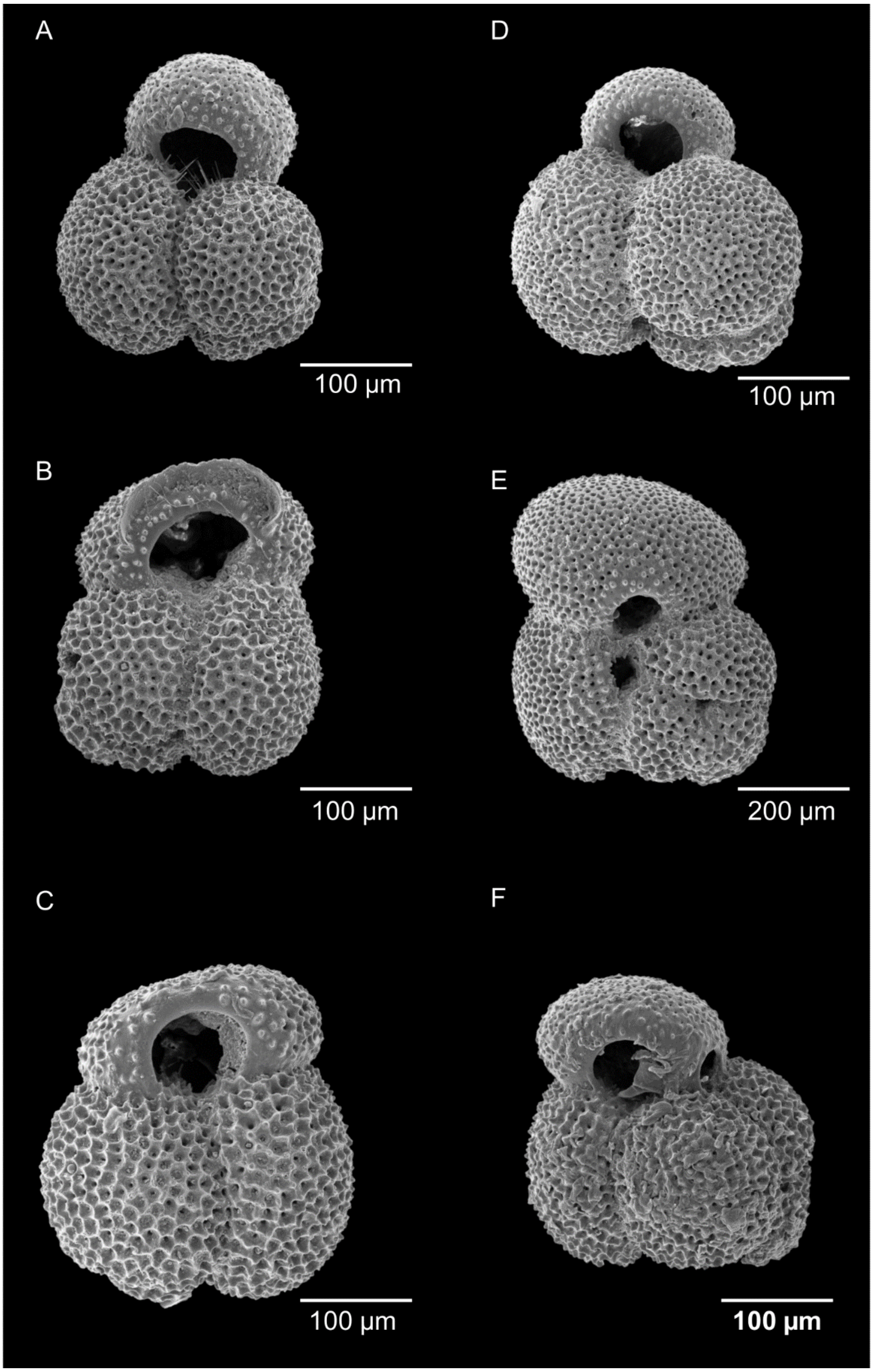

Figure 8 - Specimens of the *G. ruber* (w) *sensu lato* picked from samples of this study. It is possible to observe the morphometric variances between them.

The *G. truncatulinoides* (d) were separated into crusted (C) and non-crusted (NC) forms for the Mg/Ca analyses. For this, the tests were observed under a binocular microscope (Figure 13 and Figure 14, respectively, Appendix). This separation was determined because, in other regions, the C and NC test forms have been determined as indicative of calcification at different water depths (e.g., SPEAR et al., 2011; SALMON et al., 2016; REYNOLDS et al., 2018), and because visual discrimination of both forms can be subjective. More information regarding the discrimination of both forms is described on appendix.

2.4.2. Planktonic foraminifera test geochemical analyses

The major elements presented in the foraminifera tests (e.g. Mg and Ca) were determinated at the U.S. Geological Survey, Coastal and Marine Science Center (St. Petersburg, FL, USA), under the supervision of Dr. Julie Richey. For these analyses, ~60 tests of all four foraminifera species were gently crushed and cleaned according to the cleaning procedures by Barker et al. (2003), which consists in the removal of multiple clay minerals, and organic matter that may be attached into/onto the foraminifera tests by an oxidative step, as well as the removal of adsorbed metals by an acid leaching step. After the cleaning procedures, the tests were then analyzed on a Perkin Elmer Optima 7300 dual view inductively coupled plasma-optical emission spectrometer (ICP-OES). Mg/Ca was corrected by using the internal gravimetric standard (IGS) method after Schrag (1999).

To check for removal of clays during the cleaning procedure, samples were monitored for peaks of Fe, Mn, and Al. Although the abundance of these elements in foraminiferal calcite is typically below the detection limits on the ICP-OES, they may be detected in measurable concentrations if contaminants are present. From these elements, it is possible to identify early diagenesis (e.g., Fe and Mn), as well as contamination of clay minerals (e.g., Al). The samples that presented high peaks of one or more of these elements, combined with low or high Ca concentration (i.e., < 5 ug g^{-1} and > 30 ug g^{-1}) were excluded from the statistical analysis (see RICHEY et al., 2012). Sample replicates were performed to measure natural variations among sample aliquots and to analyze precision.

2.4.3. Data analyses and interpretation

Modern SST observations were obtained through satellite images (NASA Ocean Color database). Data of sea temperature and salinity of the water column (0 m, 10 m, 15 m, 20 m and 25 m) was obtained with the World Ocean Atlas 2013 databse (WOA13).

The statistical analysis of the Mg/Ca data were performed on the Past3 software (version 3.8). For all species, it was tested the normality (Shapiro-Wilk) to the identification of outliers through boxplot charts.

To verify if the Mg/Ca-derived SST agrees with observed modern SSTs, the species-specific (SS) equation and the general species (GE) equation developed by Anand et al. (2003) were applied for Mg/Ca ratio for all four foraminifera species. Afterwards, an ANOVA test was performed to determine if the paleotemperature equations result in sea temperature averages similar to modern SSTs gathered by satellitle images and the WOA13 temperatures. A *p*-value of 0.5 (at 95% of confidence) was stablished to accept or reject the null hypothesis (H_0), where, in all cases:

H_0: The averages of the Mg/Ca-SSTs are equal to the temperatures obtained by the satellite and WOA13;

H_1: The averages the Mg/Ca-SSTs are different to the temperatures obtained by the satellite and WOA13.

When the *p*-values from the ANOVA test were lower (greater) than 0.5, the H_0 was rejected (accepted).

2.5. Results

2.5.1. Satellite SSTs and Water Column Temperatures

The Table 18 (Appendix) contains the compiled SSTs both from the Aqua MODIS satellite and the WOA13 for all locations of this study. In summary, the highest temperatures occur in summer, followed by the autumn temperatures. For the satellite images, the SST_{AN} averages 24.5 °C (± 0.29), SST_{AU} shows an average of 25.16 °C (± 0.36), SST_{WI} presents an average of 22.1 °C (± 0.49), SST_{SP} averages 23.22 °C (± 0.36), and SST_{SU} averages 26.4 °C (± 0.18) (Figure 9).

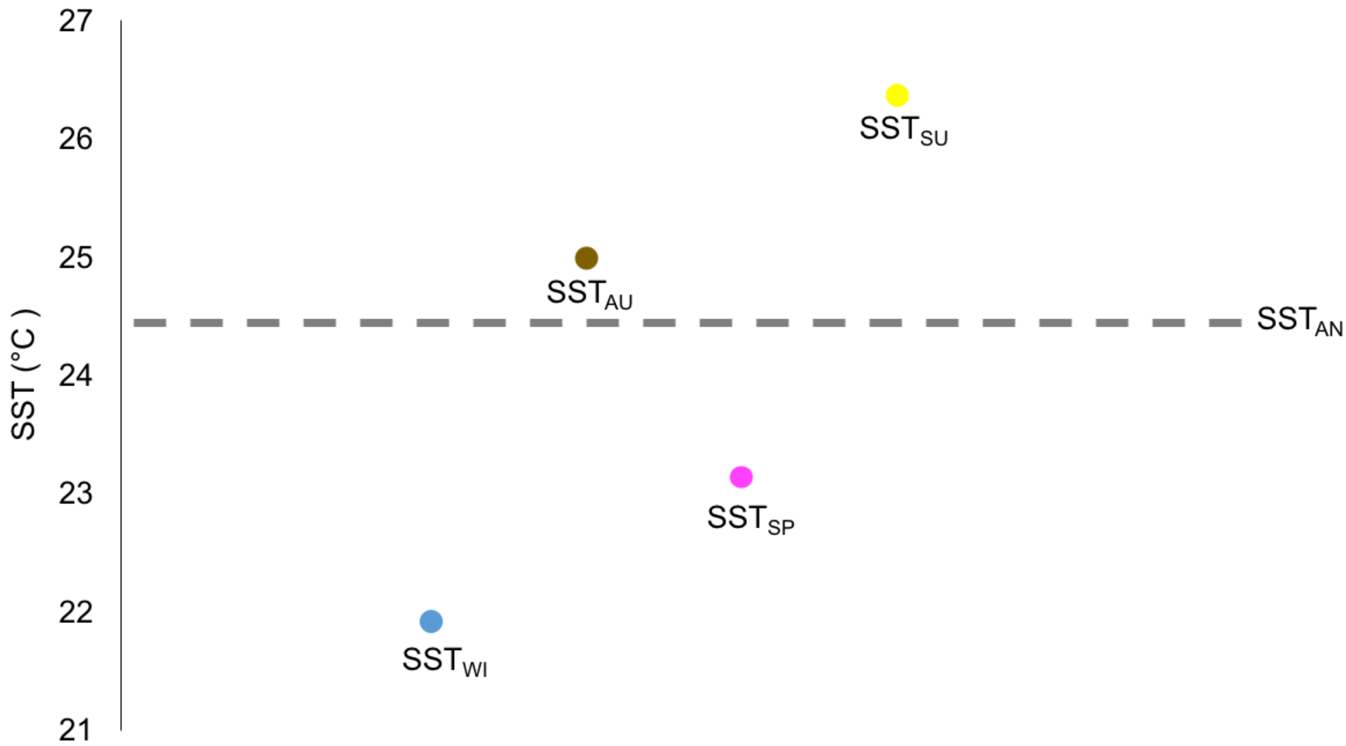

Figure 9 – Averages of the observed modern SST (in °C) gathered from the Aqua MODIS satellite.

The water column temperatures gathered from the WOA13 show lower temperatures than the satellite ones (Table 19, Figure 10). In summary, temperatures at 0 m depth shows higher temperatures than at 25 m depth, where the highest temperature at the surface was during summer (26 °C ± 0.12), and the lowest temperature during winter (21.4 °C ± 0.54), and, at 25 m depth, the highest temperature observed was in winter (16.4 °C ± 0.25), and the lowest was during summer (15.6 °C ± 0.28).

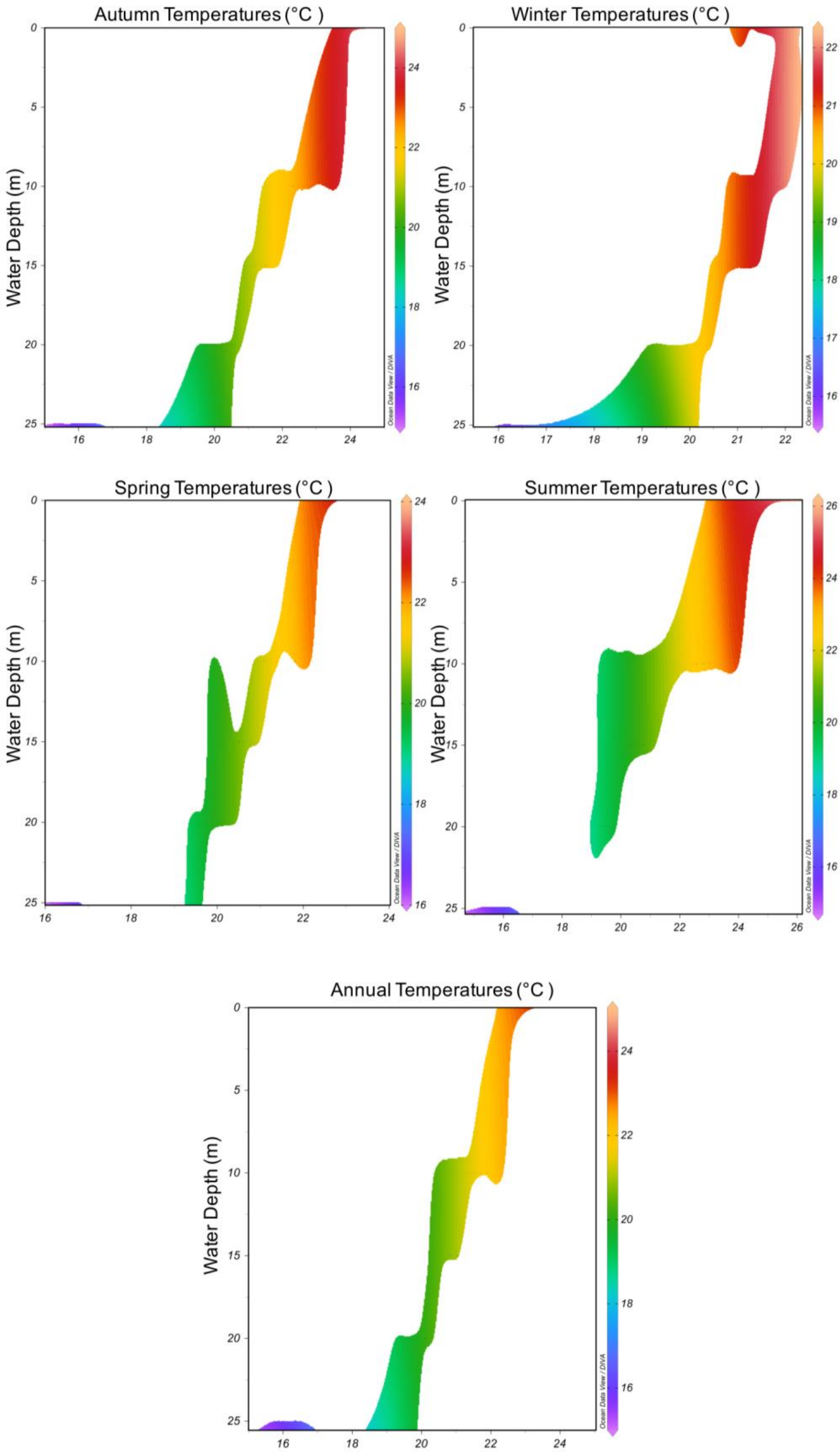

Figure 10 - Temperatures (in °C) of the water column obtained from the WOA13 database.

2.5.2. Elemental Analysis of Planktonic Foraminifera Tests and Statistical Analyses

The raw Mg/Ca data can be found in Table 20 (Appendix). A summary of the results of the ratio for all species of this research can be found in Table 21 (Appendix), as well as in Figure 11.

The Mg/Ca ratio in the *G. inflata* species (300 – 425 µm) averaged 1.78 mmol/mol (± 0.16, n = 10), where the highest value was 2.12 mmol/mol, and the lowest value was 1.53 mmol/mol.

For *G. ruber* (p) within the size fraction of 250 – 300 µm, the Mg/Ca ratio averaged 3.71 mmol/mol (± 0.32, n = 21), with a maximum of 4.42 mmol/mol, and minimum of 3.23 mmol/mol. The tests of the 300 - 355 µm size fraction of *G. ruber* (p) showed an average of 3.95 mmol/mol (± 0.24, n = 23), with a maximum of 4.58 mmol/mol, and a minimum 3.38 mmol/mol.

The *G. ruber* (w) *s.s.* species within the 250 – 300 µm size fraction presented an average of 4.04 mmol/mol (± 0.26, n = 7), ranging from 3.74– 4.49 mmol/mol. For the 300 – 355 µm size fraction, the average was 4.12 mmol/mol (± 0.24, n = 13), and ranged from 3.85–4.76 mmol/mol.

For the *G ruber* (w) *s.l.* species in the size fraction of 250 – 300 µm, the average of Mg/Ca ratio was 3.89 mmol/mol (± 0.29, n = 24), ranging from 3.37 mmol/mol to 4.54 mmol/mol. In the size fraction of 300 – 355 µm, the *G. ruber* (w) *s.l.* show an average of 3.99 mmol/mol (± 0.34, n = 16), where the highest ratio was 4.54 mmol/mol, and the lowest ratio was 3.23 mmol/mol.

The non-crusted type of *G. truncatulinoides* between the size fraction of 380 – 620 µm presented an average of 1.92 mmol/mol (± 0.18, n = 16), ranging from 1.68 mmol/mol to 2.36 mmol/mol. The crusted type of *G. truncatulinoides* (same size fraction) showed an average of 1.94 mmol/mol (± 0.17, n = 14), where the Mg/Ca ranged from 1.63 mmol/mol to 1.63 mmol/mol.

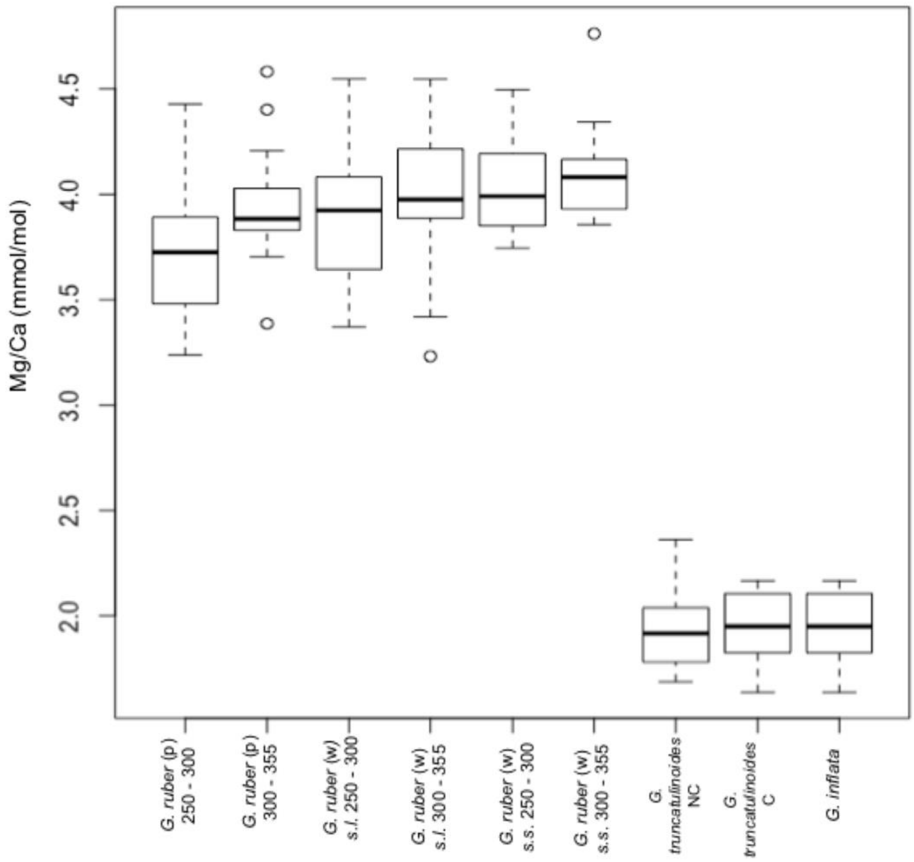

Figure 11 – Boxplot of Mg/Ca ratio from the species that were analyzed in this research project. The species that inhabit the upper water column show higher Mg/Ca ratio, while species that inhabit lower regions of the water column show lower Mg/Ca ratio. The outliers are represented as circles.

The Shapiro-Wilk test suggested that only the *G. ruber* (w) *s.s.* species in the size fraction of 300 – 355 µm does not present normality, even after transforming it into log scale. Therefore, it was chosen to keep the non-transformed data, applying a non-parametric analyses for the interpretations (*p*-value of the Kruskal-Wallis test).

The t-test suggested that the only species that have significantly different statistical means is the *G. ruber* (p), (*p*-value of 0.006), where the size fraction of 300 – 355 µm shows about 0.24 mmol/mol higher than the size fraction of 250 – 300 µm species.

Meanwhile, the other upper water column species do not show difference within their means. The *G. ruber* (w) *s.s.* showed a p-value of 0.51 between the size fractions of 250 – 300 µm and 300 – 355 µm, where the first size fraction has slightly higher Mg/Ca ratio (0.07 mmol/mol). The mean values between the two size fraction of *G. ruber* (w) *s.l.* morphotype also are not significantly different as the p-value of the t-test suggests (*p*-value of 0.30). The size fraction of 300 – 355 µm is slightly higher, showing a 0.10 mmol/mol higher than the 250 – 300 µm size fraction.

The crusted and non-crusted tests of *G. truncatulinoides* (d) species do not show the difference in their means as well (*p*-value of 0.79). Between these two forms, the crusted form has slightly higher Mg/Ca concentration, showing a difference of 0.017 mmol/mol between them.

Between the upper water column species (i.e., all the *G. ruber* species within all size fractions), the Kruskal-Wallis test suggested that there is a significant difference between the averages ($p < 0.05$). On Table 22 it is possible to see the means that are significantly different between the species that inhabit the upper water column fractions.

For the deep-dwelling species, the Kruskal-Wallis test suggested that all the means do not show significant difference within them (*p*-value of 0.95). In fact, the test showed that the *G. inflata* species shows significantly similar Mg/Ca means to the crusted form of *G. truncatulinoides* (d) (*p*-value of 0.98). The *p*-values between these species can be seen in Table 23.

2.5.3. Species-specific (SS) and general species (GE) equations to convert Mg/Ca ratios into SSTs

In Table 24 (Appendix) and Figure 12 displays all the ratio Mg/Ca converted into SSTs for each of the core-top samples from this study. Overall, the SS equations shows higher temperatures than the GE equations. Also, for the *G. ruber* species, the Mg/Ca-derived temperature is higher in the larger test size.

For the *G. ruber* (p) within the size fraction of 250 – 300 µm, when the SS equation is applied, the resulting SST is 24.4°C (± 1.5, n = 21). Meanwhile the GE equation results in 25.3°C (± 1.0, n = 21). The difference between the species-specific to the general species equation is 0.9 °C.

The SS equation for tests within 300 - 355 µm of the *G. ruber* (p) showed an average of 25.21 °C (± 0.91, n = 23), and the GE equations resulted in 26.02

°C (± 0.68, n = 23). The SS and the general species equations for this size fraction has a difference of 0.81 °C of temperature between them. When comparing with the 250 – 300 size fraction, the SS equations show a difference of 0.84 °C, while the GE equations show a difference of 0.72 °C between these two size fractions.

The *G. ruber* (w) *s.s.* species within the size fraction of 250 - 300 µm presented an average of 24.26 °C (± 0.59, n = 7) with the SS equation results. The GE equation shows an average of 26.26 °C (± 0.67, n = 7). The difference of temperature between the SS and the GE for the white *s.s.* in this size fraction is 2 °C.

For the *G. ruber* (w) *s.s.* within size fraction of 300 – 355 µm, when applied the SS equation, it is obtained 25.27 °C (± 0.66, n = 13). The GE results in 26.47 °C (± 0.63). In this size fraction, the difference of temperature between the SS and the GE is 1.19 °C. When comparing with the previous size fraction, the difference between the SS equations is 1.01 °C, and the GE is 0.21 °C.

The calculated average using the SS equation for the *G. ruber* (w) *s.l.* species, 250 – 300 µm size fraction, is 23.86 °C (± 0.74). This species showed a difference of 1.95 °C when the SS and the GE equations are compared.

In the 300 – 355 µm size fraction, the *G. ruber* (w) *s.l.*, the SS equation results in 24.89 °C (± 1.02, n = 16), while the GE equation shows an average of 26.11 °C (± 0.97, n =16). This size fraction showed a difference of 1.21 °C between the two equations applied. Between size fractions, the SS equations have 1.03 °C of difference between them, and 0.29 °C for the GE equations.

The temperature obtained with the SS equation for the *G. inflata* species (300 – 425 µm) averaged 21.42 °C (± 1.56, n = 10). The highest temperature with this equation was 23.34 °C, and the lowest was 18.49 °C. While, the GE equation results in an average of 18.11 °C (± 1.01, n = 10), where the highest temperature was 19.35 °C, and the lowest was 16.23 °C.

The non-crusted type of *G. truncatulinoides*, 380 – 620 µm size fraction, with the SS equation resulted in 18.64 °C (± 1.03, n = 16). The GE equation resulted in 18.01 °C (± 1.03, n = 16). The difference of temperature between the SS and the GE equations estimates for the *G. truncatulinoides* NC is 0.63 °C.

The average calculated after the SS equation for the crusted type of *G. truncatulinoides* (380 – 620 µm) is 18.74 °C (± 0.97), and the GE equation resulted in 18.11 °C (± 0.97, p =14). The difference of temperature between the equations for the *G. truncatulinoides* C is also 0.63 °C. These species showed the lowest difference between the equations for both crusted and non-crusted types, where the SS equations and the GE equations have a difference of 0.11 °C between them.

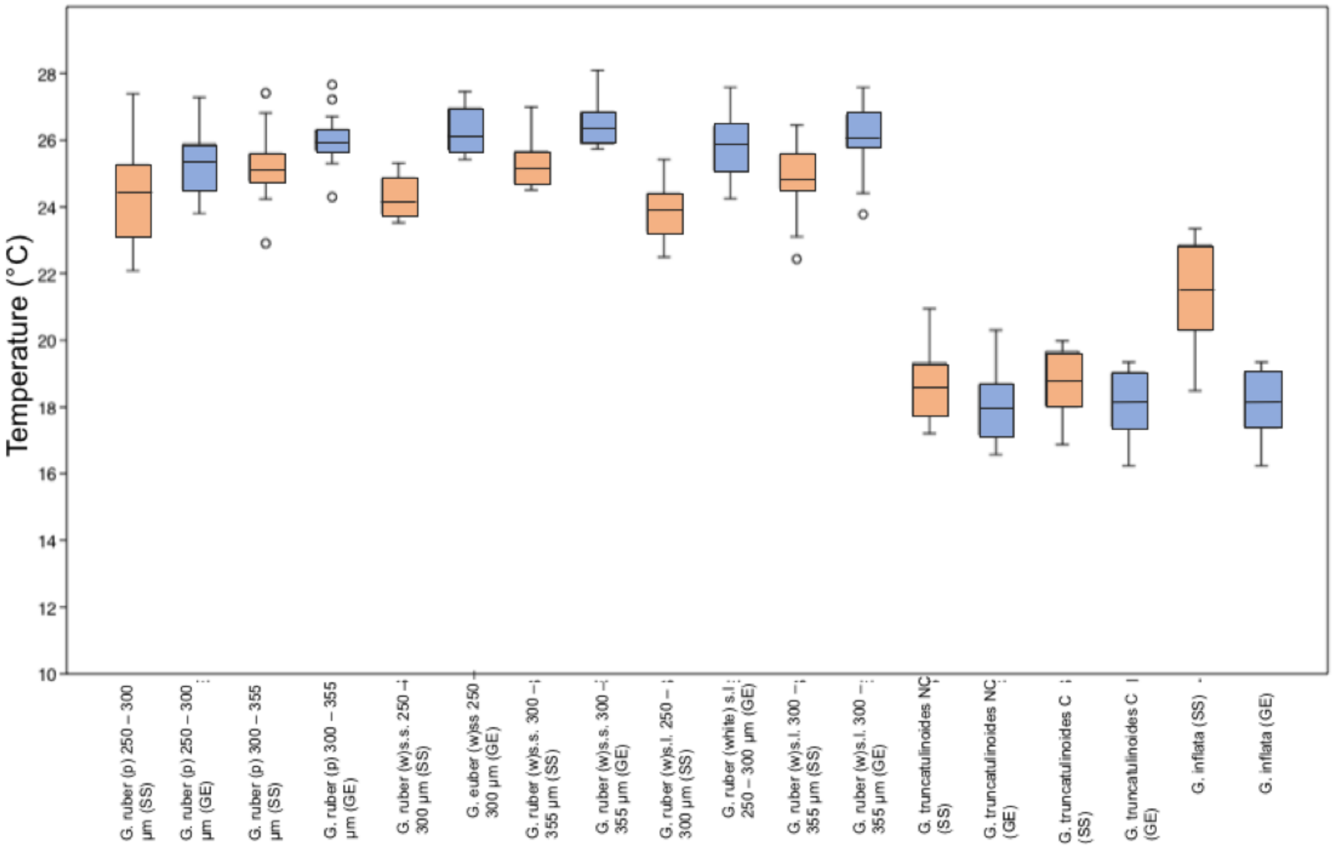

Figure 12 – Boxplot of the calculated SSTs after the Species-Specific (SS; orange boxes) Equation and General Species Equation (GE; blue boxes) for all the species analyzed in this study.

2.5.4. Comparing Mg/Ca based-SSTs to modern ocean temperatures

The differences between the calculated SSTs after the SS and the GE equations of all species analyzed in this study are represented in Figure 12.

The calculated SSTs with the SS equation of the *G. ruber* (p), 250 – 300 µm size fraction, showed significant similarity with SST_{AN} (p-value of 0.81), while the GE equation showed significant similarity with SST_{AU} (p-value of 0.51). The SS equation for *G. ruber* (p), 300 – 355 µm size fraction, tests showed an average significantly similar to SST_{AU} (25.21 °C, ± 0.91, n = 23, p-value of 0.71), while the GE equation results do not show any significant averages with annual or seasonal SST. Yet, its average is 26.02 °C (± 0.68, n = 23, p-value < 0.05), which is close to SST_{SU}.

The *G. ruber* (w) *s.s.*, 250 – 300 µm size fraction, SS equation presented an average significantly similar to the SST_{AN} (p-value of 0.20), while the GE equation results have similar averages to SST_{SU} (p-value of 0.21). Both equations of the *G. ruber* (w) *s.s.*, 300 – 355 µm size fraction, show significant similarities averages with SST_{AN} and SST_{SU}, respectively (p-value of 0.86 and p-value of 0.55). On the other hand, the calculated average using both equations of the *G. ruber* (w) *s.l.*, 250 – 300 µm size fraction, shows no siginficant similar averages to any modern SST. However, both calculated temperatures are still in the modern range of SST (23.86 °C and 25.81 °C, respectively), which are close to SST_{WI} and SST_{AU} temperatures, respectively. For the *G. ruber* (w) *s.l.*, 300 – 355 µm size fraction, the SS equation and the GE equation show significant results with SST_{AU} and SST_{SU}, respectively (p-value of 0.21 for both).

The temperature obtained with the SS equation for the *G. inflata* species (300 – 425 µm) show a strong simlarity with annual SSTs at 10 m depth (p-value of 0.89). The GE equation, however, shows no similarity with any temperature.

The non-crusted type of *G. truncatulinoides*, 380 – 620 µm size fraction, for both equations, shows no significant similar temperature averages. The crusted form shows a weak similarity of temperatures with the SS equation at 20 m on SST_{SU} (p-value of 0.06).

2.6. Discussion

2.6.1. Shallow-dwelling planktonic foraminifera from the SBB core-top samples and their Mg/Ca based-SST estimates

Comparing the core-top Mg/Ca-SSTs with observed temperatures is important to determine how accurately the Mg/Ca proxy reflects local SST (HERTZBERG et al., 2013), and to identify where in the water column the foraminifera calcifies. Overall, the Mg/Ca-inferred SSTs averages obtained in this study showed consistent results when compared to modern SSTs. The results of this study shows that there are differences on the ratio Mg/Ca between the surface and subsurface species.

The data suggest that the SS and the GE equation by Anand et al. (2003) result in different Mg/Ca-SSTs, such that the SS equation results in colder temperatures than the GE equation. Therefore, the discussion will be based on the results that showed the strongest similarities between the Mg/Ca-derived temperatures and the observational temperatures (e.g. highest *p*-values).

Overall, for the *G. ruber* species, the larger size fraction had significantly higher Mg/Ca. Between the two size fractions of the pink form, there is a significantly difference between both averages (0.24 mmol/mol, $p < 0.05$; Table 25). On the other hand, even though in other regions the *G. ruber* (w) seems to have different incorporation of Mg^{+2} in their tests, the data from this study suggests that there is no significant difference on the Mg^{+2} and Ca^{+2} uptake by *G. ruber* (w) morphotypes and their size fractions ($p > 0.05$; Table 25).

Past studies have reported the increase in Mg/Ca with increasing test size for the pink form (RICHEY et al., 2012; FRIEDRICH et al., 2013), as well as the lack of difference in the Mg/Ca content in their white forms without discriminating then into *s.s.* and *s.l*. forms (RICHEY et al., 2012). In general, these studies hypothesize that foraminifera grow larger in warmer waters. Furthermore, the pink forms seem to calcify in shallower/warmer conditions than the white forms, which was also observe previously (e.g. RICHEY et al., 2012). More recently, Richey et al. (2019) stated that the larger tests of *G. ruber* are more abundant in warmer months, and smaller sizes, specially the white form, in colder months. The different test sizes seem to have different seasonal preferences, which may be the reason of the difference between test size and the uptake of Mg/Ca.

Sousa et al. (2014) reported that in their plankton tow off the Brazilian SE continental margin, during summer, the *G. ruber* pink was the most abundant species among the surface-dwelling species, inhabiting the first 20 meters of the water column. The *G. ruber* white species was also present and abundant in the first 20-meter depth, but, in some stations, they found them within 40- to 60-meter depth, and between 80- to 100-m depth. According to these authors, the depth of the mixed layer affects the presence and abundance of both species in the area.

Converting the Mg/Ca into SSTs, the data from this study suggests that the smallest size of the pink form yields SST_{AN} estimates, while the *s.s.* form is more likely to reflect SST_{SU} temperatures. The *s.l.* form, however, did not show any strong similarity with any observational SST, but their results are closely to SST_{WI} temperatures. Within the bigger size fractions, all both pink and *s.s.* form reflect SST_{AU}. The *s.l.,* is high related to both SST_{AU} and SST_{SU} estimates. forms, reflect SST_{SU}.

In this study, the pink form within the biggest size seems to calcifies in 0.7 ± 0.4 °C warmer temperatures than the smallest size. This data that is presented here is consistent when compared to previous studies, where it was observed a significant difference in Mg/Ca-temperatures between the size fractions of the pink form only (RICHEY et al., 2012; FRIEDRICH et al., 2013), where the authors related the increase on temperature estimates with the increase of size to depth where the calcification of the tests takes place, which is influenced or by summer-weighted seasonal distribution or shallower depth habitat.

In general, the *G. ruber* is believed to be a summer-biased species, and the white forms an annual-biased species (KEMLE-VON-MUCKE AND HEMLEBEN, 1999; SCHIEBEL AND HEMLEBEN, 2017), where the *s.l.* type tends to record colder temperatures than the *s.s.* form (WANG, 2000; STEINKE et al., 2005). The results from both WOA13 and the satellite images show the the SST in autumn has warm temperatures, and it is not warmer than summer time only. The largest sizes show strong similarities in temperature averages with the SST_{AU} and SST_{SU}, which agree with previous statements. The white forms also present the increase on Mg/Ca according to shell size, but with no statistically difference between them. Yet, the *s.l.* within the smallest size is the one who derives the lowest temperatures within all shallow species.

Therefore, it is possible to suggest that, in the SBB, the smallest size of the pink forms inhabit the upper water column throughout the year, showing no seasonal preference; the *s.s.* form seems to calcifies in shallower waters, and it is a summer-biased species; the *s.l.* form is a cold-biased species, and it seems to relate more to winter time. The biggest sizes also seem to inhabit shallower waters, and all of them are warm-biased species, especially during autumn.

2.6.2. The Mg/Ca based-temperatures derived from deep-dwelling planktonic foraminifera species in the SBB: What are the *G. inflata* and the *G. truncatulinoides* (d) forms recording in their Mg/Ca content?

The *G. inflata* and the *G. truncatulinoides* (d) are deep-dwelling species (up to 400 m depth; GROENEVELD AND CHIESSI; FRANCO-FRAGAS, 2011), inhabiting greater depths in the water column than the *G. ruber* species (up tp 50 m; SOUSA et al., 2014). Also, the forms crusted and non-crusted of the *G. truncatulinoides* can be used to trace different water depth habits with the crusted forms tending to record colder temperatures than the non-crusted form (e.g. SPEAR et al., 2011; SALMON et al., 2016; REYNOLDS et al., 2018).

The data of this study shows that the *G. inflata* species have high temperature similarities with annual temperatures at 10 m depth (~20 °C) (Table 26). This is very differently from presented by Groeneveld and Chiessi (2011) have found on their core-top samples collected in the South Atlantic (ranging from 8 °S to 49 °S). These authors reported that the *G. inflata* ranges from 8 to 16 °C, and it calcifies ~ 387 m depth, recording permanent thermocline conditions. In the North Atlantic, Cléroux et al. (2007) reported that the *G. inflata* for their core-top samples seem to respond to the base of the thermocline (< 100 m depth), and that these species migrate to deeper waters when temperatures at high depths are above 16 °C.

The data from this study shows great similarities with temperatures in much shallower depths than Groeneveld and Chiessi (2011), but much more similar to what Cléroux et al. (2007) have found. An explanation for the difference between the data from this study to Groeneveld and Chiessi (2011) results is that the samples retrieved in this study come from shallower depths than them.

Groeneveld and Chiessi (2011) retrieved their samples in open water (> 3000 m), and they have a large latitudinal gradient and, therefore, larger temperature gradients as well.

The samples from this study come mainly from the continental slope, which is much shallower. This area is highly influenced by meander and eddies caused by the Brazil Current, which uplifts the SAWC, the colder and nutrient-rich waters to shallower depths (SILVEIRA et al., 2000; CAMPOS, 2000; SILVEIRA et al., 2008). Therefore, in the SBB on continental slope areas, the *G. inflata* seems to record annual temperature conditions at 10 m depth, as well as the influence of the vertical migration of the SAWC to the surface. The data reported in this study agrees with what Cléroux et al. (2007) have reported to the North Atlantic.

The *G. truncatulinoides* (d) forms do not show any statistically differences on Mg/Ca in their tests. There is no difference as well when comparing the ratio from the *G. inflata* species to both C and NC forms of the *G. truncatulinoides* (d). Even though only the C form shows a weak similarity with summer temperatures at 20 m depth, the NC form does not show averages too different from the crusted form.

Cléroux et al. (2008) found that the *G. truncatulinoides* and the *G. inflata* have similar calcifying depth preference. The data from this study shows that the difference of temperatures between both species is ~2 °C. In addition, both forms seem to fit in the SACW thermal structure (SILVEIRA, 2000).

The NC form is closely related to annual temperatures at 20 m depth, while the C form is weakly related to the summer temperatures at 20 m. The difference between both forms have been discussed in previous studies (SPEAR et al., 2011; SALMON et al., 2016; REYNOLDS et al., 2018). In this study, the Mg/Ca and temperatures are not statistically different from both forms. However, the NC seems to calcify in different conditions than the C form. The Figure 15 shows how related all the foraminifera analyzed in this study are to one another. Clearly the NC form fits into the surface species component (from here called warm-biased component), while the C and the *G. inflata* fit the second component (cold-biased component).

The same trend has been reported by other studies in different areas. Spear et al. (2011) analyzed the geochemical signs of *G. truncatulinoides* in the northern Gulf of Mexico, and they found that the C forms calcify in deeper and cooler waters, whereas the NC forms record winter mixed layer conditions. Salmon et al. (2016) noticed that in the Sargasso Sea, the C forms in their samples calcifies in much deeper depths throughout winter, and that the NC in calcifies surface waters, even at 0 m depth. Reynolds et al. (2018) used tests from sediment traps, and they also observed the different geochemical signals between both forms.

All these authors related their results to the ontogeny and life cycle of the *G. truncatulinoides* forms, where, as the test becomes more matures, it migrates to deeper waters and evolves a secondary crust (encrustation) around the test with a different chemistry composition.

In this study, the Mg/Ca ratios and temperatures are not statistically different from both forms. However, the *G. truncatulinoides* (d) NC form seems to calcify in different conditions than the *G. truncatulinoides* (d) C form. The *G. truncatulinoides* (d) NC form clearly fits into the surface species component (from here called warm-biased component), while the *G. truncatulinoides* (d) C and the *G. inflata* fit the second component (cold-biased component). Additionally, the *G. inflata* and both forms of the *G. truncatulinoides* (d) seem to reflect the SACW intrusion into the photic zone. The *G. inflata* and the *G. truncatulinoides* (d) C form seem to prefer to inhabit the thermal layer of the SACW, since their signals fits exactly in these temperatures (~16 °C), and the *G. truncatulinoides* (d) NC, seems to inhabit the upper base of the SACW (~18 °C), once it fits in-between surface and subsurface-dwelling species.

In summary, the *G. inflata* and the *G. truncatulinoides* (d) tests in this study can be used to trace the vertical variation of the SACW in the SBB, especially the *G. truncatulinoides* (d) C form. The *G. truncatulinoides* (d) NC form seems to inhabit depths quite shallower than the C form.

2.7. Final Considerations

The Mg/Ca based-temperatures derived from all the planktonic foraminifera species (*G. ruber* (p), *G. ruber* (w) *s.s.*, *G. ruber* (s) *s.l.*, *G. truncatulinoides* (d) and *G. inflata*) analyzed in this study agree well with modern ocean temperatures. Our data suggests that in in different size fractions the tested species respond differently to the most used species-specific and general species paleotemperature equations. Therefore, in order to improve the accuracy of future SST reconstructions, it is suggested to analyze what equation fits better in the area of the interest.

In the SBB, the most suitable equation for the *G. ruber* (p) species, in both the 250 - 300 µm and 300 - 355 µm size fractions, is the species-specific equation. Using this equation, the *G. ruber* (p) tests in the smallest size fraction reflect mean SST_{AN} conditions, while in largest size fraction tests reflect SST_{AU}. The Mg/Ca based-SST estimates derived from the 250 - 300 µm size fraction *G. ruber* (w) *s.s.* tests show significant results with modern SST_{SU} at 0 m, when the GE equation is applied, while for the 300 - 355 µm size fraction, the SS equation reflects SST_{AU} at 0 m. For the *G. ruber* (w) *s.l.* only the largest size fraction (300 - 355 µm) tests present similarity with modern ocean SST, and both equations reflect SST_{AU} and SST_{SU} conditions at 0 m; the smallest size fraction in this *G. ruber* (w) morphotype can be used to trace cold-seasons, especially SST_{WI} at 0 m.

The deep-dwelling species studies seem to reflect the uplift of the SACW into the surface waters in the SBB. The *G. inflata* apparently calcifies at 10 m water depth, and it can be used to trace the upwelling of the SACW, while the *G. truncatulinoides* (d) C form records the downwelling of the SACW during autumn (~20 m water depth), and the *G. truncatulinoides* (d) NC form records mean annual temperature in deeper water conditions.

This is the first study to report Mg/Ca ratios in surface-dwelling (*G. ruber*) and deep-dwelling (*G. inflata* and *G. truncatulinoides* (d)) planktonic foraminifera tests obtained in core-top samples in the SBB. This validation of the planktonic foraminifera Mg/Ca ratio conversion to temperature SS and GE equations for the surface-dwelling (*G. ruber*), and deep-dwelling (*G. inflata* and *G. truncatulinoides* (d) species in the SBB, will help to improve the accuracy of future temperature reconstructions in the area. Also, to evaluate the suggestions made by this study, it is recommended to perform sediment trap analyses along the SBB.

3. Appendix

3.1. The discrimination of the G. truncatulinoides (d) Crusted and Non-crusted forms

G. truncatulinoides (d) were discriminated into crusted (C) and non-crusted (NC) forms for the Mg/Ca analyzes. For this, the tests were observed under a binocular microscope. This separation was determined because, in other regions, the C and NC test forms have been determined to calcify at different water depths (e.g., SPEAR et al., 2011; SALMON et al., 2016; REYNOLDS et al., 2018), and because visual discrimination of both forms can be subjective.

Once the C and NC tests were separated, every single NC test was measured across the diameter of the umbilical side, from the tip of the final chamber to the opposite side, as described by Reynolds et al. (2018) (Figure 13). After taking notes of the NC test lengths, they were individually weighed on a microbalance. This test was performed to observe if the C and NC *G. truncatulinoides* (d) tests have a distinct exponential length-weight relationship, as observed by Reynolds et al. (2018) in the Gulf of Mexico, where the NC tests are mostly lighter than the C tests. It is important to highlight that only a few C tests were measured and weighed after the first test with the NC tests.

Electron images of a few tests of the discriminated C and NC forms were taken at the Electron Microscopy Laboratory at the University of South Florida, St. Petersburg (USFSP), in St. Petersburg, FL (USA) (Figure 14).

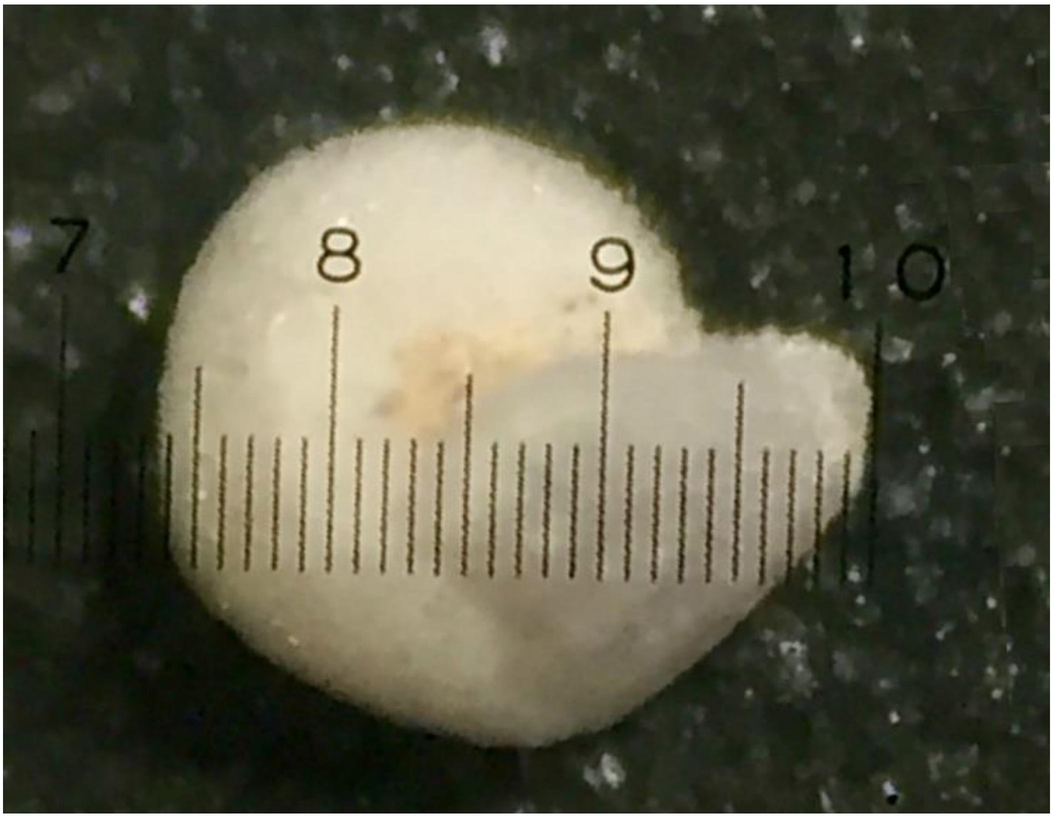

Figure 13 – Specimen of *G. truncatulinoides* (d) being measured under a binocular microscope. The scale was calibrated as every single mark equals to 20 µm.

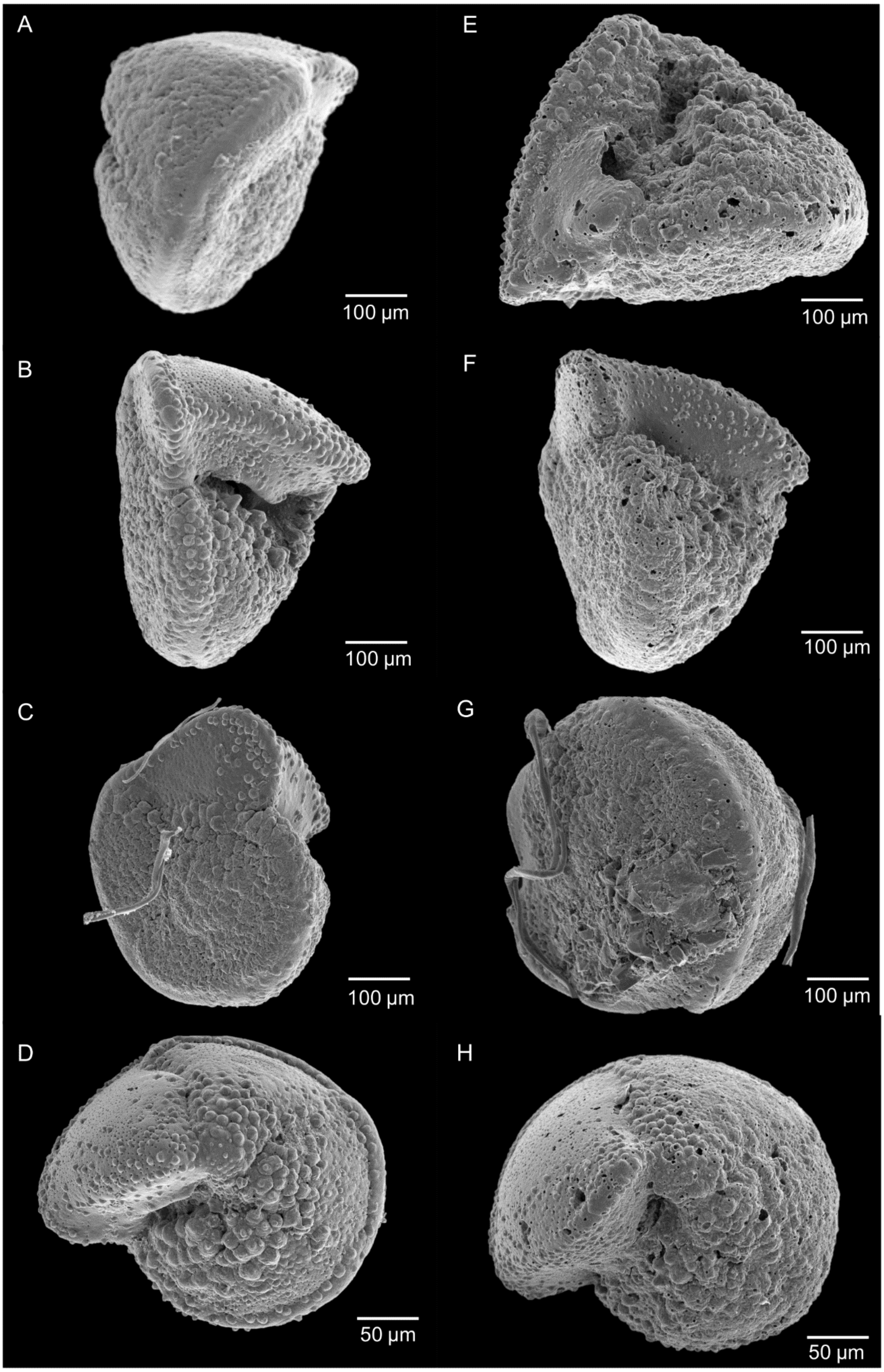

Figure 14 – Specimens of the *G. truncatulinoides* (d) picked from samples of this study. The Figure 14A to 14D are tests that were considered non-crusted under the microscope. The Figure 14E to 14H are tests that were considered crusted morphotypes under the microscope.

3.1.2 Distinction of Crusted from Non-crusted forms of *G. truncatulinoides* (d)

A general look of the data of the results of this methodology can be seen in Figure 15.

The NC tests of *G. truncatulinoides* (d) species in the 300 – 355 µm size fraction showed a mean length of 474 µm (± 37.32, n = 359), ranging from 380 µm to 560 µm. The mean weight of the tests within this size fraction was 36.93 µg (± 9.52, n = 359), as the lightest test weighed 12.5 µg and the heaviest test weighed 61.6 µg.

The NC tests of the size fraction between 355 – 425 µm presented a mean of 540 µm in their length (± 40.66, n = 202), where the test with the largest length measured 620 µm and the smallest test measured 400 µm. The weight of this size fraction showed a mean of 52.82 µg (± 10.88, n = 202), where the lightest test weighed 22.7 µg, and the heaviest test weighed 78.2 µg.

In the size fraction of 380 – 620 µm, the length average was 498.32 µm (± 46.67, n = 561), as the smallest length was 380 µm and the biggest was 620 µm. The weight in this size fraction means 42.65 µg (± 12.60, n = 561), as the lightest test weighted 12.5 µg and the heaviest weighted 78.2 µg.

For the C forms, the length ranged from 420 µm to 580 µm (± 48.26, n = 24), and the weight ranged from 23 µg to 68.2 µg (± 12.22, n = 24).

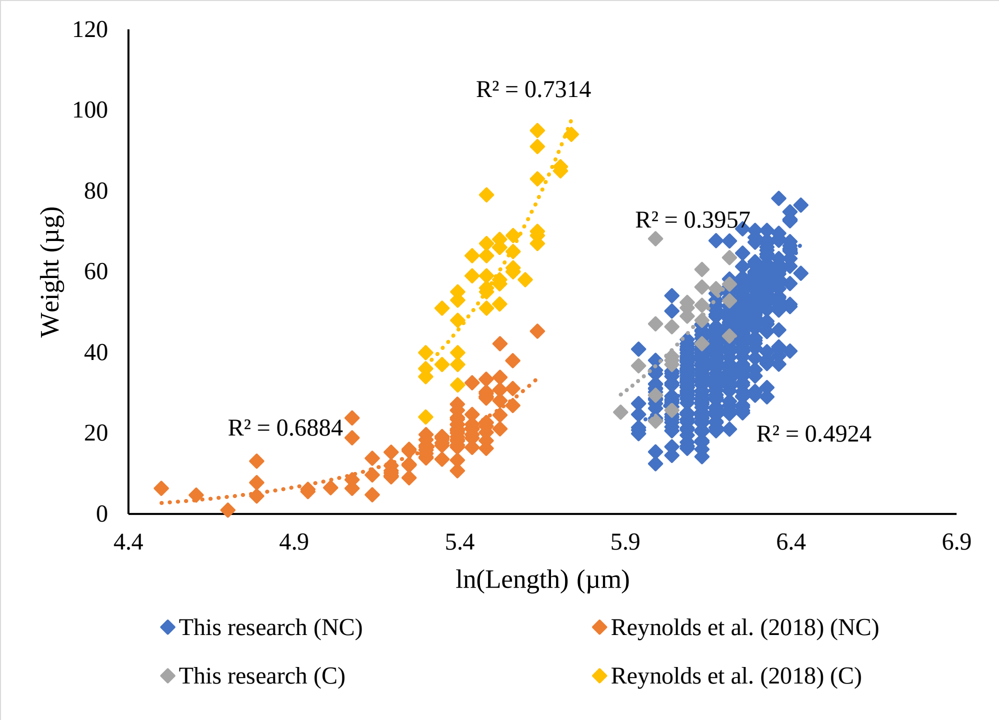

Figure 15 – Scatter plot of the length-weight relationship between the crusted (C) and non-crusted (NC) tests of *G. truncatulinoides* (d) of this research and from Reynolds et al. (2018). Besides presenting a low correlation between length and weight, the tests of this research project are located between the division of the C and NC tests observed by Reynolds et al. (2018). Consequently, the length-weight relationship cannot be applied to separate the C from NC tests in this research.

The NC tests of *G. truncatulinoides* (d) do not present a significant difference between the both sieved size fractions ($p > 0.5$). For this reason, the tests were placed as a single size fraction (300 – 425 µm), corresponding to the smallest test length to the largest length (380 – 620 µm) measured. Once it was decided to assemble the tests of *G. truncatulinoides* (d) in one size fraction (300 – 425 µm), a batch of crusted tests form (C) (n = 24) was also measured and weighed to observe the length-weight relationship between the tests.

3.1.3. The lack of difference of length-weight between the crusted and non-crusted forms of *G. truncatulinoides* (d)

The NC and the C tests of this research settle in the middle range of the NC and C tests found by Reynolds et al. (2018) (Figure 15). The length-weight correlation of C and NC tests found in this research are considerably low, where the R^2 of NC length-weight was 0.49, and the R^2 of C length-weight was 0.39.

Reynolds et al. (2018) found a high length-weight correlation between their *G. truncatulinoides* (d) C and NC tests (R^2 = 0.73 and R^2 = 0.68, respectively), which makes possible to differentiate the C and NC mathematically, avoiding visual errors.

This high correlation observed in this study may be linked to the fact that Reynolds et al. (2018) picked the most extreme examples of C and NC tests that were collected with a sediment trap and preserved in formalin. Thus, their tests have not sunk into the bottom of the ocean, and, consequently, they did not undergo any type of post-depositional process.

Apparently, in the SBB, the C and NC tests may have more aggregated material (such as crust and clay minerals) in their structures, as they sank into the bottom, which makes difficult to separate the C from NC tests as Reynolds et al. (2018) had performed. Differently than Reynolds et al. (2018), the samples of this research come from core-tops retrieved with a multiple-corer. These aggregate material can be a result of the long exposure of the sediments with the sediment-water interface, since the sedimentation rates in the SBB are lower than 2 to 68 cm. kyr^{-1} (MAHIQUES et al., 2011). As a consequence, we conclude that these metrics derived from sediment-trap samples may not be applicable in marine sediments.

The *G. truncatulinoides* (d) tests for this research were, then, visually separated as C and NC under a binocular microscope taking as a reference to distinct them the color, brightness, opacity and the presence or absence of crust around the tests.

Therefore, it is suggested that in the SBB, for paleoceanographic studies using post-depositional material, to segregate the C and NC forms of the *G. truncatulinoides* species should be performed under a visual separation instead of the mathematical way, since the tests do not agree well with the length-weight relationship.

3.2 Data analyzed in this study

The following tables contain the dataset that was used for the construction and analysis of this research project.

Table 1 – Identification of the research projects, location, and water depth (m) of the oceanographic stations from where the samples were retrieved.

Project	Station	Latitude (°S)	Longitude (°W)	Water depth (m)
GEO	NAP62-2	24.042	44.542	121
GEO	NAP63-2	24.840	44.319	840
GEO	NAP64-2	24.632	44.494	302
GEO	NAP66-2	25.605	45.104	368
GEO	NAP68-2	25.792	45.022	1393
PM	249	26.804	46.399	430
PM	250	26.825	46.406	440
PM	253	26.245	45.682	731
PM	254	26.261	45.712	747
PM	255	26.494	45.969	652
PM	256	26.447	45.968	569
PM	257	26.426	45.954	698
PM	258	26.534	46.080	543
PM	259	26.562	46.116	559
PM	260	26.561	46.124	517
PM	262	26.848	46.423	402
PM	263	26.885	46.415	477
PM	264	26.855	46.404	458
PM	265	24.671	44.081	818
PM	266	24.629	44.020	847
PM	267	24.553	43.920	805
CNT	311	24.451	44.216	432
CNT	312	24.748	44.861	1337
CNT	313	24.793	43.636	1557
CNT	314	24.738	43.690	1517

Table 2 – Values of the alkenones unsaturation index ($U^{K'}_{37}$), as well as the Sea Surface Temperatures (SST) gathered from the Aqua MODIS mission.

Station	$U^{K'}_{37}$	SST_{AN} (°C)	SST_{AU} (°C)	SST_{WI} (°C)	SST_{SP} (°C)	SST_{SU} (°C)
NAP61_2	0.826	24.23	24.67	21.48	22.84	26.57
NAP62_2	0.804	24.24	24.43	21.63	22.76	26.00
NAP63_2	0.885	24.94	25.70	22.81	23.60	26.68
NAP64_2	0.870	24.84	25.42	22.49	23.50	26.41
NAP66_2	0.834	24.13	24.43	21.41	22.77	26.08
NAP67_2	0.850	24.71	25.32	22.37	23.46	26.40
NAP68_2	0.880	24.68	25.49	22.63	23.51	26.53
249	0.863	24.33	24.99	21.82	22.94	26.39
250	0.869	24.33	24.99	21.82	22.94	26.39
253	0.895	24.39	25.18	21.90	23.05	26.54
254	0.834	24.39	25.12	21.91	23.07	26.52
255	0.851	24.33	25.04	21.77	23.03	26.49
256	0.895	24.29	25.04	21.75	23.05	26.46
257	0.895	24.30	25.06	21.75	23.00	26.45
258	0.886	24.40	25.03	21.74	23.01	26.47
259	0.868	24.35	25.00	21.84	23.02	26.46
260	0.811	24.35	25.00	21.84	23.02	26.46
262	0.902	24.26	24.99	21.81	23.00	26.38
263	0.846	24.36	25.07	21.90	23.03	26.43
264	0.863	24.34	25.05	21.86	22.96	26.43
265	0.871	25.00	25.67	22.90	23.77	26.66
266	0.859	25.05	25.65	22.90	23.75	26.63
267	0.889	24.98	25.64	22.91	23.83	26.51
311	0.854	24.72	25.41	22.43	23.31	26.27
312_1	0.877	24.45	24.76	21.92	23.22	26.16
312	0.870	24.45	24.76	21.92	23.22	26.16
313	0.872	24.98	25.69	22.92	23.63	26.73
314	0.887	24.95	25.62	22.94	23.66	26.68
7608	0.869	24.05	24.41	21.24	22.74	26.23
7609	0.858	24.13	24.44	21.40	22.82	26.25
7610	0.818	23.89	24.06	20.36	22.67	26.42
7611	0.824	23.94	24.25	20.60	22.74	26.27
7612	0.852	24.18	24.24	20.77	22.78	26.43
7613	0.818	24.02	24.20	20.83	22.69	26.22
7615	0.824	23.98	24.18	21.14	22.75	26.11
7616	0.831	23.92	24.26	20.93	22.65	26.15
7617	0.875	24.24	24.43	21.63	22.76	26.00
7618	0.865	24.77	25.44	22.65	23.32	26.28
7619	0.926	24.79	25.57	22.76	23.42	26.32

7621	0.879	24.54	25.41	22.46	23.20	26.06
7622	0.920	24.85	25.53	22.68	23.47	26.24
7623	0.909	24.81	25.48	22.52	23.46	26.26
2105-3	0.863	24.06	24.57	21.10	23.11	26.28
2106-1	0.859	24.40	24.96	21.84	23.34	26.36
2107-5	0.845	24.43	24.99	21.81	23.37	26.36
Average	0.860	24.44	24.99	21.91	23.14	26.37
STD	±0.02	±0.27	±0.39	±0.52	±0.28	±0.15
Min	0.804	23.89	24.06	20.36	22.65	26.00
Max	0.926	25.05	25.70	22.94	23.83	26.73

Table 3 – Alkenones Total Concentration (ng/g) from samples analyzed in this study and from previous published data.

Station	Total Concentration (ng/g) (C37- Alkenones)
NAP61_2	0.43
NAP62_2	0.92
NAP63_2	0.57
NAP64_2	0.17
NAP66_2	0.47
NAP67_2	0.43
NAP68_2	0.27
249	0.11
250	0.09
253	0.10
254	0.18
255	0.15
256	0.04
257	0.09
258	0.05
259	0.08
260	0.16
262	0.04
263	0.12
264	0.10
265	0.04
266	0.06
267	0.05
311	0.40
312_1	0.40
312	0.42
313	0.29
314	0.43
7608	0.08
7609	0.10
7610	0.36
7611	0.20
7612	0.37
7613	0.14
7615	0.40
7616	0.42
7617	0.24
7618	0.14
7619	0.08
7621	0.05
7622	0.24
7623	0.12
Average	0.23

STD	0.19
Min	0.04
Max	0.92

Table 4 – Summary of the alkenones unsaturation index ($U^{K'}_{37}$) and the seasonal and annual sea surface temperatures (in °C) gathered from the Aqua MODIS satellite.

	$U^{K'}_{37}$	SST_{AN}	SST_{AU}	SST_{WI}	SST_{SP}	SST_{SU}
Average	0.860	24.44	24.99	21.91	23.14	26.37
STD	±0.02	±0.27	±0.39	±0.52	±0.28	±0.15
Min	0.804	23.89	24.06	20.36	22.65	26.00
Max	0.926	25.05	25.70	22.94	23.83	26.73

Table 5 – Sea temperatures (°C) of the water column (in meters) obtained after the World Ocean Atlas (WOA13).

	Water depth (m) – Annual sea temperature (°C)					**Water depth (m) – Winter sea temperature (°C)**					**Water depth (m) – Autumn sea temperature (°C)**					**Water depth (m) – Spring sea temperature (°C)**					**Water depth (m) – Summer sea temperature (°C)**				
Station	**0**	**10**	**15**	**20**	**25**	**0**	**10**	**15**	**20**	**25**	**0**	**10**	**15**	**20**	**25**	**0**	**10**	**15**	**20**	**25**	**0**	**10**	**15**	**20**	**25**
NAP61_2	NaN	NaN	NaN	NaN	NaN	NaN	NaN	NaN	NaN	NaN	NaN	NaN	NaN	NaN	NaN	NaN	NaN	NaN	NaN	NaN	NaN	NaN	NaN	NaN	NaN
NAP62_2	23.97	21.57	21.06	19.52	NaN	22.05	21.36	21.15	19.49	NaN	24.52	22.6	21.53	19.66	NaN	23.26	21.07	20.8	19.71	NaN	26.06	19.41	20.75	19.23	NaN
NAP63_2	23.97	21.57	21.06	19.52	16.49	22.05	21.36	21.15	19.49	16.65	24.52	22.6	21.53	19.66	16.58	23.26	21.07	20.8	19.71	16.49	26.06	22.6	20.75	19.23	16.24
NAP64_2	23.97	21.57	21.06	19.52	16.13	22.05	21.36	21.15	19.49	16.23	24.52	22.6	21.53	19.66	16.2	23.26	21.07	20.8	19.71	16.16	26.06	21.89	20.75	19.23	15.92
NAP66_2	23.78	20.33	NaN	NaN	NaN	21.64	20.75	NaN	NaN	NaN	24.15	21.39	NaN	NaN	NaN	23.12	19.82	NaN	NaN	NaN	26.21	19.24	NaN	NaN	NaN
NAP67_2	23.64	21.31	20.77	20.13	NaN	21.42	21.11	20.9	20.13	NaN	23.97	22.29	21.36	20.39	NaN	23.04	20.85	20.51	20.48	NaN	26.13	22.26	20.32	19.54	NaN
NAP68_2	23.64	21.31	20.77	20.13	16.51	21.42	21.11	20.9	20.13	16.94	23.97	22.29	21.36	20.39	16.27	23.04	20.85	20.51	20.48	16.82	26.13	22.84	20.32	19.54	15.99
249	23.34	21.47	20.22	20.1	15.76	20.84	20.99	20.61	20.35	16.37	23.51	22.32	20.86	20.57	15.27	22.93	21.13	19.78	20.08	16.07	26.07	22.81	19.64	19.39	15.31
250	23.34	21.47	20.22	20.1	15.76	20.84	20.99	20.61	20.35	16.37	23.51	22.32	20.86	20.57	15.27	22.93	21.13	19.78	20.08	16.07	26.07	22.81	19.64	19.39	15.31
253	23.45	21.89	20.83	20.33	16.26	21.2	21.17	20.79	20.44	16.8	23.8	22.84	21.48	20.78	15.9	22.83	21.39	20.52	20.34	16.53	25.94	22.43	20.54	19.76	15.82
254	23.45	21.89	20.83	20.33	16.32	21.2	21.17	20.79	20.44	16.81	23.8	22.84	21.48	20.78	15.84	22.83	21.39	20.52	20.34	16.72	25.94	23.03	20.54	19.76	15.92
255	23.45	21.89	20.83	20.33	15.98	21.2	21.17	20.79	20.44	16.59	23.8	22.84	21.48	20.78	15.46	22.83	21.39	20.52	20.34	16.27	25.94	22.59	20.54	19.76	15.58
256	23.45	21.89	20.83	20.33	15.98	21.2	21.17	20.79	20.44	16.59	23.8	22.84	21.48	20.78	15.46	22.83	21.39	20.52	20.34	16.27	25.94	22.59	20.54	19.76	15.58
257	23.45	21.89	20.83	20.33	15.98	21.2	21.17	20.79	20.44	16.59	23.8	22.84	21.48	20.78	15.46	22.83	21.39	20.52	20.34	16.27	25.94	22.59	20.54	19.76	15.58
258	23.34	21.47	20.22	20.1	15.82	20.84	20.99	20.61	20.35	16.46	23.51	22.32	20.86	20.57	15.3	22.93	21.13	19.78	20.08	16.12	26.07	22.73	19.64	19.39	15.4
259	23.34	21.47	20.22	20.1	15.82	20.84	20.99	20.61	20.35	16.46	23.51	22.32	20.86	20.57	15.3	22.93	21.13	19.78	20.08	16.12	26.07	22.73	19.64	19.39	15.4
260	23.34	21.47	20.22	20.1	15.82	20.84	20.99	20.61	20.35	16.46	23.51	22.32	20.86	20.57	15.3	22.93	21.13	19.78	20.08	16.12	26.07	22.73	19.64	19.39	15.4
262	23.34	21.47	20.22	20.1	15.76	20.84	20.99	20.61	20.35	16.37	23.51	22.32	20.86	20.57	15.27	22.93	21.13	19.78	20.08	16.07	26.07	22.81	19.64	19.39	15.31
263	23.34	21.47	20.22	20.1	15.76	20.84	20.99	20.61	20.35	16.37	23.51	22.32	20.86	20.57	15.27	22.93	21.13	19.78	20.08	16.07	26.07	22.81	19.64	19.39	15.31
264	23.34	21.47	20.22	20.1	15.76	20.84	20.99	20.61	20.35	16.37	23.51	22.32	20.86	20.57	15.27	22.93	21.13	19.78	20.08	16.07	26.07	22.81	19.64	19.39	15.31
311	23.98	21.57	21.06	19.52	NaN	22.05	21.36	21.15	19.49	NaN	24.52	22.6	21.53	19.66	NaN	23.26	21.07	20.8	19.71	NaN	26.06	21.67	20.75	19.23	NaN
312_1	23.98	21.57	21.06	19.52	NaN	22.05	21.36	21.15	19.49	NaN	24.52	22.6	21.53	19.66	NaN	23.26	21.07	20.8	19.71	NaN	26.06	20.24	20.75	19.23	NaN
312	23.98	21.57	21.06	19.52	NaN	22.05	21.36	21.15	19.49	NaN	24.52	22.6	21.53	19.66	NaN	23.26	21.07	20.8	19.71	NaN	26.06	20.24	20.75	19.23	NaN
313	23.82	21.71	20.59	19.23	16.4	22.02	21.17	20.42	19.11	16.5	24.46	22.8	21.15	19.49	16.49	23.09	21.07	20.35	19.33	16.6	25.70	24.02	20.42	18.99	16.03

314	23.82	21.71	20.59	19.23	16	22.02	21.17	20.42	19.11	16.06	24.46	22.8	21.15	19.49	16.12	23.09	21.07	20.35	19.33	16.18	25.70	23.37	20.42	18.99	15.64
7608	23.54	20.94	19.32	NaN	NaN	21.05	21.09	19.78	NaN	NaN	23.6	21.79	19.76	NaN	NaN	23.15	20.64	19.01	NaN	NaN	26.35	20.56	18.71	NaN	NaN
7609	23.34	21.47	20.22	20.1	15.31	20.84	20.99	20.61	20.35	16.2	23.51	22.32	20.86	20.57	14.82	22.93	21.13	19.78	20.08	15.38	26.07	21.37	19.64	19.39	14.83
7610	23.54	20.94	19.32	NaN	NaN	21.05	21.09	19.78	NaN	NaN	23.6	21.79	19.76	NaN	NaN	23.15	20.64	19.01	NaN	NaN	26.35	18.58	18.71	NaN	NaN
7611	23.54	20.94	19.32	NaN	NaN	21.05	21.09	19.78	NaN	NaN	23.6	21.79	19.76	NaN	NaN	23.15	20.64	19.01	NaN	NaN	26.35	19.08	18.71	NaN	NaN
7612	NaN	NaN	NaN	NaN	NaN	NaN	NaN	NaN	NaN	NaN	NaN	NaN	NaN	NaN	NaN	NaN	NaN	NaN	NaN	NaN	NaN	15.43	NaN	NaN	NaN
7613	23.78	20.33	NaN	NaN	NaN	21.64	20.75	NaN	NaN	NaN	24.15	21.39	NaN	NaN	NaN	23.12	19.82	NaN	NaN	NaN	26.21	17.28	NaN	NaN	NaN
7615	23.64	21.31	20.77	20.13	NaN	21.42	21.11	20.9	20.13	NaN	23.97	22.29	21.36	20.39	NaN	23.04	20.85	20.51	20.48	NaN	26.13	20.8	20.32	19.54	NaN
7616	23.64	21.31	20.77	20.13	NaN	21.42	21.11	20.9	20.13	NaN	23.97	22.29	21.36	20.39	NaN	23.04	20.85	20.51	20.48	NaN	26.13	19.1	20.32	19.54	NaN
7617	23.98	21.57	21.06	19.52	NaN	22.05	21.36	21.15	19.49	NaN	24.52	22.6	21.53	19.66	NaN	23.26	21.07	20.8	19.71	NaN	26.06	19.41	20.75	19.23	NaN
7618	23.91	21.64	20.07	18.79	NaN	22.35	21.06	19.78	18.51	NaN	24.59	22.65	20.58	19.05	NaN	23.32	21.26	19.95	18.92	NaN	25.36	21.14	19.97	18.66	NaN
7619	23.91	21.64	20.07	18.79	NaN	22.35	21.06	19.78	18.51	NaN	24.59	22.65	20.58	19.05	NaN	23.32	21.26	19.95	18.92	NaN	25.36	21.14	19.97	18.66	NaN
7621	24.32	22.73	21.36	20.31	NaN	22.7	21.77	20.86	20.02	NaN	24.98	23.62	21.98	20.71	NaN	23.82	22.45	21.28	20.47	NaN	25.77	21.37	21.31	20.03	NaN
7622	23.82	21.71	20.59	19.23	15.59	22.02	21.17	20.42	19.11	15.67	24.46	22.8	21.15	19.49	15.72	23.09	21.17	20.35	19.33	15.74	25.70	22.53	20.42	18.99	15.22
7623	23.98	21.57	21.06	19.52	NaN	22.05	21.36	21.15	19.49	NaN	24.52	22.6	21.53	19.66	NaN	23.26	21.07	20.8	19.71	NaN	26.06	21.67	20.75	19.23	NaN
2105-3	23.28	21.42	19.78	18.39	14.98	20.62	20.95	20.14	19.15	15.85	23.53	22	20.17	18.32	14.45	22.91	21.07	19.26	18.06	15.09	26.20	21.66	17.79	17.43	14.53
2106-1	23.47	22.42	21.13	19.85	16.18	21.04	21.31	20.85	20.07	16.72	23.92	23.07	21.7	20.04	15.59	22.92	22.02	20.87	19.7	16.68	26.35	23.3	18.56	17.83	15.71
2107-5	23.47	22.42	21.13	19.85	16.18	21.04	21.31	20.85	20.07	16.72	23.92	23.07	21.7	20.04	15.59	22.92	22.02	20.87	19.7	16.68	25.40	23.3	19.28	17.52	15.71
Average	23.64	21.53	20.55	19.80	15.94	21.46	21.15	20.66	19.87	16.44	24.02	22.47	21.11	20.10	15.57	23.07	21.10	20.25	19.88	16.20	26.01	21.49	20.03	19.21	15.52
STD	0.27	0.45	0.53	0.49	0.35	0.55	0.19	0.42	0.57	0.29	0.43	0.43	0.54	0.61	0.50	0.20	0.45	0.58	0.52	0.40	0.24	1.81	0.76	0.58	0.38
Min	23.28	20.33	19.32	18.39	14.98	20.62	20.75	19.78	18.51	15.67	23.51	21.39	19.76	18.32	14.45	22.83	19.82	19.01	18.06	15.09	25.36	15.43	17.79	17.43	14.53
Max	24.32	22.73	21.36	20.33	16.51	22.70	21.77	21.15	20.44	16.94	24.98	23.62	21.98	20.78	16.58	23.82	22.45	21.28	20.48	16.82	26.35	24.02	21.31	20.03	16.24

Table 6 – Pearson's correlation matrix between $U^{K'}_{37}$ and annual and seasonal sea surface temperatures. The values that are highlighted show the highest correlation value and the lowest *p*-value.

	$U^{K'}_{37}$	SST_{AN}	SST_{WI}	SST_{AU}	SST_{SP}	SST_{SU}
***p*-value**		< 0.01	< 0.01	< 0.01	< 0.01	0.17
SST_{AN}	0.54					
SST_{WI}	0.58	0.96				
SST_{AU}	**0.61**	0.93	0.95			
SST_{SP}	0.52	0.94	0.90	0.89		
SST_{SU}	0.20	0.49	0.41	0.56	0.52	

Table 7 - Pearson's correlation matrix between $U^{K'}_{37}$ and annual and seasonal sea temperatures obtained with the WOA13. The highlighted value in bold shows the highest correlation with a significant *p*-value

	Annual sea temperatures					
	$U^{K'}_{37}$	**0m**	**10m**	**15m**	**20m**	**25m**
$U^{K'}_{37}$		0.33	< 0.05	0.34	0.17	0.88
0m	0.16		0.54	< 0.05	< 0.05	< 0.05
10m	0.37	0.10		< 0.05	0.43	0.08
15m	0.16	0.51	0.67		0.22	< 0.05
20m	-0.24	-0.43	0.14	0.21		0.18
25m	0.03	0.54	0.37	0.78	0.29	
	Winter sea temperatures					
	$U^{K'}_{37}$	**0m**	**10m**	**15m**	**20m**	**25m**
$U^{K'}_{37}$		0.10	0.16	1.00	0.08	0.26
0m	0.26		< 0.05	0.18	< 0.05	0.63
10m	0.22	0.59		< 0.05	0.17	0.15
15m	0.00	0.22	0.54		< 0.05	< 0.05
20m	-0.30	-0.73	-0.24	0.34		< 0.05
25m	-0.25	-0.11	0.31	0.64	0.57	
	Autumn sea temperatures					
	$U^{K'}_{37}$	**0m**	**10m**	**15m**	**20m**	**25m**
$U^{K'}_{37}$		0.11	< 0.05	0.33	0.27	0.27
0m	0.26		< 0.05	< 0.05	< 0.05	< 0.05
10m	**0.43**	0.43		< 0.05	0.71	< 0.05
15m	0.16	0.51	0.80		0.13	< 0.05
20m	-0.19	-0.55	0.07	0.26		0.61
25m	0.24	0.83	0.51	0.67	-0.11	
	Spring sea temperatures					

	$U^{K'}_{37}$	0m	10m	15m	20m	25m
$U^{K'}_{37}$		0.59	< 0.05	0.29	0.17	0.75
0m	0.09		0.75	< 0.05	0.19	0.86
10m	0.34	0.05		< 0.05	0.73	0.07
15m	0.18	0.31	0.53		0.13	< 0.05
20m	-0.24	-0.23	0.06	0.26		< 0.05
25m	-0.07	0.04	0.38	0.73	0.50	

	Summer sea temperatures					
	$U^{K'}_{37}$	**0m**	**10m**	**15m**	**20m**	**25m**
$U^{K'}_{37}$		< 0.05	< 0.05	0.12	0.98	0.76
0m	-0.42		< 0.05	< 0.05	0.20	0.26
10m	0.41	-0.35		0.86	0.60	< 0.05
15m	0.26	-0.34	0.03		< 0.05	< 0.05
20m	0.00	0.22	-0.09	0.68		0.27
25m	0.07	-0.24	0.54	0.67	0.24	

Table 8 - Calculated SSTs after $U^{K'}_{37}$ based equations (in °C).

	Inferred SSTs (°C)			
Station	**Prahl et al. (1988)**	**Muller et al. (1998)**	**Conte et al. (2006)**	**Tierney and Tingley (2018)**
NAP61_2	23.73	23.70	25.68	23.02
NAP62_2	23.06	23.03	25.14	22.32
NAP63_2	25.52	25.48	27.21	25.21
NAP64_2	25.06	25.03	26.81	24.58
NAP66_2	23.97	23.94	25.88	23.31
NAP67_2	24.46	24.42	26.28	23.87
NAP68_2	25.36	25.33	27.07	24.97
249	24.85	24.82	26.62	24.33
250	25.03	25.00	26.78	24.56
253	25.82	25.79	27.48	25.62
254	23.97	23.94	25.88	23.34
255	24.49	24.45	26.31	23.90
256	25.82	25.79	27.48	25.62
257	25.82	25.79	27.48	25.62
258	25.55	25.52	27.24	25.24
259	25.00	24.97	26.75	24.50
260	23.27	23.24	25.31	22.59
262	26.03	26.00	27.68	25.98
263	24.33	24.30	26.18	23.71
264	24.85	24.82	26.62	24.35
265	25.09	26.35	26.83	24.65
266	24.73	25.99	26.52	24.20
267	25.64	26.90	27.32	25.34
311	24.58	24.55	26.39	24.03

312_1	25.27	25.24	26.99	24.91
312	25.06	25.03	26.81	24.61
313	25.12	25.09	26.86	24.68
314	25.58	25.55	27.26	25.28
7608	25.03	25.00	26.78	24.57
7609	24.70	24.67	26.49	24.18
7610	23.49	23.45	25.48	22.80
7611	23.67	23.64	25.63	22.95
7612	24.52	24.48	26.33	23.90
7613	23.49	23.45	25.48	22.78
7615	23.67	23.64	25.63	22.94
7616	23.88	23.85	25.80	23.19
7617	25.21	25.18	26.94	24.83
7618	24.91	24.88	26.67	24.40
7619	26.76	26.73	28.36	27.14
7621	25.33	25.30	27.05	24.96
7622	26.58	26.55	28.19	26.78
7623	26.24	26.21	27.88	26.26
2105-3	24.85	24.82	26.62	24.35
2106-1	24.73	24.70	26.52	24.21
2107-5	24.30	24.27	26.15	23.68
Average	24.85	24.91	26.64	24.40
STD	0.86	0.94	0.74	1.08
Min	23.06	23.03	25.14	22.32
Max	26.76	26.90	28.36	27.14

Table 9 - Values of the sea surface temperatures anomalies (Δ_{sst}) calculated after the Prahl et al. (1988) equation against seasonal and annual temperatures, as well as previous SST-$U^{K'}_{37}$ equations.

	SST (°C)	SST (°C) Aqua MODIS					Published Equations SSTs (°C)		
Station	Prahl et al. (1988)	Δsst Annual	Δsst Winter	Δsst Autumn	Δsst Spring	Δsst Summer	Δsst Muller et al. (1998)	Δsst Conte et al. (2006)	Tierney and Tingley (2018)
NAP61_2	23.73	0.50	-2.25	0.94	-0.89	2.84	1.15	-0.82	1.84
NAP62_2	23.06	1.18	-1.43	1.37	-0.30	2.94	1.82	-0.28	2.54
NAP63_2	25.52	-0.57	-2.71	0.18	-1.92	1.16	-0.63	-2.36	-0.36
NAP64_2	25.06	-0.22	-2.57	0.36	-1.56	1.35	-0.18	-1.95	0.28
NAP66_2	23.97	0.16	-2.56	0.46	-1.20	2.11	0.91	-1.02	1.55
NAP67_2	24.46	0.25	-2.09	0.87	-0.99	1.95	0.43	-1.43	0.98
NAP68_2	25.36	-0.69	-2.73	0.13	-1.85	1.17	-0.48	-2.22	-0.12
249	24.85	-0.52	-3.03	0.14	-1.91	1.54	0.03	-1.77	0.52
250	25.03	-0.70	-3.21	-0.04	-2.09	1.36	-0.15	-1.93	0.30
253	25.82	-1.43	-3.92	-0.64	-2.77	0.72	-0.94	-2.63	-0.76
254	23.97	0.42	-2.06	1.15	-0.90	2.55	0.91	-1.02	1.51
255	24.49	-0.16	-2.72	0.55	-1.46	2.00	0.40	-1.46	0.96
256	25.82	-1.53	-4.07	-0.78	-2.77	0.64	-0.94	-2.63	-0.77
257	25.82	-1.52	-4.07	-0.76	-2.82	0.63	-0.94	-2.63	-0.77
258	25.55	-1.14	-3.81	-0.52	-2.54	0.92	-0.67	-2.38	-0.39
259	25.00	-0.65	-3.16	0.00	-1.98	1.46	-0.12	-1.90	0.35
260	23.27	1.08	-1.43	1.73	-0.25	3.19	1.61	-0.45	2.27
262	26.03	-1.77	-4.22	-1.04	-3.03	0.35	-1.15	-2.83	-1.13
263	24.33	0.03	-2.43	0.74	-1.30	2.10	0.55	-1.33	1.14
264	24.85	-0.51	-2.99	0.20	-1.89	1.58	0.03	-1.77	0.51
265	25.09	-0.09	-2.19	0.58	-1.32	1.57	-1.50	-1.98	0.20
266	24.73	0.32	-1.83	0.92	-0.98	1.90	-1.13	-1.66	0.65
267	25.64	-0.65	-2.73	0.00	-1.81	0.87	-2.04	-2.47	-0.49

311	24.58	0.14	-2.15	0.83	-1.27	1.69	0.30	-1.53	0.82
312_1	25.27	-0.83	-3.35	-0.51	-2.05	0.89	-0.39	-2.14	-0.05
312	25.06	-0.62	-3.14	-0.30	-1.84	1.10	-0.18	-1.95	0.24
313	25.12	-0.14	-2.20	0.57	-1.49	1.61	-0.24	-2.01	0.18
314	25.58	-0.63	-2.64	0.04	-1.92	1.10	-0.70	-2.41	-0.43
7608	25.03	-0.98	-3.79	-0.62	-2.29	1.20	-0.15	-1.93	0.28
7609	24.70	-0.56	-3.30	-0.26	-1.88	1.55	0.18	-1.64	0.67
7610	23.49	0.41	-3.13	0.57	-0.82	2.93	1.40	-0.62	2.06
7611	23.67	0.28	-3.07	0.58	-0.93	2.60	1.21	-0.77	1.90
7612	24.52	-0.34	-3.75	-0.28	-1.74	1.91	0.37	-1.48	0.96
7613	23.49	0.53	-2.66	0.71	-0.80	2.73	1.40	-0.62	2.08
7615	23.67	0.31	-2.53	0.51	-0.92	2.44	1.21	-0.77	1.91
7616	23.88	0.04	-2.95	0.38	-1.23	2.27	1.00	-0.95	1.66
7617	25.21	-0.97	-3.58	-0.78	-2.45	0.79	-0.33	-2.09	0.02
7618	24.91	-0.14	-2.26	0.53	-1.59	1.37	-0.03	-1.82	0.46
7619	26.76	-1.97	-4.00	-1.19	-3.34	-0.44	-1.88	-3.51	-2.28
7621	25.33	-0.80	-2.87	0.08	-2.13	0.73	-0.45	-2.19	-0.10
7622	26.58	-1.73	-3.90	-1.05	-3.11	-0.34	-1.70	-3.34	-1.93
7623	26.24	-1.43	-3.72	-0.76	-2.78	0.02	-1.36	-3.02	-1.40
2105-3	24.85	-0.79	-3.75	-0.28	-1.74	1.43	0.03	-1.77	0.50
2106-1	24.73	-0.33	-2.89	0.23	-1.39	1.63	0.15	-1.66	0.64
2107-5	24.30	0.12	-2.49	0.69	-0.93	2.06	0.58	-1.30	1.18
Average	24.85	-0.41	-2.94	0.14	-1.71	1.52	-0.06	-1.79	0.45
STD	0.87	0.74	0.72	0.68	0.75	0.85	0.95	0.75	1.10
Max	26.76	1.18	-1.43	1.73	-0.25	3.19	1.82	-0.28	2.54
Min	23.06	-1.97	-4.22	-1.19	-3.34	-0.44	-2.04	-3.51	-2.28

Table 10 - Values of the sea surface temperatures anomalies (Δ_{sst}) calculated after the Muller et al. (1998) equation against seasonal and annual temperatures, as well as previous SST-$U^{K'}_{37}$ equations.

	SST (°C)	SST (°C) Aqua MODIS					Published Equations SSTs (°C)		
Station	**Muller et al. (1998)**	**Δsst Annual**	**Δsst Winter**	**Δsst Autumn**	**Δsst Spring**	**Δsst Summer**	**Δsst Prahl et al. (1988)**	**Δsst Conte et al. (2006)**	**Tierney and Tingley (2018)**
NAP61_2	23.70	0.53	-2.22	0.97	-0.86	2.87	1.18	-0.77	1.89
NAP62_2	23.03	1.21	-1.40	1.40	-0.27	2.97	1.85	-0.23	2.59
NAP63_2	25.48	-0.54	-2.67	0.22	-1.88	1.20	-0.61	-2.30	-0.30
NAP64_2	25.03	-0.19	-2.54	0.39	-1.53	1.38	-0.15	-1.90	0.33
NAP66_2	23.94	0.19	-2.53	0.49	-1.17	2.14	0.94	-0.97	1.60
NAP67_2	24.42	0.29	-2.05	0.90	-0.96	1.98	0.45	-1.37	1.04
NAP68_2	25.33	-0.65	-2.70	0.16	-1.82	1.20	-0.46	-2.17	-0.06
249	24.82	-0.49	-3.00	0.17	-1.88	1.57	0.06	-1.71	0.58
250	25.00	-0.67	-3.18	-0.01	-2.06	1.39	-0.12	-1.87	0.35
253	25.79	-1.40	-3.89	-0.61	-2.74	0.75	-0.91	-2.58	-0.71
254	23.94	0.45	-2.03	1.18	-0.87	2.58	0.94	-0.97	1.57
255	24.45	-0.12	-2.68	0.59	-1.42	2.04	0.42	-1.40	1.01
256	25.79	-1.50	-4.04	-0.75	-2.74	0.67	-0.91	-2.58	-0.71
257	25.79	-1.49	-4.04	-0.73	-2.79	0.66	-0.91	-2.58	-0.71
258	25.52	-1.12	-3.78	-0.49	-2.51	0.95	-0.64	-2.33	-0.34
259	24.97	-0.62	-3.13	0.03	-1.95	1.49	-0.09	-1.84	0.40
260	23.24	1.11	-1.40	1.76	-0.22	3.22	1.63	-0.40	2.32
262	26.00	-1.74	-4.19	-1.01	-3.00	0.38	-1.12	-2.77	-1.07
263	24.30	0.06	-2.40	0.77	-1.27	2.13	0.57	-1.27	1.20
264	24.82	-0.48	-2.96	0.23	-1.86	1.61	0.06	-1.71	0.56
265	26.35	-1.35	-3.45	-0.68	-2.58	0.31	-0.18	-1.92	0.26
266	25.99	-0.94	-3.09	-0.34	-2.24	0.64	0.18	-1.61	0.70
267	26.90	-1.91	-3.99	-1.26	-3.07	-0.39	-0.73	-2.41	-0.43

311	24.55	0.17	-2.12	0.86	-1.24	1.72	0.33	-1.48	0.88
312_1	25.24	-0.79	-3.32	-0.48	-2.02	0.92	-0.36	-2.08	0.00
312	25.03	-0.58	-3.11	-0.27	-1.81	1.13	-0.15	-1.90	0.30
313	25.09	-0.11	-2.17	0.60	-1.46	1.64	-0.21	-1.95	0.23
314	25.55	-0.60	-2.61	0.07	-1.89	1.13	-0.67	-2.36	-0.37
7608	25.00	-0.95	-3.76	-0.59	-2.26	1.23	-0.12	-1.87	0.34
7609	24.67	-0.54	-3.27	-0.23	-1.85	1.58	0.21	-1.58	0.73
7610	23.45	0.44	-3.09	0.61	-0.78	2.97	1.42	-0.57	2.11
7611	23.64	0.30	-3.04	0.61	-0.90	2.63	1.24	-0.72	1.96
7612	24.48	-0.30	-3.71	-0.24	-1.70	1.95	0.39	-1.43	1.01
7613	23.45	0.57	-2.62	0.75	-0.76	2.77	1.42	-0.57	2.13
7615	23.64	0.34	-2.50	0.54	-0.89	2.47	1.24	-0.72	1.96
7616	23.85	0.07	-2.92	0.41	-1.20	2.30	1.03	-0.89	1.72
7617	25.18	-0.94	-3.55	-0.75	-2.42	0.82	-0.30	-2.03	0.08
7618	24.88	-0.11	-2.23	0.56	-1.56	1.40	0.00	-1.77	0.51
7619	26.73	-1.94	-3.97	-1.16	-3.31	-0.41	-1.85	-3.46	-2.23
7621	25.30	-0.76	-2.84	0.11	-2.10	0.76	-0.43	-2.14	-0.05
7622	26.55	-1.70	-3.87	-1.02	-3.08	-0.31	-1.67	-3.28	-1.87
7623	26.21	-1.40	-3.69	-0.73	-2.75	0.05	-1.33	-2.97	-1.35
2105-3	24.82	-0.76	-3.72	-0.25	-1.71	1.46	0.06	-1.71	0.56
2106-1	24.70	-0.30	-2.86	0.26	-1.36	1.66	0.18	-1.61	0.70
2107-5	24.27	0.16	-2.46	0.72	-0.90	2.09	0.60	-1.25	1.23
Average	24.91	-0.47	-3.00	0.08	-1.77	1.46	0.06	-1.73	0.50
STD	0.95	0.78	0.71	0.71	0.78	0.92	0.87	0.75	1.10
Min	26.90	1.21	-1.40	1.76	-0.22	3.22	1.85	-0.23	2.59
Max	23.03	-1.94	-4.19	-1.26	-3.31	-0.41	-1.85	-3.46	-2.23

Table 11 - Values of the sea surface temperatures anomalies (Δ_{sst}) calculated after the Conte et al. (2006) equation against seasonal and annual temperatures, as well as previous SST-$U^{K'}_{37}$ equations.

	SST (°C)	SST (°C) Aqua MODIS					Published Equations SSTs (°C)		
Station	Conte et al. (2006)	Δsst Annual	Δsst Winter	Δsst Autumn	Δsst Spring	Δsst Summer	Δsst Prahl et al. (1988)	Δsst Muller et al. (1998)	Tierney and Tingley (2018)
NAP61_2	25.68	-1.44	-4.20	-1.01	-2.84	0.89	2.91	2.94	3.63
NAP62_2	25.14	-0.89	-3.51	-0.71	-2.38	0.86	3.58	3.61	4.33
NAP63_2	27.21	-2.26	-4.40	-1.51	-3.61	-0.53	1.13	1.16	1.43
NAP64_2	26.81	-1.96	-4.32	-1.39	-3.31	-0.40	1.58	1.61	2.07
NAP66_2	25.88	-1.74	-4.47	-1.45	-3.11	0.20	2.67	2.70	3.34
NAP67_2	26.28	-1.58	-3.91	-0.96	-2.82	0.12	2.19	2.22	2.77
NAP68_2	27.07	-2.40	-4.44	-1.58	-3.56	-0.54	1.28	1.31	1.67
249	26.62	-2.29	-4.80	-1.63	-3.68	-0.23	1.79	1.82	2.31
250	26.78	-2.45	-4.96	-1.79	-3.84	-0.39	1.61	1.64	2.09
253	27.48	-3.09	-5.58	-2.30	-4.43	-0.94	0.82	0.85	1.03
254	25.88	-1.49	-3.97	-0.76	-2.81	0.64	2.67	2.70	3.30
255	26.31	-1.98	-4.54	-1.27	-3.28	0.18	2.16	2.19	2.74
256	27.48	-3.19	-5.73	-2.44	-4.43	-1.02	0.82	0.85	1.02
257	27.48	-3.19	-5.73	-2.42	-4.48	-1.03	0.82	0.85	1.02
258	27.24	-2.83	-5.50	-2.21	-4.23	-0.77	1.09	1.12	1.40
259	26.75	-2.40	-4.91	-1.75	-3.73	-0.29	1.64	1.67	2.14
260	25.31	-0.95	-3.47	-0.31	-2.29	1.15	3.37	3.40	4.05
262	27.68	-3.41	-5.87	-2.69	-4.68	-1.30	0.61	0.64	0.66
263	26.18	-1.82	-4.28	-1.11	-3.15	0.25	2.31	2.34	2.93
264	26.62	-2.28	-4.76	-1.57	-3.66	-0.19	1.79	1.82	2.29
265	26.83	-1.84	-3.93	-1.16	-3.06	-0.17	1.55	0.29	1.99
266	26.52	-1.47	-3.62	-0.87	-2.77	0.11	1.91	0.65	2.44
267	27.32	-2.34	-4.41	-1.68	-3.49	-0.81	1.00	-0.25	1.30

311	26.39	-1.67	-3.96	-0.98	-3.08	-0.12	2.06	2.09	2.61
312_1	26.99	-2.55	-5.07	-2.23	-3.77	-0.83	1.37	1.40	1.73
312	26.81	-2.36	-4.89	-2.05	-3.59	-0.65	1.58	1.61	2.03
313	26.86	-1.88	-3.94	-1.17	-3.23	-0.13	1.52	1.55	1.96
314	27.26	-2.32	-4.32	-1.64	-3.60	-0.58	1.06	1.09	1.36
7608	26.78	-2.73	-5.54	-2.37	-4.04	-0.55	1.61	1.64	2.07
7609	26.49	-2.36	-5.09	-2.05	-3.67	-0.24	1.94	1.97	2.46
7610	25.48	-1.59	-5.12	-1.42	-2.81	0.94	3.16	3.19	3.85
7611	25.63	-1.68	-5.03	-1.38	-2.89	0.64	2.97	3.00	3.69
7612	26.33	-2.16	-5.56	-2.09	-3.55	0.10	2.13	2.16	2.74
7613	25.48	-1.46	-4.65	-1.28	-2.79	0.74	3.16	3.19	3.87
7615	25.63	-1.64	-4.49	-1.45	-2.88	0.48	2.97	3.00	3.70
7616	25.80	-1.88	-4.87	-1.54	-3.15	0.35	2.76	2.79	3.45
7617	26.94	-2.69	-5.31	-2.51	-4.18	-0.94	1.43	1.46	1.81
7618	26.67	-1.91	-4.02	-1.23	-3.35	-0.39	1.73	1.76	2.24
7619	28.36	-3.57	-5.60	-2.79	-4.94	-2.04	-0.12	-0.09	-0.50
7621	27.05	-2.51	-4.59	-1.64	-3.85	-0.99	1.31	1.34	1.68
7622	28.19	-3.34	-5.51	-2.66	-4.72	-1.95	0.06	0.09	-0.14
7623	27.88	-3.06	-5.36	-2.40	-4.42	-1.62	0.40	0.43	0.38
2105-3	26.62	-2.56	-5.52	-2.05	-3.51	-0.34	1.79	1.82	2.29
2106-1	26.52	-2.12	-4.68	-1.56	-3.18	-0.16	1.91	1.94	2.43
2107-5	26.15	-1.73	-4.34	-1.16	-2.78	0.21	2.34	2.37	2.96
Average	26.64	-2.20	-4.73	-1.65	-3.50	-0.27	1.79	1.73	2.24
STD	0.75	0.64	0.65	0.59	0.64	0.74	0.87	0.95	1.10
Max	28.36	-0.89	-3.47	-0.31	-2.29	1.15	3.58	3.61	4.33
Min	25.14	-3.57	-5.87	-2.79	-4.94	-2.04	-0.12	-0.25	-0.50

Table 12 - Values of the sea surface temperatures anomalies (Δ_{sst}) calculated after the Tierney and Tingley (2018) equation against seasonal and annual temperatures, as well as previous SST-$U^{K'}_{37}$ equations.

	SST (°C)	SST (°C) Aqua MODIS					SST (°C) Previous Equations		
Station	**Tierney and Tingley (2018)**	**Δsst Annual**	**Δsst Winter**	**Δsst Autumn**	**Δsst Spring**	**Δsst Summer**	**Δsst Prahl**	**Δsst Muller**	**Δsst Conte**
NAP61_2	23.02	0.17	2.92	-0.27	1.56	-2.17	0.68	0.70	-1.27
NAP62_2	22.32	0.16	-2.77	0.03	-1.64	1.60	-1.34	-1.37	0.73
NAP63_2	25.21	-0.54	-1.59	1.30	-0.80	2.28	1.11	1.08	2.80
NAP64_2	24.58	-0.44	-1.91	1.02	-0.90	2.01	0.66	0.63	2.40
NAP66_2	23.31	0.27	-2.99	0.03	-1.63	1.68	-0.43	-0.46	1.47
NAP67_2	23.87	-0.30	-2.03	0.92	-0.94	2.00	0.05	0.02	1.88
NAP68_2	24.97	-0.27	-1.77	1.09	-0.89	2.13	0.96	0.93	2.67
249	24.33	0.08	-2.58	0.59	-1.46	1.99	0.44	0.42	2.22
250	24.56	0.08	-2.58	0.59	-1.46	1.99	0.63	0.60	2.37
253	25.62	0.01	-2.50	0.78	-1.35	2.14	1.41	1.39	3.08
254	23.34	0.02	-2.49	0.72	-1.33	2.12	-0.43	-0.46	1.47
255	23.90	0.08	-2.63	0.64	-1.37	2.09	0.08	0.05	1.90
256	25.62	0.11	-2.65	0.64	-1.35	2.06	1.41	1.39	3.08
257	25.62	0.11	-2.65	0.66	-1.40	2.05	1.41	1.39	3.08
258	25.24	0.00	-2.66	0.63	-1.39	2.07	1.14	1.12	2.83
259	24.50	0.05	-2.56	0.60	-1.38	2.06	0.60	0.57	2.35
260	22.59	0.05	-2.56	0.60	-1.38	2.06	-1.13	-1.16	0.90
262	25.98	0.14	-2.59	0.59	-1.40	1.98	1.63	1.60	3.27
263	23.71	0.04	-2.50	0.67	-1.37	2.03	-0.07	-0.10	1.78
264	24.35	0.07	-2.54	0.65	-1.44	2.03	0.44	0.42	2.22
265	24.65	-0.59	-1.50	1.27	-0.63	2.26	0.69	1.95	2.43
266	24.20	-0.64	-1.50	1.25	-0.65	2.23	0.32	1.58	2.11
267	25.34	-0.58	-1.49	1.24	-0.57	2.11	1.23	2.49	2.91

311	24.03	-0.31	-1.97	1.01	-1.09	1.87	0.17	0.15	1.98
312_1	24.91	-0.04	-2.48	0.36	-1.18	1.76	0.87	0.84	2.59
312	24.61	-0.04	-2.48	0.36	-1.18	1.76	0.66	0.63	2.40
313	24.68	-0.57	-1.48	1.29	-0.77	2.33	0.72	0.69	2.45
314	25.28	-0.54	-1.46	1.22	-0.74	2.28	1.17	1.15	2.86
7608	24.57	0.36	-3.16	0.01	-1.66	1.83	0.63	0.60	2.37
7609	24.18	0.27	-3.00	0.04	-1.58	1.85	0.29	0.27	2.09
7610	22.80	0.51	-4.04	-0.34	-1.73	2.02	-0.92	-0.95	1.07
7611	22.95	0.46	-3.80	-0.15	-1.66	1.87	-0.74	-0.76	1.22
7612	23.90	0.23	-3.63	-0.16	-1.62	2.03	0.11	0.08	1.93
7613	22.78	0.38	-3.57	-0.20	-1.71	1.82	-0.92	-0.95	1.07
7615	22.94	0.42	-3.26	-0.22	-1.65	1.71	-0.74	-0.76	1.22
7616	23.19	0.48	-3.47	-0.14	-1.75	1.75	-0.53	-0.55	1.40
7617	24.83	0.16	-2.77	0.03	-1.64	1.60	0.81	0.78	2.53
7618	24.40	-0.36	-1.75	1.04	-1.08	1.88	0.50	0.48	2.27
7619	27.14	-0.39	-1.64	1.17	-0.98	1.92	2.35	2.33	3.96
7621	24.96	-0.13	-1.94	1.01	-1.20	1.66	0.93	0.90	2.64
7622	26.78	-0.45	-1.72	1.13	-0.93	1.84	2.17	2.15	3.79
7623	26.26	-0.41	-1.88	1.08	-0.94	1.86	1.84	1.81	3.47
2105-3	24.35	0.34	-3.30	0.17	-1.29	1.88	0.44	0.42	2.22
2106-1	24.21	0.01	-2.56	0.56	-1.06	1.96	0.32	0.30	2.11
2107-5	23.68	-0.02	-2.59	0.59	-1.03	1.96	-0.10	-0.13	1.75
Average	24.40	-0.03	-2.36	0.58	-1.20	1.87	0.48	0.53	2.18
STD	0.84	0.27	0.67	0.41	0.35	0.25	0.65	0.73	0.65
Min	22.32	-0.64	-4.04	-0.34	-1.75	-2.17	-1.34	-1.37	-1.27
Max	27.14	0.51	2.92	1.30	1.56	2.33	2.35	2.49	3.96

Table 13 - Results of the Kruskal-Wallis test with the temperatures gathered from the conversion of $U^{K'}_{37}$ using previous equations, as well as the equation performed in this study, against the seasonal and annual SSTs obtained with the Aqua MODIS Satellite. For this test, *p*-values higher than 0.05 indicates that the means that are being compared have no significant difference.

	Prahl et al. (1988)	**Muller et al. (1998)**	**Conte et al. (2006)**	**Tierney and Tingley (2018)**
Prahl et al. (1988)				
Muller et al. (1998)	**0.97**			
Conte et al. (2006)	< 0.05	< 0.05		
Tierney and Tingley (2018)	< 0.05	< 0.05	< 0.05	
SST_{AN}	< 0.05	< 0.05	< 0.05	**0.87**
SST_{WI}	< 0.05	< 0.05	< 0.05	< 0.05
SST_{AU}	**0.47**	**0.61**	< 0.05	< 0.05
SST_{SP}	< 0.05	< 0.05	< 0.05	< 0.05
SST_{SU}	< 0.05	< 0.05	< 0.05	< 0.05

Table 14 - Values of chlorophyll-a concentration (in mg dm^{-3}) from the sample locations of this master's degree thesis. The values were gathered with the Aqua MODIS satellite.

	Chl-*a* (mg/dm^{-3})				
Station	**Autumn**	**Winter**	**Spring**	**Summer**	**Annual**
NAP61_2	0.78	0.96	0.89	0.59	0.80
NAP62_2	0.24	0.35	0.28	0.26	0.28
NAP63_2	0.11	0.16	0.12	0.11	0.13
NAP64_2	0.12	0.19	0.16	0.14	0.15
NAP66_2	0.25	0.44	0.29	0.28	0.31
NAP67_2	0.13	0.25	0.14	0.14	0.16
NAP68_2	0.12	0.18	0.13	0.12	0.14
249	0.13	0.18	0.15	0.11	0.14
250	0.13	0.18	0.15	0.11	0.14
253	0.14	0.22	0.16	0.16	0.17
254	0.13	0.23	0.16	0.16	0.17
255	0.13	0.27	0.17	0.11	0.17
256	0.13	0.26	0.17	0.12	0.17
257	0.13	0.26	0.17	0.12	0.17
258	0.13	0.24	0.16	0.11	0.16
259	0.13	0.21	0.16	0.10	0.15
260	0.13	0.21	0.16	0.10	0.15
262	0.12	0.18	0.15	0.12	0.14
263	0.12	0.18	0.15	0.11	0.14
264	0.12	0.18	0.15	0.11	0.14
265	0.11	0.16	0.12	0.10	0.12
266	0.12	0.16	0.12	0.10	0.12
267	0.12	0.16	0.13	0.11	0.13
311	0.13	0.21	0.18	0.14	0.16
312_1	0.16	0.25	0.18	0.17	0.19
312	0.16	0.25	0.18	0.17	0.19
313	0.11	0.15	0.12	0.09	0.12
314	0.11	0.15	0.12	0.10	0.12
7608	0.16	0.30	0.21	0.16	0.21
7609	0.17	0.28	0.21	0.15	0.20
7610	0.23	0.57	0.30	0.23	0.33
7611	0.19	0.38	0.25	0.19	0.25
7612	0.30	0.74	0.44	0.30	0.45
7613	0.27	0.56	0.34	0.29	0.37
7615	0.24	0.36	0.29	0.24	0.28
7616	0.26	0.42	0.33	0.29	0.33
7617	0.23	0.34	0.27	0.25	0.27
7618	0.14	0.20	0.17	0.11	0.16
7619	0.13	0.19	0.16	0.11	0.14
7621	0.16	0.22	0.18	0.11	0.17
7622	0.14	0.19	0.16	0.11	0.15

7623	0.13	0.20	0.17	0.13	0.16
2105-3	0.15	0.26	0.19	0.14	0.19
2106-1	0.12	0.18	0.14	0.10	0.13
2107-5	0.11	0.18	0.14	0.10	0.13
Average	0.17	0.27	0.20	0.16	0.20
STD	0.11	0.16	0.13	0.09	0.12

Table 15 - Pearson’s Correlation Matrix against $U^{K'}_{37}$ values of this study against the chlorophyll-*a* concentration gathered from the Aqua MODIS Satellite. The table contains the correlation value and the *p*-values of the test.

	$U^{K'}_{37}$	Autumn	Winter	Spring	Summer	Annual
$U^{K'}_{37}$		< 0.05	< 0.05	< 0.01	< 0.01	< 0.01
Autumn	-0.51		< 0.05	< 0.01	< 0.01	< 0.01
Winter	**-0.55**	0.92		< 0.01	< 0.01	< 0.01
Spring	-0.52	0.98	0.95		< 0.01	< 0.01
Summer	-0.53	0.94	0.92	0.94		< 0.01
Annual	-0.54	0.97	0.98	0.98	0.96	

Table 16 - Amount (in percentage) of the nannoplankton species that were found in 21 samples collected for this research.

Sample	***C. leptoporus***	***Calciosolenia***	***E. huxleyi***	***F. profunda***	***Medium Gephyr.***	***Large Gephyr.***	***Gephyr. Total***	***Helicosphaera***	***Rhabdosphaera***	***Syracosphaera***	***Umbellosphaera***	***Umbilicosphaera***	**Total w/o *F. Profunda* (%)**	**Total (%)**
PM-249	2.62	0.75	9.74	59.93	12.73	8.24	20.97	0.37	0	0.37	0.37	4.87	40.07	100
PM-250	1.87	0.37	8.24	64.79	10.49	9.74	20.22	1.50	0	0	0	3.00	35.21	100
PM-253	0	0	15.00	56.43	14.29	8.57	22.86	0.71	0	0	0.71	4.29	43.57	100
PM-254	0.94	0	13.44	67.69	6.84	5.42	12.26	0.94	0	0.71	0.94	3.07	32.31	100
PM-255	0.56	0	10.34	73.50	7.14	5.83	12.97	0.38	0.19	0	0	2.07	26.50	100
PM-256	4.00	0	24.00	36.00	16.00	13.78	29.78	0.00	0.44	1.78	0	4.00	64.00	100
PM-257	1.67	0	12.86	64.52	10.48	4.76	15.24	0.48	0.24	0.71	0.71	3.57	35.48	100
PM-258	2.16	0	16.55	48.92	18.71	8.63	27.34	0.72	0	1.44	0.72	2.16	51.08	100
PM-259	2.76	0	10.11	66.62	10.26	6.89	17.15	0.46	0	0.61	0.46	1.84	33.38	100
PM-260	3.80	0	9.49	60.13	13.92	6.96	20.89	1.90	1.27	0	0	2.53	39.87	100
PM-262	0.82	0	20.65	60.05	9.51	3.26	12.77	0.82	0	0.82	1.09	2.99	39.95	100
PM-263	0.75	0	12.31	61.56	11.31	7.54	18.84	1.51	0.25	0.50	1.26	3.02	38.44	100
PM-264	1.89	0	7.08	64.15	15.57	7.08	22.64	1.89	0	0.47	0.94	0.94	35.85	100
PM-265	3.27	0	14.25	42.99	18.22	15.65	33.88	2.10	0	1.64	1.87	0	57.01	100
PM-266	1.27	0	15.22	62.58	10.15	5.71	15.86	0.63	0.21	0.42	0.42	3.38	37.42	100
PM-267	2.18	0.24	21.12	58.98	8.50	2.91	11.41	0.49	0.24	1.21	1.21	2.91	41.02	100
CNT-311	0.36	0.36	15.33	54.38	18.25	6.20	24.45	0.36	0.36	0.73	1.46	2.19	45.62	100
CNT-312 (0-0.5cm)	1.84	0.41	34.76	36.61	17.18	4.09	21.27	0.41	1.02	0.20	0.82	2.66	63.39	100
CNT-312 (0.5-1cm)	0.42	0.21	19.45	51.16	15.43	4.23	19.66	0.85	2.11	1.27	2.33	2.54	48.84	100
CNT-313	1.60	0	37.30	38.90	9.61	3.66	13.27	0.92	0	0.69	2.97	4.35	61.10	100
CNT-314	0.53	0	32.63	43.50	15.12	1.86	16.98	0.27	0.27	0.53	2.92	2.39	56.50	100

Table 17 - Values of the *E.huxleyi-C.leptoporus* dissolution index calculated after Boeckel and Baumann (2004) (CEX’). This index is used to verify if the sample present high dissolution influence, where values under 0.6 are considered high dissolved, and values higher than 0.6 are considered non-influenced by dissolution.

Sample	CEX'
PM-249	0.87
PM-250	0.91
PM-253	1.00
PM-254	0.95
PM-255	0.97
PM-256	0.90
PM-257	0.91
PM-258	0.92
PM-259	0.86
PM-260	0.81
PM-262	0.97
PM-263	0.96
PM-264	0.88
PM-265	0.90
PM-266	0.94
PM-267	0.92
CNT-311	0.98
CNT-312 (0-0.5cm)	0.95
CNT-312 (0.5-1cm)	0.98
CNT-313	0.96
CNT-314	0.98
Average	0.93
STD	0.04
Min	0.81
Max	1.00

Table 18 – SSTs gathered from the Aqua MODIS mission.

Sample ID	SSTAn	SSTWi	SSTAu	SSTSp	SSTSu
NAP62	24.24	21.63	24.43	22.76	26
NAP63	24.94	22.81	25.7	23.6	26.68
NAP64	24.84	22.49	25.42	23.5	26.41
NAP66	24.13	21.41	24.43	22.77	26.08
NAP68	24.68	22.63	25.49	23.51	26.53
PM249	24.33	21.82	24.99	22.94	26.39
PM250	24.33	21.82	24.99	22.94	26.39
PM253	24.39	21.9	25.18	23.05	26.54
PM254	24.39	21.91	25.12	23.07	26.52
PM255	24.33	21.77	25.04	23.03	26.49
PM256	24.29	21.75	25.04	23.05	26.46
PM257	24.30	21.75	25.06	23	26.45
PM258	24.40	21.74	25.03	23.01	26.47
PM259	24.35	21.84	25	23.02	26.46
PM260	24.35	21.84	25	23.02	26.46
PM262	24.26	21.81	24.99	23	26.38
PM263	24.36	21.9	25.07	23.03	26.43
PM264	24.34	21.86	25.05	22.96	26.43
PM265	25.00	22.9	25.67	23.77	26.66
PM266	25.05	22.9	25.65	23.75	26.63
PM267	24.98	22.91	25.64	23.83	26.51
CTN311	24.72	22.43	25.41	23.31	26.27
CTN312(0.5-1)	24.45	21.92	24.76	23.22	26.16
CTN312(0-0.5)	24.45	21.92	24.76	23.22	26.16
CTN313	24.98	22.92	25.69	23.63	26.73

CTN314	24.95	22.94	25.62	23.66	26.68
Average	24.53	22.14	25.16	23.22	26.44
STD	0.29	0.49	0.37	0.33	0.18
Min	24.13	21.41	24.43	22.76	26.00
Max	25.05	22.94	25.70	23.83	26.73

Table 19 – Water column temperatures gathered from the WOA13.

Sample ID	Annual SST (0m)	Annual SST (10m)	Annual SST (15m)	Annual SST (20m)	Annual SST (25m)	Winter SST (0m)	Winter SST (10m)	Winter SST (15m)	Winter SST (20m)	Winter SST (25m)	Autumn SST (0m)	Autumn SST (10m)	Autumn SST (15m)	Autumn SST (20m)	Autumn SST (25m)	Spring SST (0m)	Spring SST (10m)	Spring SST (15m)	Spring SST (20m)	Spring SST (25m)	Summer SST (0m)	Summer SST (10m)	Summer SST (15m)
NAP62	23.97	21.57	21.06	19.52	NaN	22.05	21.36	21.15	19.49	NaN	24.52	22.6	21.53	19.66	NaN	23.26	21.07	20.8	19.71	NaN	26.06	19.41	20.75
NAP63	23.97	21.57	21.06	19.52	16.49	22.05	21.36	21.15	19.49	16.65	24.52	22.6	21.53	19.66	16.58	23.26	21.07	20.8	19.71	16.49	26.06	22.6	20.75
NAP64	23.97	21.57	21.06	19.52	16.13	22.05	21.36	21.15	19.49	16.23	24.52	22.6	21.53	19.66	16.2	23.26	21.07	20.8	19.71	16.16	26.06	21.89	20.75
NAP66	23.78	20.33	NaN	NaN	NaN	21.64	20.75	NaN	NaN	NaN	24.15	21.39	NaN	NaN	NaN	23.12	19.82	NaN	NaN	NaN	26.21	19.24	NaN
NAP68	23.64	21.31	20.77	20.13	16.51	21.42	21.11	20.9	20.13	16.94	23.97	22.29	21.36	20.39	16.27	23.04	20.85	20.51	20.48	16.82	26.13	22.84	20.32
PM249	23.34	21.47	20.22	20.1	15.76	20.84	20.99	20.61	20.35	16.37	23.51	22.32	20.86	20.57	15.27	22.93	21.13	19.78	20.08	16.07	26.07	22.81	19.64
PM250	23.34	21.47	20.22	20.1	15.76	20.84	20.99	20.61	20.35	16.37	23.51	22.32	20.86	20.57	15.27	22.93	21.13	19.78	20.08	16.07	26.07	22.81	19.64
PM253	23.45	21.89	20.83	20.33	16.26	21.2	21.17	20.79	20.44	16.8	23.8	22.84	21.48	20.78	15.9	22.83	21.39	20.52	20.34	16.53	25.94	22.43	20.54
PM254	23.45	21.89	20.83	20.33	16.32	21.2	21.17	20.79	20.44	16.81	23.8	22.84	21.48	20.78	15.84	22.83	21.39	20.52	20.34	16.72	25.94	23.03	20.54
PM255	23.45	21.89	20.83	20.33	15.98	21.2	21.17	20.79	20.44	16.59	23.8	22.84	21.48	20.78	15.46	22.83	21.39	20.52	20.34	16.27	25.94	22.59	20.54
PM256	23.45	21.89	20.83	20.33	15.98	21.2	21.17	20.79	20.44	16.59	23.8	22.84	21.48	20.78	15.46	22.83	21.39	20.52	20.34	16.27	25.94	22.59	20.54
PM257	23.45	21.89	20.83	20.33	15.98	21.2	21.17	20.79	20.44	16.59	23.8	22.84	21.48	20.78	15.46	22.83	21.39	20.52	20.34	16.27	25.94	22.59	20.54
PM258	23.34	21.47	20.22	20.1	15.82	20.84	20.99	20.61	20.35	16.46	23.51	22.32	20.86	20.57	15.3	22.93	21.13	19.78	20.08	16.12	26.07	22.73	19.64
PM259	23.34	21.47	20.22	20.1	15.82	20.84	20.99	20.61	20.35	16.46	23.51	22.32	20.86	20.57	15.3	22.93	21.13	19.78	20.08	16.12	26.07	22.73	19.64
PM260	23.34	21.47	20.22	20.1	15.82	20.84	20.99	20.61	20.35	16.46	23.51	22.32	20.86	20.57	15.3	22.93	21.13	19.78	20.08	16.12	26.07	22.73	19.64
PM262	23.34	21.47	20.22	20.1	15.76	20.84	20.99	20.61	20.35	16.37	23.51	22.32	20.86	20.57	15.27	22.93	21.13	19.78	20.08	16.07	26.07	22.81	19.64
PM263	23.34	21.47	20.22	20.1	15.76	20.84	20.99	20.61	20.35	16.37	23.51	22.32	20.86	20.57	15.27	22.93	21.13	19.78	20.08	16.07	26.07	22.81	19.64
PM264	23.34	21.47	20.22	20.1	15.76	20.84	20.99	20.61	20.35	16.37	23.51	22.32	20.86	20.57	15.27	22.93	21.13	19.78	20.08	16.07	26.07	22.81	19.64
PM265	24.13	22.37	21.03	19.67	16.05	22.17	21.85	21.25	19.93	16.01	24.75	23.32	21.52	19.74	16.22	23.41	21.81	20.6	19.58	16.19	26.19	22.51	20.77
PM266	24.13	22.37	21.03	19.67	16.05	22.17	21.85	21.25	19.93	16.01	24.75	23.32	21.52	19.74	16.22	23.41	21.82	20.6	19.58	16.19	26.19	22.51	20.77
PM267	24.20	22.37	21.02	19.62	16.01	21.46	22.06	21.46	20.1	16.04	24.82	23.7	21.92	20.04	16.14	23.48	22.21	21	19.89	16.15	26.13	23	21.13
CTN311	23.98	21.57	21.06	19.52	NaN	22.05	21.36	21.15	19.49	NaN	24.52	22.6	21.53	19.66	NaN	23.26	21.07	20.8	19.71	NaN	26.06	21.67	20.75
CTN312(0.5-1)	23.98	21.57	21.06	19.52	NaN	22.05	21.36	21.15	19.49	NaN	24.52	22.6	21.53	19.66	NaN	23.26	21.07	20.8	19.71	NaN	26.06	20.24	20.75
CTN312(0-0.5)	23.98	21.57	21.06	19.52	NaN	22.05	21.36	21.15	19.49	NaN	24.52	22.6	21.53	19.66	NaN	23.26	21.07	20.8	19.71	NaN	26.06	20.24	20.75
CTN313	23.82	21.71	20.59	19.23	16.4	22.02	21.17	20.42	19.11	16.5	24.46	22.8	21.15	19.49	16.49	23.09	21.07	20.35	19.33	16.6	25.70	24.02	20.42
CTN314	23.82	21.71	20.59	19.23	16	22.02	21.17	20.42	19.11	16.06	24.46	22.8	21.15	19.49	16.12	23.09	21.07	20.35	19.33	16.18	25.70	23.37	20.42

Average	23.67	21.65	20.69	19.88	16.02	21.46	21.23	20.86	20.01	16.43	24.06	22.61	21.28	20.21	15.74	23.07	21.19	20.36	19.95	16.26	26.04	22.27	20.33
std	0.31	0.40	0.36	0.37	0.25	0.54	0.30	0.29	0.46	0.26	0.49	0.44	0.33	0.50	0.47	0.21	0.41	0.43	0.33	0.23	0.12	1.17	0.51
min	23.34	20.33	20.22	19.23	15.76	20.84	20.75	20.42	19.11	16.01	23.51	21.39	20.86	19.49	15.27	22.83	19.82	19.78	19.33	16.07	25.70	19.24	19.64
max	24.20	22.37	21.06	20.33	16.51	22.17	22.06	21.46	20.44	16.94	24.82	23.70	21.92	20.78	16.58	23.48	22.21	21.00	20.48	16.82	26.21	24.02	21.13

Table 20 – Data of the ratio Mg/Ca after the analytical control. The “NaN” refers to the samples that did not have enough calcite to perform the analyses.

	Schrag Mg/Ca (mMol/Mol)								
Sample ID	*G. ruber* (p) 250 - 300	*G. ruber* (p) 300 - 355	*G. ruber* (w) *s.s.* 250 - 300	*G. ruber* (w) *s.s.* 300 - 355	*G. ruber* (w) *s.l.* 250 - 300	*G. ruber* (w) *s.l.* 300 - 355	*G. truncatulinoides* NC	*G. truncatulinoides* C	*G. inflata*
NAP62	4.42	NaN	NaN	NaN	4.01	NaN	NaN	NaN	NaN
NAP63	3.74	4.04	NaN	NaN	4.07	NaN	NaN	NaN	NaN
NAP64	3.78	NaN	NaN	NaN	4.55	NaN	NaN	NaN	NaN
NAP66	3.91	4.21	NaN	NaN	4.10	NaN	NaN	NaN	NaN
NAP68	4.43	NaN	NaN	NaN	NaN	NaN	NaN	NaN	NaN
PM249	3.86	4.01	4.49	4.76	3.94	4.20	2.36	1.93	1.93
PM250	3.55	4.11	NaN	NaN	3.91	3.96	2.03	2.17	2.17
PM253	3.24	3.39	NaN	NaN	NaN	NaN	1.69	NaN	NaN
PM254	NaN	3.70	NaN	NaN	3.88	NaN	NaN	NaN	NaN
PM255	3.41	3.85	4.09	3.86	3.37	3.42	1.72	1.87	1.87
PM256	3.34	3.81	3.84	4.12	3.57	3.92	1.99	1.80	1.80
PM257	NaN	NaN	NaN	NaN	NaN	NaN	NaN	NaN	NaN
PM258	3.66	3.78	3.86	4.08	3.65	4.55	1.96	2.05	2.05
PM259	NaN	3.81	3.74	3.88	3.50	3.23	1.84	1.95	1.95
PM260	3.42	3.96	NaN	4.34	3.60	3.86	2.05	2.11	2.11
PM262	NaN	4.14	NaN	3.98	3.89	4.38	2.15	2.11	2.11
PM263	NaN	3.87	3.99	3.90	4.10	3.99	2.17	1.95	1.95
PM264	3.25	3.88	NaN	4.34	3.64	NaN	1.74	2.11	2.11
PM265	3.68	3.85	NaN	NaN	3.71	3.99	NaN	NaN	NaN
PM266	3.85	3.88	NaN	4.17	3.74	3.92	1.92	2.09	2.09
PM267	3.51	3.97	NaN	3.93	3.48	3.72	1.79	1.82	1.82
CTN311	3.48	4.40	NaN	NaN	3.96	4.20	1.91	NaN	NaN
CTN312(0.5-1)	3.93	3.88	4.29	4.08	4.09	4.23	1.77	1.66	1.66
CTN312(0-0.5)	4.04	4.58	NaN	NaN	4.12	NaN	NaN	NaN	NaN

CTN313	3.89	4.02	NaN	NaN	4.07	3.96	1.79	1.64	1.64
CTN314	3.72	4.01	NaN	4.14	4.51	4.44	NaN	NaN	NaN
Average	3.72	3.96	4.05	4.12	3.89	4.00	1.93	1.95	1.95
std	0.33	0.24	0.25	0.24	0.30	0.34	0.18	0.17	0.17
min	3.24	3.39	3.74	3.86	3.37	3.23	1.69	1.64	1.64
max	4.43	4.58	4.49	4.76	4.55	4.55	2.36	2.17	2.17

Table 21- Summary of the Mg/Ca ratio analysis performed at the U.S. Geological Survey. The data below was calculated after the quality control with the respective calculates SSTs.

Species	**Size Fraction**	**Number of Samples**	**Average (mmol/mol)**	**SDV**	**Min (mmol/mol)**	**Max (mmol/mol)**	**SS Eq. (°C)**	**SDV**	**Min (°C)**	**Max (°C)**	**GE Eq. (°C)**	**SDV**	**Min (°C)**	**Max (°C)**
G. inflata	300 - 425	10	1.78	± 0.10	1.53	2.12	21.42	1.56	18.49	23.34	18.11	1.01	16.23	19.35
G. ruber (p)	250 - 300	21	3.71	± 0.32	3.23	4.42	24.37	1.48	22.08	27.39	25.31	0.97	23.81	27.28
G. ruber (p)	300 - 355	23	3.95	± 0.24	3.38	4.58	25.21	0.91	22.90	27.41	26.02	0.68	24.30	27.66
G. ruber (w) *s.s.*	250 - 300	7	4.04	± 0.26	3.74	4.49	24.26	0.59	23.52	25.31	26.26	0.67	25.42	27.45
G. ruber (w) *s.s.*	300 - 355	13	4.12	± 0.24	3.85	4.76	25.27	0.66	24.51	26.99	26.47	0.63	25.74	28.09
G. ruber (w) *s.l.*	250 - 300	24	3.89	± 0.29	3.37	4.54	23.86	0.74	22.49	25.42	25.81	0.84	24.25	27.58
G. ruber (w) *s.l.*	300 - 355	16	3.99	± 0.34	3.23	4.54	24.89	1.02	22.43	26.45	26.11	0.97	23.78	27.58
G. truncatulinoides (d) NC	380 – 620	16	1.92	± 0.18	1.68	2.36	18.64	1.03	17.19	20.94	18.01	1.03	16.56	20.30
G. truncatulinoides (d) C	380 - 620	14	1.94	± 0.17	1.63	2.16	18.74	0.97	16.86	19.98	18.11	0.97	16.23	19.35

Table 22 - Results of the test of significancy of the difference between the Mg/Ca means within the surface-dwelling species analyzed in the research project. The values in the table are the uncorrected *p*-value of the Kruskal-Wallis test.

	G. ruber **(p) – 250-300 µm**	***G. ruber*** **(p) – 300-355 µm**	***G. ruber*** **(w)** ***s.s.*** **– 250 – 300 µm**	***G. ruber*** **(w) s.s. – 300 – 355 µm**	***G. ruber*** **(w)** ***s.l.*** **– 250 – 300 µm**	***G. ruber (*****w)** ***s.l.*** **– 300 – 355 µm**
G. ruber **(p) – 250-300 µm**						
G. ruber **(p) – 300-355 µm**	< 0.05					
G. ruber **(w)** ***s.s.*** **– 250 – 300 µm**	< 0.05	**0.70**				
G. ruber **(w)** ***s.s.*** **– 300 – 355 µm**	< 0.05	< 0.05	**0.40**			
G. ruber **(w)** ***s.l.*** **– 250 – 300 µm**	**0.05**	**0.50**	**0.35**	< 0.05		
G. ruber **(w)** ***s.l.*** **– 300 – 355 µm**	< 0.05	**0.46**	**1**	**0.56**	**0.25**	

Table 23 – Results of the test of significancy of the difference between means within the deep-dwelling species analyzed in the research project. The values in the table are the uncorrected *p*-value of ANOVA test.

	G. truncatulinoides **(d) NC**	***G. truncatulinoides*** **(d) C**
G. truncatulinoides **(d) NC**		
G. truncatulinoides **(d) C**	**0.60**	
G. inflata	**0.60**	**0.98**

Table 24 – Calculated SSTs based on ratio Mg/Ca from samples collected along the SBB.

	G. ruber (p) - 250 - 300		*G. ruber* (p) - 300 - 355		*G. white* s.s - 250 - 300		*G. white s.s* - 300 - 355		*G. white s.l*- 250 - 300		*G. white s.l* - 300 - 355		*G. truncatulinoides* (d) NC		*G. truncatulinoides* (d) C		*G. inflata*	
Sample ID	SS (°C)	GE (°C)	SS (°C)	GE (°C)	SS (°C)	GE (°C)	SS (°C)	GE (°C)	SS (°C)	GE (°C)	SS (°C)	GE (°C)	SS (°C)	GE (°C)	SS (°C)	GE (°C)	SS (°C)	GE (°C)
NAP62	27.34	27.25	NaN	NaN	NaN	NaN	NaN	NaN	24.19	26.18	NaN	NaN	NaN	NaN	NaN	NaN	NaN	NaN
NAP63	24.53	25.41	25.52	26.25	NaN	NaN	NaN	NaN	24.33	26.34	NaN	NaN	NaN	NaN	NaN	NaN	NaN	NaN
NAP64	24.68	25.51	NaN	NaN	NaN	NaN	NaN	NaN	25.42	27.58	NaN	NaN	NaN	NaN	NaN	NaN	NaN	NaN
NAP66	25.30	25.91	26.14	26.71	NaN	NaN	NaN	NaN	24.42	26.44	NaN	NaN	NaN	NaN	NaN	NaN	NaN	NaN
NAP68	27.39	27.28	NaN	NaN	NaN	NaN	NaN	NaN	NaN	NaN	NaN	NaN	NaN	NaN	NaN	NaN	NaN	NaN
PM249	25.07	25.76	25.43	26.18	25.31	27.45	26.99	28.09	24.02	25.98	25.51	26.69	20.94	20.30	18.71	18.08	21.37	18.08
PM250	23.63	24.82	25.80	26.46	NaN	NaN	NaN	NaN	23.94	25.90	24.83	26.05	19.24	18.61	19.98	19.35	23.34	19.35
PM253	22.08	23.81	22.90	24.30	NaN	NaN	NaN	NaN	NaN	NaN	NaN	NaN	17.19	16.56	NaN	NaN	NaN	NaN
PM254	NaN	NaN	24.24	25.30	NaN	NaN	NaN	NaN	23.88	25.82	NaN	NaN	NaN	NaN	NaN	NaN	NaN	NaN
PM255	22.94	24.37	24.81	25.72	24.40	26.41	24.51	25.74	22.49	24.25	23.10	24.41	17.40	16.77	18.31	17.68	20.75	17.68
PM256	22.63	24.16	24.67	25.62	23.78	25.71	25.30	26.49	23.06	24.89	24.70	25.92	19.01	18.38	17.92	17.29	20.14	17.29
PM257	NaN	NaN	NaN	NaN	NaN	NaN	NaN	NaN	NaN	NaN	NaN	NaN	NaN	NaN	NaN	NaN	NaN	NaN
PM258	24.16	25.17	24.53	25.51	23.81	25.75	25.17	26.37	23.28	25.15	26.45	27.58	18.84	18.20	19.34	18.71	22.35	18.71
PM259	NaN	NaN	24.67	25.62	23.52	25.42	24.58	25.81	22.86	24.67	22.43	23.78	18.18	17.55	18.80	18.17	21.50	18.17
PM260	22.99	24.40	25.24	26.05	NaN	NaN	25.89	27.05	23.12	24.97	24.51	25.75	19.34	18.71	19.69	19.06	22.89	19.06
PM262	NaN	NaN	25.88	26.52	NaN	NaN	24.88	26.09	23.89	25.84	26.01	27.16	19.90	19.27	19.68	19.05	22.88	19.05
PM263	NaN	NaN	24.90	25.79	24.14	26.13	24.64	25.86	24.40	26.42	24.92	26.13	19.98	19.35	18.80	18.17	21.50	18.17
PM264	22.12	23.83	24.92	25.81	NaN	NaN	25.91	27.07	23.23	25.09	NaN	NaN	17.52	16.89	19.65	19.02	22.83	19.02
PM265	24.27	25.24	24.81	25.72	NaN	NaN	NaN	NaN	23.42	25.31	24.90	26.12	NaN	NaN	NaN	NaN	NaN	NaN
PM266	25.04	25.74	24.95	25.83	NaN	NaN	25.42	26.60	23.52	25.42	24.70	25.92	18.64	18.01	19.59	18.96	22.73	18.96
PM267	23.45	24.70	25.27	26.06	NaN	NaN	24.74	25.96	22.81	24.61	24.09	25.35	17.86	17.23	18.07	17.43	20.37	17.43

CTN311	23.31	24.61	26.81	27.22	NaN	NaN	NaN	NaN	24.08	26.06	25.51	26.69	18.57	17.94	NaN	NaN	NaN	NaN
CTN312(0.5-1)	25.38	25.97	24.95	25.83	24.86	26.94	25.18	26.38	24.40	26.41	25.60	26.78	17.76	17.13	17.00	16.37	18.71	16.37
CTN312(0-0.5)	25.85	26.27	27.41	27.66	NaN	NaN	NaN	NaN	24.45	26.47	NaN	NaN	NaN	NaN	NaN	NaN	NaN	NaN
CTN313	25.20	25.85	25.46	26.21	NaN	NaN	NaN	NaN	24.34	26.35	24.82	26.04	17.82	17.19	16.86	16.23	18.49	16.23
CTN314	24.45	25.36	25.42	26.17	NaN	NaN	25.35	26.54	25.33	27.48	26.17	27.31	NaN	NaN	NaN	NaN	NaN	NaN
Average	24.37	25.31	25.21	26.02	24.26	26.26	25.27	26.47	23.86	25.81	24.89	26.11	18.64	18.01	18.74	18.11	21.42	18.11
STD	1.48	0.97	0.91	0.68	0.59	0.67	0.66	0.63	0.74	0.84	1.02	0.97	1.03	1.03	0.97	0.97	1.56	1.01
Min	22.08	23.81	22.90	24.30	23.52	25.42	24.51	25.74	22.49	24.25	22.43	23.78	17.19	16.56	16.86	16.23	18.49	16.23
Max	27.39	27.28	27.41	27.66	25.31	27.45	26.99	28.09	25.42	27.58	26.45	27.58	20.94	20.30	19.98	19.35	23.34	19.35

Table 25 – Results of the *p*-value of the Kruskal-Wallis test performed with the Mg/Ca within all species. *P*-values lower than 0.05 suggest that there is a significant difference of Mg/Ca between the size fractions; *p*-values greater than 0.05 suggest that there is no significant difference between the Mg/Ca values within the size fractions.

	G. ruber **(p) 250-300**	***G. ruber*** **(p) 300-355**	***G. ruber*** **(w)** ***ss*** **250-300**	***G. ruber*** **(w)** ***ss*** **300-355**	***G. ruber*** **(w)** ***sl*** **250-300**	***G. ruber*** **(w)** ***sl*** **300-355**	***G. truncatulinoides*** **NC**	***G. truncatulinoides*** **C**	***G. inflata***
G. ruber **(p) 250-300**									
G. ruber **(p) 300-355**	< 0.05								
G. ruber **(w)** ***ss*** **250-300**	< 0.05	0.70							
G. ruber **(w)** ***ss*** **300-355**	< 0.05	< 0.05	0.40						
G. ruber **(w)** ***sl*** **250-300**	0.05	0.50	0.35						
G. ruber **(w)** ***sl*** **300-355**	< 0.05	0.47	1	0.57	0.25				
G. truncatulinoides **NC**	< 0.05	< 0.05	< 0.05	< 0.05	< 0.05	< 0.05		0.60	0.60
G. truncatulinoides **C**	< 0.05	< 0.05	< 0.05	< 0.05	< 0.05	< 0.05	0.60		0.98
G. inflata	< 0.05	< 0.05	< 0.05	< 0.05	< 0.05	< 0.05	0.60	0.98	

Table 26 – Values of the *p*-value of the Kruskal-Wallis test performed with the SST obtained with the SS equation against the sea temperatures from the WOA13. *P*-values greater than 0.5 indicates that the calculated averages are similar to the observed temperature.

***G. inflata* (SS Equation)**	***p*-value**
Annual SST (0m)	< 0.05
Annual SST (10m)	**0.89**
Annual SST (15m)	< 0.05
Annual SST (20m)	< 0.05
Annual SST (25m)	< 0.05
Winter SST (0m)	0.63
Winter SST (10m)	0.21
Winter SST (15m)	0.08
Winter SST (20m)	< 0.05
Winter SST (25m)	< 0.05
Autumn SST (0m)	< 0.05
Autumn SST (10m)	0.06
Autumn SST (15m)	0.60
Autumn SST (20m)	< 0.05
Autumn SST (25m)	< 0.05
Spring SST (0m)	< 0.05
Spring SST (10m)	0.24
Spring SST (15m)	< 0.05
Spring SST (20m)	< 0.05
Spring SST (25m)	< 0.05
Summer SST (0m)	< 0.05
Summer SST (10m)	0.15
Summer SST (15m)	< 0.05
Summer SST (20m)	< 0.05
Summer SST (25m)	< 0.05

4. References

Anand, P., Elderfield, H. and Conte, M.H., 2003. Calibration of Mg/Ca thermometry in planktonic foraminifera from a sediment trap time series. *Paleoceanography*, *18*(2).

Antunes, R.L. *Introdução ao estudo dos nanofósseis calcários*. UFRJ/IG. 1997.

Barker, S., Greaves, M. and Elderfield, H., 2003. A study of cleaning procedures used for foraminiferal Mg/Ca paleothermometry. *Geochemistry, Geophysics, Geosystems*, *4*(9).

Baumann, K.H., Čepek, M. and Kinkel, H., 1999. Coccolithophores as indicators of ocean water masses, surface-water temperature, and paleoproductivity—examples from the South Atlantic. In *Use of Proxies in Paleoceanography* (pp. 117-144). Springer, Berlin, Heidelberg.

Benthien, A., Müller, P. J. 2000. Anomalously low alkenone temperatures caused by lateral particle and sediment transport in the Malvinas Current region, western Argentine Basin. *Deep Sea Research Part I: Oceanographic Research Papers*, *47*(12), 2369-2393.

Boeckel, B. and Baumann, K.H. Distribution of coccoliths in surface sediments of the south-eastern South Atlantic Ocean: ecology, preservation and carbonate contribution. *Marine Micropaleontology*, *51*(3), pp.301-320. 2004.

Boeckel, B., Baumann, K.H., Henrich, R. and Kinkel, H., 2006. Coccolith distribution patterns in South Atlantic and Southern Ocean surface sediments in relation to environmental gradients. *Deep Sea Research Part I: Oceanographic Research Papers*, *53*(6), pp.1073-1099.

Boyle, E.A., 1983. Manganese carbonate overgrowths on foraminifera tests. Earth and Planetary Science Letters 53, 11–35.

Braga, E.S., Chiozzini, VC., Berbel, G.B., Maluf, J.C., Aguiar, V.M., Charo, M., Molina, D., Romero, S.I. and Eichler, B.B. Nutrient distributions over the Southwestern South Atlantic continental shelf from Mar del Plata (Argentina) to Itajaí (Brazil): Winter–summer aspects. *Continental Shelf Research*, *28*(13), pp.1649-1661. 2008.

Brandini F.P. 1990a. Producão primária e características fotossintéticas do fitoplâncton ¸ na região sueste do Brasil. Brazilian Journal of Oceanography 38:147–159 DOI 10.1590/S1679-87591990000200004.

Brandini, F.P., 1990b. Hydrography and characteristics of the phytoplankton in shelf and oceanic waters off southeastern Brazil during winter (July/August 1982) and summer (February/March 1984). *Hydrobiologia*, *196*(2), pp.111-148.

Brandini, F.P., Moraes, C.L.B. and Thamm, C.A., 1989. Shelf-break upwelling, subsurface maxima of chlorophyll and nitrite, and vertical distribution of a subtropical nano-microplankton community off southeastern Brazil. *Memórias do III Encontro Brasileiro de Plâncton (FP Brandini, coord.), Curitiba*, pp.47-55.

Brandini F. P., Boltovskoy D., Piola A., Kocmur S., Röttgers R., P., Lopes R. 2000. Multiannual trends in fronts and distribution of nutrients and chlorophyll in the southwestern Atlantic (30–62◦ S). Deep-Sea Research Part I: Oceanographic Research Papers 47:1015–1033 DOI 10.1016/S0967-0637(99)00075-8.

Brandini, F.P., Nogueira Jr, M., Simião, M., Codina, J.C.U. and Noernberg, M.A., 2014. Deep chlorophyll maximum and plankton community response to oceanic bottom intrusions on the continental shelf in the South Brazilian Bight. *Continental Shelf Research*, *89*, pp.61-75.

Brassell, S.C., Brereton, R.G., Eglinton, G., Grimalt, J., Liebezeit, G., Marlowe, I.T., Pflaumann, U. and Sarnthein, M., 1986. Palaeoclimatic signals recognized by chemometric treatment of molecular stratigraphic data. *Organic Geochemistry*, *10*(4-6), pp.649-660.

Brassell, S.C., Eglinton, G., Marlowe, I.T., Pflaumann, U. and Sarnthein, M., 1986. Molecular stratigraphy: a new tool for climatic assessment. *Nature*, *320*(6058), p.129.

Campos, E.J., Velhote, D. and da Silveira, I.C. Shelf break upwelling driven by Brazil Current cyclonic meanders. *Geophysical Research Letters*, *27*(6), pp.751-754. 2000.

Castelao, R.M., Campos, E.J. and Miller, J.L. A modelling study of coastal upwelling driven by wind and meanders of the Brazil Current. *Journal of Coastal Research*, pp.662-671. 2004.

Castro, B.M., Brandini, F.P., Pires-Vanin, A.M.S. and Miranda, L.B., 2006. Multidisciplinary oceanographic processes on the Western Atlantic continental shelf between 4 N and 34 S. *The sea*, *11*, pp.209-251.

Chiessi, C.M., Mulitza, S., Groeneveld, J., Silva, J.B., Campos, M.C. and Gurgel, M.H., 2014. Variability of the Brazil Current during the late Holocene. *Palaeogeography, Palaeoclimatology, Palaeoecology*, *415*, pp.28-36.

Cléroux, C., Cortijo, E., Anand, P., Labeyrie, L., Bassinot, F., Caillon, N. and Duplessy, J.C., 2008. Mg/Ca and Sr/Ca ratios in planktonic foraminifera: Proxies for upper water column temperature reconstruction. *Paleoceanography and Paleoclimatology*, *23*(3).

Conte, M.H., Sicre, M.A., Rühlemann, C., Weber, J.C., Schulte, S., Schulz-Bull, D., Blanz, T., 2006. Global temperature calibration of the alkenone unsaturation index (UK′ 37) in surface waters and comparison with surface sediments. *Geochemistry, Geophysics, Geosystems*, *7*(2).

Cordeiro, L.G.M.S., Belem, A.L., Bouloubassi, I., Rangel, B., Sifeddine, A., Capilla, R. and Albuquerque, A.L.S., 2014. Reconstruction of southwestern Atlantic sea surface temperatures during the last Century: Cabo Frio continental shelf (Brazil). *Palaeogeography, Palaeoclimatology, Palaeoecology*, *415*, pp.225-232.

Dauner, A.L.L., Mollenhauer, G., Bícego, M.C., de Souza, M.M., Nagai, R.H., Figueira, R.C.L., de Mahiques, M.M., e Sousa, S.H.D.M. and Martins, C.C., 2019. Multi-proxy reconstruction of sea surface and subsurface temperatures in the western South Atlantic over the last~ 75 kyr. *Quaternary Science Reviews*, *215*, pp.22-34.

Dekens, P.S., Lea, D.W., Pak, D.K. and Spero, H.J., 2002. Core top calibration of Mg/Ca in tropical foraminifera: Refining paleotemperature estimation. *Geochemistry, Geophysics, Geosystems*, *3*(4), pp.1-29.

Dittert, N., Baumann, K.H., Bickert, T., Henrich, R., Huber, R., Kinkel, H. and Meggers, H. Carbonate dissolution in the deep-sea: methods, quantification and paleoceanographic application. In *Use of proxies in paleoceanography* (pp. 255-284). Springer, Berlin, Heidelberg. 1999.

Eggins, S., De Deckker, P., Marshall, J. Mg/Ca variation in planktonic foraminifera tests: implications for reconstructing palaeo-seawater temperature and habitat migration. *Earth and Planetary Science Letters*, *212*(3-4), pp.291-306. 2003.

Elderfield, H. and Ganssen, G., 2000. Past temperature and δ 18 O of surface ocean waters inferred from foraminiferal Mg/Ca ratios. *Nature*, *405*(6785), p.442.

Evans, D., Wade, B.S., Henenhan, M., Erez, J. and Müller, W. Revisiting carbonate chemistry controls on planktic foraminifera Mg/Ca: implications for sea surface temperature and hydrology shifts over the Paleocene–Eocene Thermal Maximum and Eocene–Oligocene transition. *Climate of the Past*, *12*(4), pp.819-835. 2016.

Farmer, J.R., Cronin, T.M., De Vernal, A., Dwyer, G.S., Keigwin, L.D. and Thunell, R.C., 2011. Western Arctic Ocean temperature variability during the last 8000 years. *Geophysical Research Letters*, *38*(24).

Franco-Fraguas, P; Costa, K. B.; Toledo, F. A. L. Relationship between isotopic composition (Δ18O and Δ13C) and plaktonic foraminifera test size in core tops from the Brazilian Continental Margin. *Braz. j. oceanogr*. 2011, vol.59, n.4, pp.327-338. ISSN 1982-436X. http://dx.doi.org/10.1590/S1679-87592011000400003. 2011.

Friedrich, O., Schiebel, R., Wilson, P.A., Weldeab, S., Beer, C.J., Cooper, M.J. and Fiebig, J. Influence of test size, water depth, and ecology on Mg/Ca, Sr/Ca, δ18O and δ13C in nine modern species of planktic foraminifers. *Earth and Planetary Science Letters*, *319*, pp.133-145. 2012.

Gaeta, S.A. and Brandini, F.P. Produção primária do fitoplâncton na região entre o Cabo de São Tomé (RJ) eo Chuí (RS). *O ambiente oceanográfico da plataforma continental e do talude na região sudeste-sul do Brasil, São Paulo, SP, Brasil, EDUSP*, pp.219-264. 2006.

Groeneveld, J.; Chiessi, C. M. Mg/Ca of Globorotalia inflata as a recorder of permanent thermocline temperatures in the South Atlantic. Paleoceanography, 26(2). 2011.

Hertzberg, J.E. and Schmidt, M.W. Refining Globigerinoides ruber Mg/Ca paleothermometry in the Atlantic Ocean. *Earth and Planetary Science Letters*, *383*, pp.123-133. 2013.

Jin, X., Liu, C., Poulton, A.J., Dai, M. and Guo, X. Coccolithophore responses to environmental variability in the South China Sea: species composition and calcite content. *Biogeosciences*, *13*(16), pp.4843-4861. 2016.

Kemle-von Mücke, S. and Hemleben, C. Foraminifera. *South Atlantic Zooplankton*, *1*, pp.43-73. 1999.

Koch, C. and Young, J.R. A simple weighing and dilution technique for determining absolute abundances of coccoliths from sediment samples. *Journal of Nannoplankton Research*, *29*(1), pp.67-69. 2007.

Kucera, M., 2007. Chapter six planktonic foraminifera as tracers of past oceanic environments. *Developments in marine geology*, *1*, pp.213-262.
Lea, D.W., Mashiotta, T.A., Spero, H.J. Controls on magnesium and strontium uptake in planktonic foraminifera determined by live culturing. *Geochimica et Cosmochimica Acta*, *63*(16), pp.2369-2379. 1999.

Leduc, G., Schneider, R., Kim, J.H. and Lohmann, G., 2010. Holocene and Eemian sea surface temperature trends as revealed by alkenone and Mg/Ca paleothermometry. *Quaternary Science Reviews*, *29*(7), pp.989-1004.

Lee, K.E., Kim, J.H., Wilke, I., Helmke, P. and Schouten, S., 2008. A study of the alkenone, TEX86, and planktonic foraminifera in the Benguela Upwelling System: Implications for past sea surface temperature estimates. *Geochemistry, Geophysics, Geosystems*, *9*(10).

Leeuw, S.W., Perram, J.W. and Smith, E.R., 1980. Simulation of electrostatic systems in periodic boundary conditions. I. Lattice sums and dielectric constants. *Proc. R. Soc. Lond. A*, *373*(1752), pp.27-56.

Leider, A., Hinrichs, K. U., Mollenhauer, G., Versteegh, G. J. 2010. Core-top calibration of the lipid-based and TEX 86 temperature proxies on the southern Italian shelf (SW Adriatic Sea, Gulf of Taranto). *Earth and Planetary Science Letters*, *300*(1), 112-124.

Lessa, D.V., Venancio, I.M., Dos Santos, T.P., Belem, A.L., Turcq, B.J., Sifeddine, A., Albuquerque, A.L.S. Holocene oscillations of Southwest Atlantic shelf circulation based on planktonic foraminifera from an upwelling system (off Cabo Frio, Southeastern Brazil). The Holocene, 26(8), pp.1175-1187. 2016.

Lima, J.A.M. Oceanic circulation on the Brazil Current shelf break and slope at 22S. Sydney: University of New South Wales. 1997.

Locarnini, R.A., Mishonov, A.V., Antonov, J.I., Boyer, T.P., Garcia, H.E., Baranova, O.K., Zweng, M.M., Paver, C.R., Reagan, J.R., Johnson, D.R. and Hamilton, M. World ocean atlas 2013. Volume 1, Temperature. 2013.

Lourenço, R.A. *Aplicação de marcadores orgânicos moleculares em estudos oceanográficos e paleoceanográficos: Estudo de caso na margem continental superior do sudeste do Brasil* (Doctoral dissertation, Universidade de São Paulo). 2007.

Lourenço, R. A., Magalhães, C. A., de Mahiques, M. M., Taniguchi, S., Bícego, M. C. 2017. Distribution of terrigenous and marine material along the Southeastern Brazilian continental margin. *Regional Studies in Marine Science*, *14*, 118-125.

Mahiques, M.M., da Silveira, I.C.A., e Sousa, S.H.D.M. and Rodrigues, M., 2002. Post-LGM sedimentation on the outer shelf–upper slope of the northernmost part of the São Paulo Bight, southeastern Brazil. *Marine Geology*, *181*(4), pp.387-400.

Mahiques, M.M., Mishima, Y. and Rodrigues, M., 1999. Characteristics of the sedimentary organic matter on the inner and middle continental shelf between Guanabara Bay and São Francisco do Sul, southeastern Brazilian margin. *Continental Shelf Research*, *19*(6), pp.775-798.

Mahiques, M.M., Sousa, S.H., Burone, L., Nagai, R.H., Silveira, I.C., Figueira, R.C., Soutelino, R.G., Ponsoni, L. and Klein, D.A., 2011. Radiocarbon geochronology of the sediments of the São Paulo Bight (southern Brazilian upper margin). *Anais da Academia Brasileira de Ciências*, *83*(3), pp.817-834.

Mahiques, M.M., Tessler, M.G., Ciotti, A.M., da Silveira, I.C.A., e Sousa, S.H.D.M., Figueira, R.C.L., Tassinari, C.C.G., Furtado, V.V. and Passos, R.F.,

2004. Hydrodynamically driven patterns of recent sedimentation in the shelf and upper slope off Southeast Brazil. *Continental Shelf Research*, *24*(15), pp.1685-1697.

Mahiques, M.M.D., Bícego, M.C., Silveira, I.C., Sousa, S.H., Lourenço, R.A. and Fukumoto, M.M., 2005. Modern sedimentation in the Cabo Frio upwelling system, Southeastern Brazilian shelf. *Anais da Academia Brasileira de Ciências*, *77*(3), pp.535-548.

Mahiques, M.M.D., Burone, L., Figueira, R.C.L., Lavenére-Wanderley, A.A.D.O., Capellari, B., Rogacheski, C.E., Barroso, C.P., dos Santos, S., Augusto, L., Cordero, L.M. and Cussioli, M.C., 2009. Anthropogenic influences in a lagoonal environment: a multiproxy approach at the valo grande mouth, Cananéia-Iguape system (SE Brazil). *Brazilian Journal of Oceanography*, *57*(4), pp.325-337.

Matsuura, Y. A probable cause of recruitment failure of the Brazilian sardine Sardinella aurita population during the 1974/75 spawning season. *South African Journal of Marine Science*, *17*(1), pp.29-35. 1986.

McGillicuddy Jr, D.J., 2016. Mechanisms of physical-biological-biogeochemical interaction at the oceanic mesoscale. *Annual Review of Marine Science*, *8*, pp.125-159.

Moser, G.A.O., Gianesella-Galvão, S.M.F. 1997. Biological and oceanography upwelling indicators at Cabo Frio (RJ). *Rev Bras Oceanogr* 45:11–23.

Müller, P.J., Kirst, G., Ruhland, G., Von Storch, I. and Rosell-Melé, A., 1998. Calibration of the alkenone paleotemperature index U 37 K′ based on core-tops from the eastern South Atlantic and the global ocean (60 N-60 S). *Geochimica et Cosmochimica Acta*, *62*(10), pp.1757-1772.

Nagai, R.H., Sousa, S.H.M., Burone, L. and Mahiques, M.M., 2009. Paleoproductivity changes during the Holocene in the inner shelf of Cabo Frio, southeastern Brazilian continental margin: Benthic foraminifera and sedimentological proxies. *Quaternary International*, *206*(1-2), pp.62-71.

Nürnberg, D., Bijma, J., Hemleben, C., Assessing the reliability of magnesium in foraminiferal calcite as a proxy for water mass temperatures. *Geochimica et Cosmochimica Acta*, *60*(5), pp.803-814. 1996.

Odebrecht, C. and Castello, J.P. The convergence ecosystem in the Southwest Atlantic. In *Coastal marine ecosystems of Latin America* (pp. 147-165). Springer, Berlin, Heidelberg. 2001.

Okada, H. and Honjo, S., 1973, April. The distribution of oceanic coccolithophorids in the Pacific. In *Deep Sea Research and Oceanographic Abstracts* (Vol. 20, No. 4, pp. 355-374). Elsevier.

Okada, H. and McIntyre, A., 1979. Seasonal distribution of modern coccolithophores in the western North Atlantic Ocean. *Marine Biology*, *54*(4), pp.319-328.

Pelejero, C. and Calvo, E., 2003. The upper end of the UK′ 37 temperature calibration revisited. *Geochemistry, Geophysics, Geosystems*, *4*(2).

Pivel, M.A.G., Santarosa, A.C.A., Toledo, F.A.L. and Costa, K.B. The Holocene onset in the southwestern South Atlantic. *Palaeogeography, Palaeoclimatology, Palaeoecology*, *374*, pp.164-172. 2013.

Prahl, F.G. and Wakeham, S.G. Calibration of unsaturation patterns in long-chain ketone compositions for palaeotemperature assessment. *Nature*, *330*(6146), p.367. 1987.

Prahl, F.G., Wakeham, S.G., 1987. Calibration of unsaturation patterns in long-chain ketone compositions for palaeotemperature assessment. *Nature*, *330*(6146), pp.367-3.

Quadros, J.P.D. *Nanofósseis calcários da margem continental nordeste do Brasil: uma contribuição à paleoceanografia do Atlântico Sul nos últimos 25.000 anos* (Doctoral dissertation, Universidade de São Paulo). 2007.

Reynolds, C.E., Richey, J.N., Fehrenbacher, J.S., Rosenheim, B.E. and Spero, H.J. Environmental controls on the geochemistry of Globorotalia truncatulinoides in the Gulf of Mexico: Implications for paleoceanographic reconstructions. *Marine Micropaleontology*. 2018.

Ribeiro, C.G., dos Santos, A.L., Marie, D., Pellizari, V.H., Brandini, F.P., Vaulot, D. Pico and nanoplankton abundance and carbon stocks along the Brazilian Bight. *PeerJ*, *4*, p.2587. 2016.

Richey, J.N., Poore, R.Z., Flower, B.P. and Hollander, D.J. Ecological controls on the shell geochemistry of pink and white Globigerinoides ruber in the northern Gulf of Mexico: Implications for paleoceanographic reconstruction. *Marine Micropaleontology*, *82*, pp.28-37. 2012.

Richey, J.N., Thirumalai, K., Khider, D., Reynolds, C.E., Partin, J.W. and Quinn, T.M. Considerations for Globigerinoides ruber (white and pink) paleoceanography: comprehensive insights from a long-running sediment trap. *Paleoceanography and Paleoclimatology*. 2019.

Riveiros, N., Govin, A., Waelbroeck, C., Mackensen, A., Michel, E., Moreira, S., Bouinot, T., Caillon, N., Orgun, A. and Brandon, M. Mg/Ca thermometry in planktic foraminifera: Improving paleotemperature estimations for G. bulloides and N. pachyderma left. *Geochemistry, Geophysics, Geosystems*, *17*(4), pp.1249-1264. 2016.

Rosell-Melé, A., Eglinton, G., Pflaumann, U., Sarnthein, M. Atlantic core-top calibration of the U37K index as a sea-surface palaeotemperature indicator. *Geochimica et Cosmochimica Acta*, *59*(15), 3099-3107. 1995.

Rosenthal, Y. and Lohmann, G.P. Accurate estimation of sea surface temperatures using dissolution-corrected calibrations for Mg/Ca paleothermometry. *Paleoceanography*, *17*(3), pp.16-1. 2002.

Saavedra-Pellitero, M., Flores, J.A., Baumann, K.H. and Sierro, F.J., 2010. Coccolith distribution patterns in surface sediments of Equatorial and Southeastern Pacific Ocean. *Geobios*, *43*(1), pp.131-149.

Salmon, K.H., Anand, P., Sexton, P.F., Conte, M., 2016. Calcification and growth processes in planktonic foraminifera complicate the use of B/Ca and U/Ca as carbonate chemistry proxies. Earth Planet. Sci. Lett. 449, 372–381. http://dx.doi.org/10.1016/j.epsl.2016.05.016.

Santos, T.P., Belem, A.L., Barbosa, C.F., Dokken, T., Albuquerque, A.L.S. Paleoceanographic reconstruction of the western equatorial Atlantic during the last 40kyr. Palaeogeography, Palaeoclimatology, Palaeoecology, 415, pp.14-20. 2014.

Santos, T.P., Lessa, D.O., Venancio, I.M., Chiessi, C.M., Mulitza, S., Kuhnert, H., Albuquerque, A.L.S. The impact of the AMOC resumption in the western South Atlantic thermocline at the onset of the Last Interglacial. Geophysical Research Letters. 2017.

Schiebel R, Hemleben C. Planktic Foraminifers in the Modern Ocean. Berlin, Heidelberg: Springer. 2017.

Schrag, D.P. Rapid analysis of high-precision Sr/Ca ratios in corals and other marine carbonates. *Paleoceanography*, *14*(2), pp.97-102. 1999.

Silveira, I.C.A., Schmidt, A.C.K., Campos, E.J.D., de Godoi, S.S. and Ikeda, Y. A corrente do Brasil ao largo da costa leste brasileira. *Revista Brasileira de Oceanografia*, *48*(2), pp.171-183. 2000.

Silveira, I.C.A., Calado, L., Castro, B.M., Cirano, M., Lima, J.A.M. and Mascarenhas, A.D.S., 2004. On the baroclinic structure of the Brazil Current–Intermediate Western Boundary Current system at 22–23 S. *Geophysical Research Letters*, *31*(14).

Silveira, I.C.A. Lima, J.A., Schmidt, A.C.K., Ceccopieri, W., Sartori, A., Franscisco, C.P.F., Fontes, R.F.C. Is the meander growth in the Brazil Current system off Southeast Brazil due to baroclinic stability? Dynamics of Atmospheres and Oceans. 45(3/4): 187-207. 2008.

Sonzogni, C., Bard, E., Rostek, F., Dollfus, D., Rosell-Melé, A. and Eglinton, G. Temperature and salinity effects on alkenone ratios measured in surface sediments from the Indian Ocean. *Quaternary Research*, *47*(3), pp.344-355. 1997.

Souza, R.B. and Robinson, I.S., 2004. Lagrangian and satellite observations of the Brazilian Coastal Current. *Continental Shelf Research*, *24*(2), pp.241-262.

Sousa, S.H.M., de Godoi, S.S., Amaral, P.G.C., Vicente, T.M., Martins, M.V.A., Sorano, M.R.G.S., Gaeta, S.A., Passos, R.F. and Mahiques, M.M. Distribution of living planktonic foraminifera in relation to oceanic processes on the southeastern continental Brazilian margin (23° S–25° S and 40° W–44° W). *Continental Shelf Research*, *89*, pp.76-87. 2014.

Spear, J.W., Poore, R.Z., Quinn, T.M., 2011. Globorotalia truncatulinoides (dextral) Mg/Ca as a proxy for Gulf of Mexico winter mixed-layer temperature: evidence from a sediment trap in the northern Gulf of Mexico. Mar. Micropaleontol. 80 (3–4), 53–61.

Steinke, S., Chiu, H.Y., Yu, P.S., Shen, C.C., Löwemark, L., Mii, H.S. and Chen, M.T., 2005. Mg/Ca ratios of two Globigerinoides ruber (white) morphotypes: Implications for reconstructing past tropical/subtropical surface water conditions. *Geochemistry, Geophysics, Geosystems*, *6*(11).

Ternois, Y., Sicre, M.A., Boireau, A., Marty, J.C. and Miquel, J.C., 1996. Production pattern of alkenones in the Mediterranean Sea. *Geophysical Research Letters*, *23*(22), pp.3171-3174.

Thirumalai, K., Quinn, T.M. and Marino, G., 2016. Constraining past seawater δ18O and temperature records developed from foraminiferal geochemistry. *Paleoceanography*, *31*(10), pp.1409-1422.

Toledo, F.A., Cachão, M., Costa, K.B. and Pivel, M.A., 2007. Planktonic foraminifera, calcareous nannoplankton and ascidian variations during the last 25 kyr in the Southwestern Atlantic: A paleoproductivity signature? *Marine Micropaleontology*, *64*(1-2), pp.67-79.

Volkman, J.K., Eglinton, G., CoRNER, E.D. and Forsberg, T.E.V., 1980. Long-chain alkenes and alkenones in the marine coccolithophorid Emiliania huxleyi. *Phytochemistry*, *19*(12), pp.2619-2622.

Wang, L., 2000. Isotopic signals in two morphotypes of Globigerinoides ruber (white) from the South China Sea: implications for monsoon climate change during the last glacial cycle. *Palaeogeography, Palaeoclimatology, Palaeoecology*, *161*(3-4), pp.381-394.

Wefer G, Berger WH, Bijma J, Fischer G. Clues to ocean history: a brief overview of proxies. InUse of proxies in paleoceanography. 1999. (pp. 1-68). Springer, Berlin, Heidelberg.

Weldeab, S., Schneider, R.R. and Kölling, M., 2006a. Comparison of foraminiferal cleaning procedures for Mg/Ca paleothermometry on core material deposited under varying terrigenous-input and bottom water conditions. *Geochemistry, Geophysics, Geosystems*, *7*(4).

Young, J.R., Geisen, M., Cros, L., Kleijne, A., Sprengel, C., Probert, I. and Østergaard, J. A guide to extant coccolithophore taxonomy. *Journal of Nannoplankton Research, Special Issue*, *1*, pp.1-132. 2003.

Young, J.R., Bown, P.R., and Lees, J.A. Nannotax3 website. International Nannnoplankton Association. URL: https://ina.tmsoc.org/Nannotax3. 2014.